Universidade do Porto
Faculdade de Engenharia
FEUP

Simulated Moving Bed Separators/Reactors:
Application to the Synthesis of 1,1-Dibutoxyethane (DBE)

A Dissertation Presented to the Faculdade de Engenharia da Universidade do Porto for the degree of PhD in Chemical and Biological Engineering.

by

Nuno André Barbosa dos Santos Graça

Supervised by Professor Alírio Egídio Rodrigues and
Professor Luís Manuel Santos Pais

Laboratory of Separation and Reaction Engineering
Department of Chemical Engineering
Faculty of Engineering, University of Porto
Porto, Portugal

Março 2012

Acknowledgments

À Susana

"One never notices what has been done;
one can only see what remains to be done"

Marie Curie

Resumo

O objetivo do presente trabalho consistiu no estudo da reação de síntese do acetal 1,1-dibutoxietano (DBE) a partir de 1-butanol e acetaldeido, usando a resina de permuta iónica Amberlyst-15 como catalisador, de forma a obter dados termodinâmicos, cinéticos e de adsorção que sustentem a implementação de um processo integrado de separação/reação numa unidade de leito móvel simulado (SMB, *Simulated Moving Bed*).

A determinação dos dados cinéticos foi levada a cabo numa instalação experimental com um reator fechado, sistema automático de amostragem e aquisição de dados. A constante de equilíbrio químico foi calculada experimentalmente na gama de temperaturas 20-40 ºC a 6 atm. Os dados cinéticos obtidos experimentalmente são descritos por um modelo matemático de reator fechado, que considera difusão nos poros da partícula de catalisador e usa uma lei cinética com dois parâmetros baseada no modelo de Langmuir-Hinshelwood.

A síntese do DBE foi levada a cabo num reator cromatográfico de leito fixo. Experiências de adsorção/desorção, usando pares não reativos, foram realizadas para a obtenção dos parâmetros da isotérmica de adsorção. Um modelo matemático do reator cromatográfico, que inclui dispersão axial e resistências à transferência de massa internas e externas, foi usado para simular o comportamento dinâmico do reator.

A reação foi realizada numa unidade piloto de SMB Licosep 12-26 (Novasep, França), existente no LSRE. A operação do SMBR é simulada, usando os dados de reação e adsorção anteriormente obtidos, através do modelo matemático do reator de leito móvel verdadeiro (TMBR, *True Moving Bed Reactor*).

A influência da temperatura na operação isotérmica do reator de leito fixo foi estudada experimentalmente. Os dados de adsorção obtidos a diferentes temperaturas permitem o desenvolvimento de modelos matemáticos e a simulação da operação não isotérmica dos reatores de leito fixo e leito móvel simulado.

Abstract

The general objective of the present work is the study of the synthesis of 1,1-dibutoxyethane (DBE) from 1-butanol and acetaldehyde using the ion-exchange resin Amberlyst-15 as catalyst in order to obtain thermodynamic, kinetic and adsorption data that support the implementation of an integrated reaction/separation process in a simulated moving bed (SMB) unit.

The measurement of thermodynamic and kinetic data was performed in a laboratory scale batch reactor, with automatic sampling system and data acquisition. The reaction equilibrium constant was evaluated in the temperature range 20-40ºC, at 6 atm. The experimental kinetic results are described by a mathematical model of the batch reactor, which includes diffusion inside the catalyst particle and uses a two-parameter kinetic law based on the Langmuir-Hinshelwood model.

The synthesis of DBE was carried out in a fixed-bed adsorptive reactor. Adsorption/desorption experiments with non-reactive binary mixtures were performed in order to obtain the adsorption isotherm parameters. A mathematical model of the adsorptive reactor, which includes axial dispersion and internal and external mass-transfer resistances, was used to simulate the dynamic behavior of the reactor.

The reaction was performed in a SMB pilot unit Licosep 12-26 (Novasep, France), available at LSRE. The SMBR operation was simulated with the obtained reaction kinetic and adsorption data through a mathematical model of true moving bed reactor (TMBR).

The influence of temperature on the isothermal operation of the fixed-bed adsorptive reactor was experimentally studied. The adsorption data obtained at different temperatures allowed the development of mathematical models and simulation of the non-isothermal operation of fixed-bed and simulated moving bed adsorptive reactors.

Resumé

Le but générique de ce travail est l'étude de la synthèse du 1,1-dibutoxyéthane (DBE) à partir du mélange 1-butanol et acétaldéhyde, catalysée par la résine échangeuse d'ions Amberlyst-15, en vue d'obtenir données thermodynamiques, cinétiques et d'adsorption qui permettent la mise on œuvre d'une approche intégrée de réaction/séparation dans une unité a lit mobile simulé (SMB, *Simulated Moving Bed*).

Les mesures des données thermodynamiques et cinétiques ont été effectuées dans un réacteur fermé équipé avec un système automatique pour l'échantillonnage et l'acquisition des donnés. La constante d'équilibre a été calculé dans une gamme de températures 20-40ºC, à 6 atm. Les résultats cinétiques sont décrits par un modèle du réacteur fermé avec diffusion dans les pores de catalyseur, qui utilise une vitesse de réaction décrite par un modèle à deux paramètres basé sur l'expression de Langmuir-Hinshelwood.

La synthèse du DBE a été effectuée dans un réacteur adsorptive en lit fixe. Expériences d'adsorption/désorption ont été réalisés avec binaires non-réactives en vue de l'obtention de paramètres isothermes d'adsorption. Un modèle mathématique du réacteur adsorptive, avec dispersion axiale et résistances internes et externes au transport de matière, a été utilisé pour la simulation du comportement dynamique du réacteur.

La réaction a été conduite dans une unité pilote Licosep 12-16 (Novasep, France), disponible au LSRE. L'opération du SMBR a été simulée, a partir des données cinétiques et d'adsorption précédemment mesurées, grâce au modèle mathématique d'un vrai système à contre-courant (TMBR, *True Moving Bed Reactor*).

L'influence de la température sur le fonctionnement isotherme du réacteur en lit fixe a été étudiée expérimentalement. Les donnés d'adsorption obtenues à des températures différentes ont permis le développement des modèles mathématiques et la simulation du fonctionnement non-isotherme du réacteur en lit fixe et du réacteur a lit mobile simulé.

Table of Contents

List of Figures

Chapter 4

Chapter 5

Chapter 6

List of Tables

1. Introduction

1.1. Relevance and Motivation

Acetals are used in several areas, such as in agricultural chemicals, perfumes, pharmaceuticals and food flavoring. However, one of the most promising applications is its potential as oxygenated additive. In the path of the global trend to develop environmental friendly gasolines and fuels, the use of bio-derivable oxygenated additives, such as acetals, allows to reduce the tailpipe hazard emissions, such as the CO, NOx and particulate matter, in an environmental sustainable way.

Compounds like ethanol, which can be obtained from sugar cane, and acetaldehyde, which can be produced from ethanol, can be used as bio-derivable reactants to produce the acetal 1,1-diethoxyethane. Another bio-derivable compound, 1-butanol, which has been considered as alternative to ethanol as biofuel, can be used to produce the acetal 1,1- dibutoxyethane by means of natural resources.

The use of heterogeneous catalysts, such as a solid acid catalyst, presents several advantages over the homogenous catalysis. One of the most important advantages of the heterogeneous catalysts is their capability to be reused, which increases the productivity of the chemical processes and reduces their environmental impact.

The reactants conversion of equilibrium limited reactions, such acetalization, can be enhanced by using integrated reaction and separation processes to displace the chemical equilibrium to the products side. These integrated systems are one of the more important components of process intensification leading to cheaper, safer and sustainable technologies. The use of a simulated moving bed adsorptive reactor to deal with equilibrium limited reactions presents several advantages, such as continuous operation mode, and can be used with temperature sensitive compounds; it has the advantages of a countercurrent process avoiding the drawbacks of the true moving bed adsorptive reactor, and presents a more effective use of the desorbent and adsorbent phases as compared with rotating annular adsorptive reactor.

In short, the bio-derivable compounds 1-butanol and acetaldehyde can be used to produce the acetal 1,1-dibutoxyethane by means of natural resources and using a simulated moving bed adsorptive reactor packed with a solid acid catalyst, allows a continuous, sustainable and environmental friendly production of the acetal 1,1-dibutoxyethane.

1.2. Objectives and Outline

The main objective of the present thesis is to study and determine the thermodynamics, reaction kinetics and adsorption parameters in order to implement the synthesis of the acetal 1,1-dibutoxyethane in a simulated moving bed adsorptive reactor.

The thesis presented here includes six chapters dealing with the different aspects of the 1,1-dibutoxyethane synthesis:

In Chapter 1 the motivation and the main objectives of the thesis are presented.

Chapter 2 contains a literature survey on the acetals synthesis and applications. The acid catalyzed reaction for the synthesis of acetals from alcohols and aldehydes is presented and the advantages of using heterogeneous catalysis are referred. Some examples of integrated reaction and separation processes, namely reactive distillation and adsorptive reaction, are described. A brief description of patents related with acetals synthesis and applications is also presented.

Chapter 3 contains a detailed description of the experimental set-up used for thermodynamic and reaction kinetics data acquisition. Experimental results for the liquid-phase reaction of the synthesis of 1,1-dibutoxyethane from 1-butanol and acetaldehyde catalyzed by the commercial ion-exchange resin Amberlyst-15 are presented. The reaction equilibrium constant was evaluated based on experimental results at different temperatures. A mathematical model of the batch reactor, which includes diffusion inside the catalyst particles and uses a two-parameter kinetic law based on the Langmuir-Hinshelwood model, was used to obtain the kinetic parameters.

In Chapter 4, a study of the dynamic behavior of the 1,1-dibutoxyethane synthesis in a fixed bed adsorptive reactor is presented. Experimental adsorption/desorption experiments performed with the non-reactive binary pairs allowed to obtain the

parameters of the multicomponet Langmuir type isotherm. Reaction and regeneration experiments were performed in a fixed-bed column packed with Amberlyst-15. A mathematical model including axial dispersion and internal and external mass-transfer resistances was used to simulate the dynamic behavior of the fixed bed adsorptive reactor.

Chapter 5 presents the performance of a SBMR pilot unit for the synthesis of 1,1-dibutoxyethane. The SMBR operation was simulated with the obtained reaction kinetic and adsorption data through a mathematical model of a true moving bed reactor. The concept of reaction/separation region was used in order to evaluate the influence of the different operation parameters on the reactor performance.

Chapter 6 presents a study of the thermal effects on fixed-bed and simulated moving bed adsorptive reactors. Adsorption data were obtained at different temperatures in order to develop mathematical models and to simulate the non-isothermal operation of the fixed-bed and simulated moving bed adsorptive reactors.

Chapter 7 presents the general conclusions of this work and suggestions for future work.

2. Acetals: Synthesis and Applications

This chapter presents a literature survey on acetals synthesis, applications and production from the point of view of process intensification.

2.1. Synthesis of Acetals

Acetals can be produced by the acid-catalyzed addition of 2 mol of a monohydric alcohol and 1 mol of an aldehyde (Guinot, 1932). *Figure 2.1* presents the detailed mechanism of the formation of an acetal molecule. The formation of an acetal molecule occurs when the aldehyde molecule becomes protonated in acidic medium, the carbocation formed is then rapidly attacked by a molecule of alcohol losing a proton, the hydroxyl group of the hemiacetal formed previously becomes protonated and is lost as water, the carbocation formed is then attacked by a molecule of alcohol to form the acetal molecule.
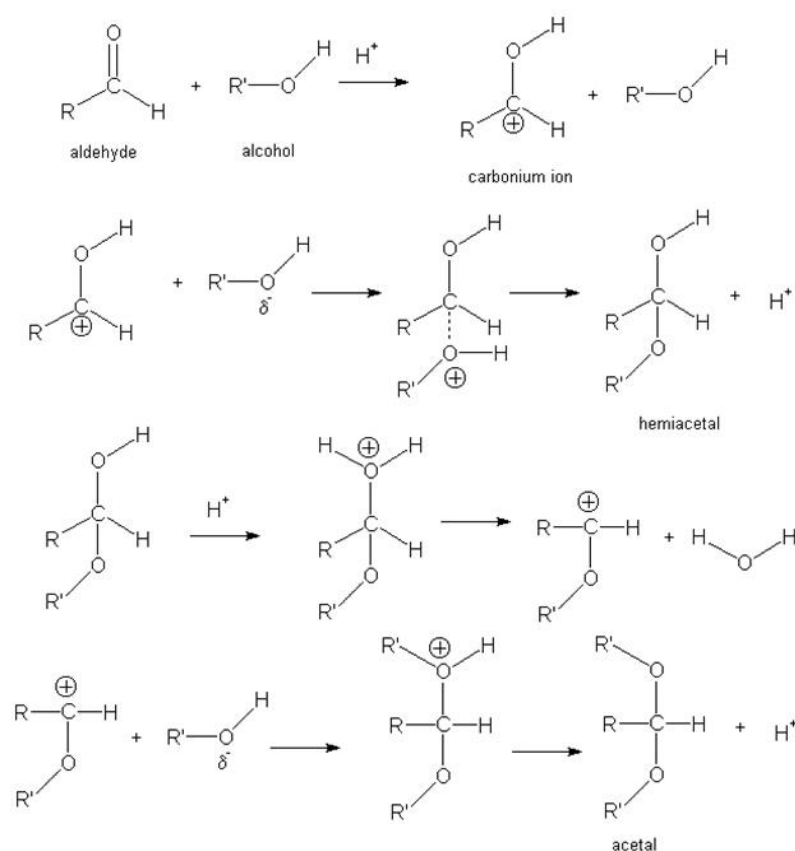
Figure 2.1. Mechanism of hemiacetal and acetal formation

According to the previous mechanism, for the formation of one molecule of acetal two molecules of alcohol are needed for each molecule of aldehyde. In this reaction it is also formed one molecule of water for each molecule of acetal. The global reaction is then:

$$Aldehyde \; + \; 2\,Alcohol \; \Longleftrightarrow \; Acetal \; + \; Water$$

This is a reversible reaction, hence the conversion of reactants is limited by the chemical equilibrium. To overcome this limitation the use of integrated processes of reaction and separation seems to be a good solution.

Table 2.1 presents a literature survey on synthesis of acetals with different alcohols and aldehydes performed in different kinds of reactors.

Table 2.1. Literature survey on synthesis of acetals.

Alcohol	Aldehyde	Acetal	Reactor	References
Methanol	Acetaldehyde	Acetaldehyde dimethylacetal	Batch/Fixed-Bed	(Gandi et al., 2007)
			SMBR	(Pereira et al., 2008)
	Formaldehyde	Formaldehyde dimethylacetal	Batch/Reactive Distillation	(Kolah et al., 1996)
Ethanol	Acetaldehyde	Acetaldehyde diethylacetal	Batch	(Silva and Rodrigues, 2001) (Silva and Rodrigues, 2006) (Capeletti et al., 2000)
			Fixed-Bed	(Silva and Rodrigues, 2002) (Gomez et al., 2004)
			SMBR	(Silva and Rodrigues, 2005)

There is a particular interest in using ethanol and acetaldehyde as reactants, because they can be produced from natural resources such as sugar cane and therefore the acetal 1,1-diethoxyethane can be produced by means of natural resources. Recently 1-butanol has been considered as alternative to ethanol as biofuel (Dürre, 2007); butanol has several advantages over ethanol, such as higher energy content, lower water absorption, better blending ability and can be used in conventional combustion engines without modifications. Therefore, 1-butanol is also a possible bio-derivable reactant to produce the acetal 1,1-dibutoxyethane.

2.2.1   Catalyst

The synthesis of oxygenated compounds, such as acetals, is typically carried out using homogenous catalysts, such as strong liquid inorganic acids, whose separation from the reaction products and reuse is a major concern (Lilja et al., 2002). The reuse of the catalyst is indeed a fundamental aspect, since it allows the increase of the overall productivity of chemical processes while minimizing their environmental impact (Barbara and Liguori, 2009). Therefore, the use of solid catalysts seems to be a good alternative. There is wide range of solid acid catalysts that can be used, such as iodine (Ramalinga et al., 2002), acid-treated clays (Chopade and Sharma, 1996), ZSM-5 (Ma et al., 1996), Zeolite-T membrane (Tanaka et al., 2002).

Some publications report the use of ion-exchange resins on the production of oxygenated compounds, such as the synthesis of MTBE (Caetano et al., 1994, Ziyang et al., 2001), ETBE (Umar et al., 2008), TAME (Mao et al., 2008, Vilarinho Ferreira and Loureiro, 2001), 1,1-dimethoxyethane (Gandi et al., 2005) and 1,1-diethoxyethane (Silva and Rodrigues, 2006).

Conventional ion-exchange resins are composed of copolymers of divinylbenzene (DVB), styrene and sulfonic acid groups. *Table 2.2* shows the physical properties of three ion-exchange resins, all of which are commercially available.

Moreover, ion-exchange resins, such as Amberlyst-15 and Amberlyst-18, can act as both catalyst and selective adsorbent, which makes them very attractive to be used in integrated reaction/separation processes. Published works report the use of Amberlys-18

in a fixed-bed adsorptive reactor (Silva and Rodrigues, 2002) and Amberlyst-15 in a simulated moving bed adsorptive Reactor (Silva and Rodrigues, 2005).

Table 2.2. Physical properties of some ion-exchange resins.

Catalyst	Surface area (m^2/g)	Pore Volume (mL/g)	Capacity (meqH$^+$/g)
Amberlyst®-15 Wet	53	0.4	4.7
Amberlyst®-16 Wet	30	0.2	4.8
Amberlyst®-35 Wet	50	0.35	5.2

2.2. Applications

Acetals are a useful starting material for perfumes, agricultural chemicals and pharmaceuticals (Iwasaky et al., 1998); they also can be used in the flavoring of food, in the design of synthetic perfumes in order to increase the resistance to oxidation and therefore the lifetime of perfumes (Kohlpaintner et al., 1999), as mineral oil substitute (Hille et al., 1998), in the production of polyvinylic ethers (Egwaw et al., 1997) and as intermediate in condensation reactions (Weizmann, 1949).

2.2.1. Oxygenated Compounds

In the last years there has been a growing interest in the development of environmentally friendly gasoline and fuels. Oxygenated additives can be used in order to reduce NOx and CO emissions and provide high octane quality of unleaded gasoline. Methyl tert-butyl ether (MTBE) is widely used as additive for gasoline, providing the enhancement of octane number and a significantly reduction of tailpipe pollution. However, there are concerns related with the detection of MTBE in ground water on U.S. (Rasa et al., 2011); moreover, some studies consider MTBE as possible carcinogen (Mehlman, 2001).

Emissions from a regular diesel engine consist mainly on solid carbonaceous particles, which can have compounds adsorbed on their surface. Besides the solid material, the emissions contain also volatile material particles of hydrocarbon, sulfuric acid or similar (*Figure 2.2*).
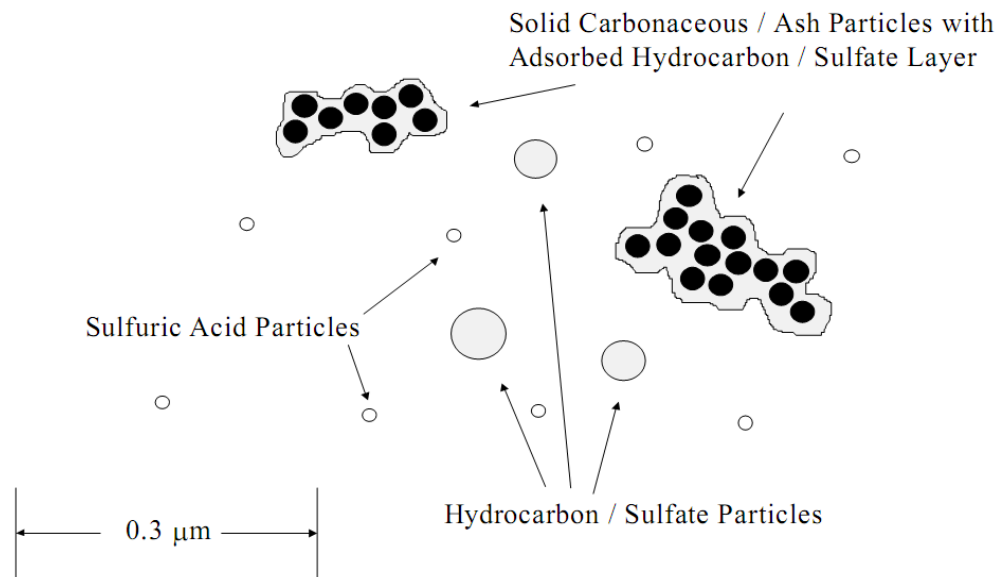
Figure 2.2. Typical diesel engine emission particle structure (Kittellson, 2000).

Due to their small size, the particles can travel long distances and be inhaled and trapped on respiratory tract. Studies performed by the World Health Organization, concluded that there is an increase on mortality as a consequence of increasing particulate emissions (Filliger and Schneider, 1999).

The increase of oxygen content in diesel fuel reduces significantly the particulate levels. Miyamoto and co-workers found that the Bosh smoke number (a measure of the particulate or soot levels in diesel exhaust) falls from about 55% for conventional diesel fuel to less than 1% when the oxygen content of fuel is above 25% by mass (Miyamoto et al., 1998). The use of the acetal 1,1-diethoxyethane (DEE) as diesel fuel additive has shown a marked reduction of exhaust smoke. However, the blends present a flash point below the European regulation limit (55 ºC) (see *Table 2.3*) (Frusteri et al., 2007). Therefore, the blends DEE/diesel cannot be used in vehicles without the adoption of an adequate safety system. Moreover, the use of another bio-derived acetal with higher flash point, such 1,1-dibutoxyethane (DBE) (46.2 ºC) could be explored.

Table 2.3. Flash point for the DEE/diesel fuel blends
(Frusteri et al., 2007)

Fuels	Flash point (ºC)
100% diesel fuel	73
5% DEE/95% diesel fuel	45
10% DEE/90% diesel fuel	32
20% DEE/80% diesel fuel	28

2.3. Patent Overview

The great number of patents shows an increasing interest in the acetals production and their applications. A brief description of a few patents is shown in *Table 2.4.*

Table 2.4. Patents related with the production and use of the acetals

Distilleries Des Deux-Sevres (Guinot, 1932)	Separation of pure acetal by distillation in three stages. In the first stage, whole acetaldehyde and part of alcohol is removed by distillation, leaving as residue the acetal, the water and the remainder of alcohol; the second stage consists in the removal of this residue of water and alcohol by distillation, by the use of an auxiliary liquid insoluble in water; In the third stage the auxiliary liquid is recovered by washing, and the alcohol by distillation, and in causing them to enter the cycle operations.
Polymerisable Products Ltd. (Weizmann, 1949)	Condensation reactions can be carried out easily and with satisfactory yields by the use of the complex formed by combining potassium hydroxide and a substance containing two ether oxygen atoms , and in particular a substance belonging to the class of acetals and dialkyl ether of ethylene glycol. Such complex can be obtained by combining potassium hydroxide and acetaldehyde dibutylacetal.

Distillers Co. (Bramwyche et al., 1950)	The production of diethyl acetal is carried out by reacting acetaldehyde with ethanol in presence of a strong acid and in presence of an inert eluent, substantially immiscible with water. The two phases formed are then separated and acetal is recovered from the diluents phase by distillation.
Dow Chemical (Frevel and Hedelund, 1950)	Acetals can be obtained by reacting a saturated aliphatic aldehyde containing 1 to 7 carbon atoms in the molecule with a primary or a secondary monohydric alkyl alcohol containing 1 to 6 carbon atoms in vapor phase and in absence of catalyst, when at least one of the reactants contains not more than one carbon in the molecule.
Union Rheinische **Braunkohlen** **Kraftstoff** **Aktiengesellschaft.** (Korff et al., 1981)	The improved process for the production of acetaldehyde dimethylacetal by reacting methanol with carbon monoxide and hydrogen in the presence of a cobalt-containing catalyst, halogen or halide as promoter and a 3-valent phosphorus compound as ligand using a nickel compound as a co-catalyst was presented.
Degusa Aktiengesellschaft (Andrade et al., 1986)	Method for the preparation of acetals through the conversion of aldehydes with alcohols in a liquid phase in presence of a solid acid catalyst, such as a strongly acid ion exchange resin or zeolite. The acetal is extracted by means of water and by means of water insoluble organic solvents.
Showa Denko K.K. (Aizawa et al., 1994)	A process for producing acetaldehyde dimethylacetal comprising reacting acetaldehyde and methanol in the presence of an acid catalyst in a part of a rectification tower while conducting rectification to withdraw the water by-produced from the bottom of the tower and to recover a distillate containing the acetic acid produced from the top of the tower.

Huels Aktiengesellschaft (Kaufhold and El-Chahawi, 1996)	An industrial process for preparing acetaldehyde diethyl acetal by reaction of acetaldehyde with ethanol in presence of an acid catalyst, and in the presence of an entrainer having a boiling point from 25° to 75°C.
Idemitsu Kosan Co. (Egwaw et al., 1997)	Method of production a polyvinyl ether which comprises polymerizing a vinyl ether compound in presence of a Lewis acid catalyst and a specific acetal or a method of producing a polyvinyl ether compound which comprises forming an acetal by reaction of a vinyl ether compound with a specific alcohol in presence of a Lewis acid catalyst, then adding the vinyl ether compound to the acetal and polymerizing the vinyl ether compound.
Hoechst Aktiengesellschaft (Hille et al., 1998)	Acetals are used as a mineral oil substitute, oil component or base oil in invert-emulsion drilling muds, emulsion drilling muds, engine oils, gearbox oils, lubricants oils and also metal-working fluids, coolants, cooling lubricants and hydraulic fluids. As compared with conventional mineral oils, acetals show good biodegradability and are less toxic.
Catalytic Distillation Technologies (Smith and Arganbright, 2000)	A process for production of acetals by contacting an alcohol and an aldehyde in a distillation reactor containing an acidic catalyst. The acetal is withdrawn from the top of the distillation column reactor and the water from the bottom. The alcohol and aldehyde are kept within the distillation reaction zone.
Clariant GmbH (Hille et al., 2000)	The direct use of liquid vegetable or animal oils without prior esterification as diesel fuel is possible with the simultaneous use of acetals.
Universidade do Porto (Rodrigues and Silva, 2009)	Industrial process for produce acetals using a simulated moving bed reactor. The separation of reaction products from reaction medium as they are formed, allows the enhancement of reactants conversion.

2.4. Process Intensification

Process intensification consists in the development of innovative frameworks and techniques that improve the chemical manufacture processes by decreasing equipment volume, energy consumption, or waste formation, and ultimately leading to cheaper, safer and sustainable technologies (Stankiewicz and Moulijn, 2000).

One of the basic and more important components of process intensification are the multifunctional reactors (*Figure 2.3*). The integration of the reaction and separation in a single unit presents the most important class of multifunctional reactors (Stankiewicz, 2003). The main advantage of these integrated systems is the possibility to shift the chemical equilibrium to the product side.
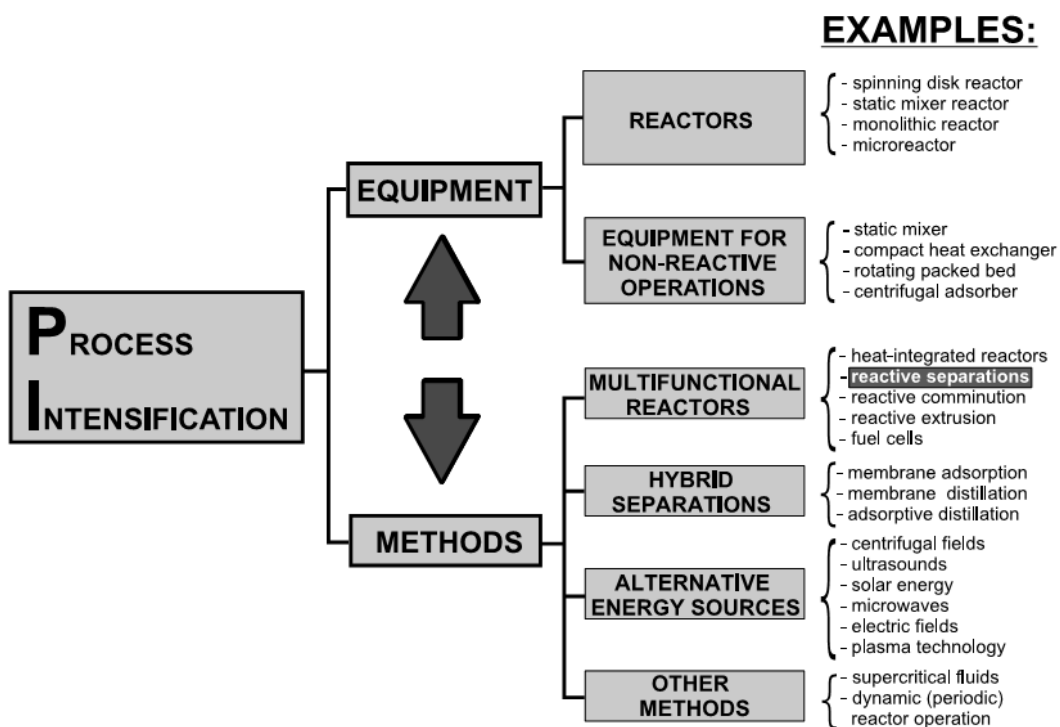
Figure 2.3. Process Intensification and its components (Stankiewicz, 2003)

Usually reaction and separation stages are carried out in separated equipment units, the conventional process consists of a reactor followed by a separation unit to remove the unconverted reactants from the desired product and recycle them to the reactor (*Figure 2.4*).
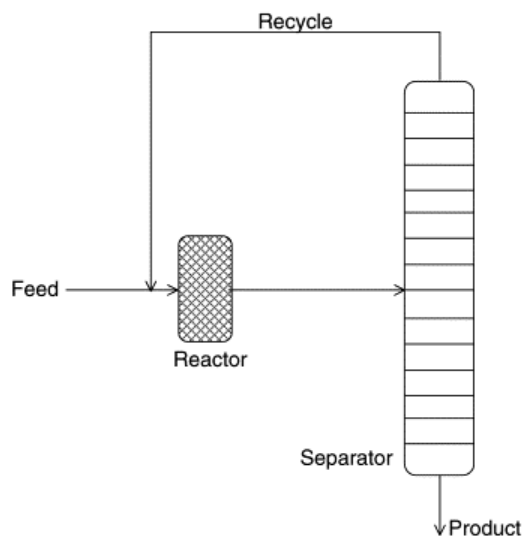
Figure 2.4. Conventional flowsheet of a process consisting of a reactor followed by a separation unit.

Using separated equipments to reaction and separation leads to an increase of equipment and energy costs. The processes of integrated reaction and separation seem to be the best alternative to the conventional process leading to a reduced investment cost and significant energy recovery and savings. However, the coupling of two or more process steps into a single unit reduces the degrees of freedom of the integrated process; therefore, the control is often much more complex than for non-integrated units.

2.4.1.   Reactive Distillation

Reactive distillation (RD) is a combination of separation and reaction in a single unit (*Figure 2.5*). The RD unit consists on a distillation column filled with a catalytically active packing. The reaction takes place on the catalyst while the reaction products are continuously separated by fraction as they are formed (displacing the chemical equilibrium towards products formation).
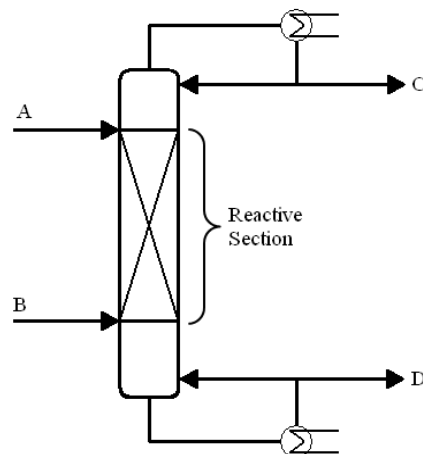
Figure 2.5. Typical Reactive Distillation Column ($T_{b,C} < T_{b,B} < T_{b,A} < T_{b,D}$)

The RD process presents some potential applications, such as (Sundmarcher and Kienle, 2003):

- Surpass equilibrium limitation;

- Achieve high selectivity towards a desired product;

- Achieve energy integration;

- Perform difficult separations;

The advantages of coupling chemical reaction with distillation have been exploited since 1921 (Bakhaus, 1921) for the production of esters. RD technology has been used to produce some oxygenated compounds, such as tert-butyl ether (MTBE) (Sneesby et al., 1998, Sundmacher et al., 1999), ethyl tert-butyl ether (ETBE) (Oudshoorn et al., 1999) and tertiary amyl methyl ether (TAME) (Oost and Hoffmann, 1996)

A prime example of RD is the methyl acetate process by Eastman Chemical (Siirola, 1995). The replacement of conventional reactors and separation units by an integrated reactive distillation column, allowed a significant reduction on equipment volume (*Figure 2.6*).
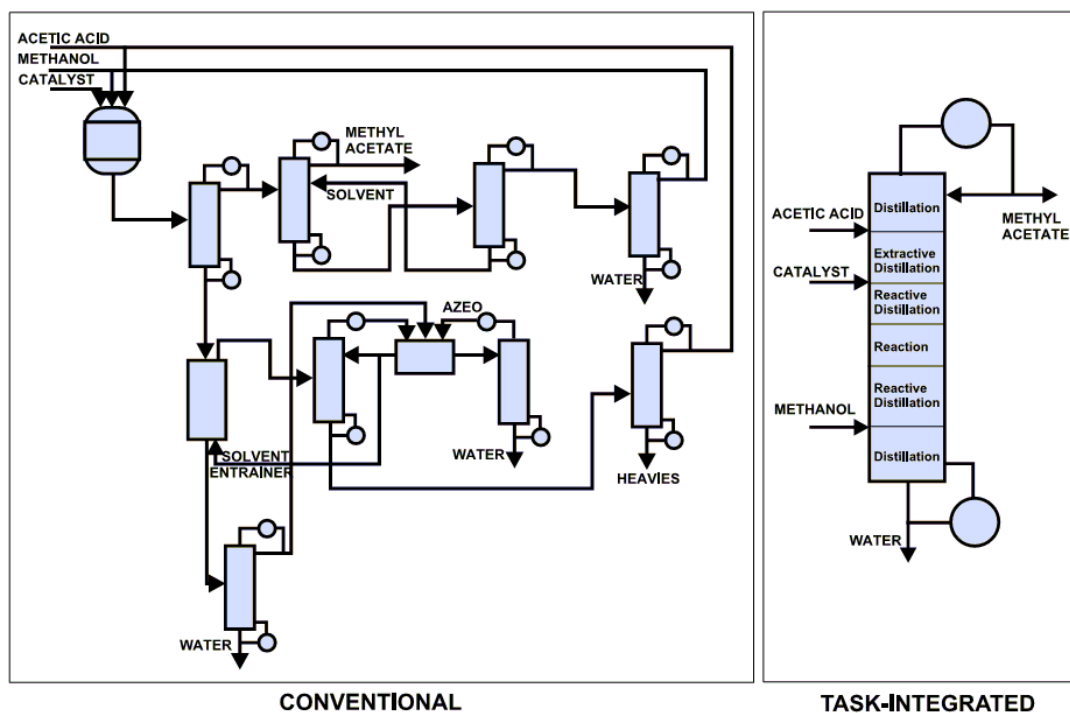
Figure 2.6. Plant integration in methyl acetate separative reactor by Eastman Chemical (Stankiewicz, 2003).

However the RD process presents some limitations and difficulties (Taylor and Krishna, 2000):

- Volatility constraints. The volatility of reagents and products must allow maintaining high concentrations of reactants and low concentrations of products in the reaction zone.

- Residence time requirement. If the reaction requires a long residence time, a large column size and large tray hold-ups will be needed and it may be more economic to use a reactor-separator configuration.

- Scale up to large flows. Due to liquid distribution problems in packed RD columns, it is difficult to design RD processes for very large flow rates.

- Process conditions mismatch. The optimum conditions of temperature and pressure for the distillation could be far from optimal for reaction and vice versa.

2.4.2. Adsorptive Reactors

An adsorptive reactor can be defined as a chromatographic system used to carry out a chemical reaction and simultaneously separate one or more of the reaction products formed. The adsorptive reactor comprises a stationary phase, which acts as adsorbent and catalyst, in continuous contact with a mobile phase; therefore, reaction and separation occur simultaneously inside the reactor. Since the reaction products are separated from reactants as they are formed, the adsorptive reactor concept applied to equilibrium limited reactions allows displacing the chemical equilibrium towards the product formation.

2.4.2.1.Fixed Bed Adsorptive Reactor.

The operation principle of a fixed bed adsorptive reactor for the reversible reaction $A \Leftrightarrow B + C$ is presented in *Figure 2.7*. A pulse of reactant A is injected into the fixed bed column and is converted to products B and C as it travels through the column. Due to different affinities with solid phase, C < A< B, the components travel through the column with different velocities, consequently, the components are separated from each other. The continuous separation of products from each other and from the reactant displaces the chemical equilibrium to the product side, increasing the reactant conversion.
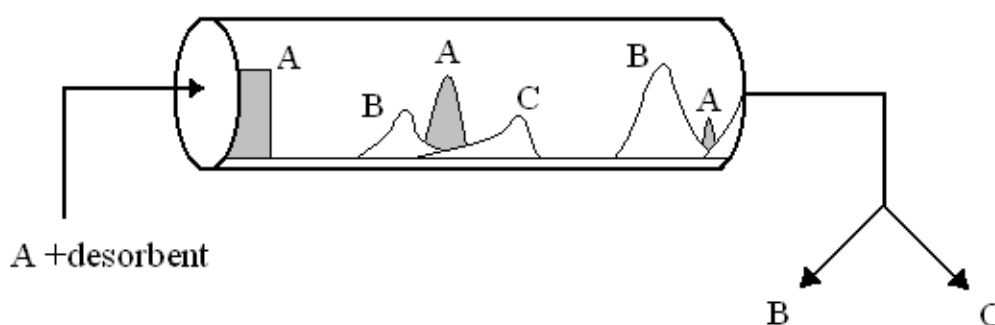
Figure 2.7. Fixed Bed adsorptive reaction operation principle.

Mazzotti and co-workers (Mazzotti et al., 1997) studied the dynamics of a fixed bed adsorptive reactor for the synthesis of ethyl acetate from ethanol and acetic acid in a laboratory-scale apparatus. The experimental results obtained were in good agreement with the results obtained with a fully predictive equilibrium dispersive model.

A study of the synthesis of the acetal 1,1-diethoxyethane in a fixed bed adsorptive reactor, packed with the ion-exchange resin Amberlyst-18, was published by Silva and Rodrigues (Silva and Rodrigues, 2002). The adsorption equilibrium was described by a multicomponent Langmuir type isotherm, obtained by performing adsorption experiments with binary nonreactive mixtures. The mathematical model of fixed bed adsorptive reactor, which includes axial dispersion, external and internal mass transfer resistance, multicomponent Langmuir isotherm and reaction kinetic obtained in a previous work (Silva and Rodrigues, 2001), was validated by the experimental results of reaction and regeneration steps. A similar study was performed for the synthesis of the acetal 1,1-dimethoxyethane in a fixed bed adsorptive reactor, packed with the ion-exchange resin Amberlyst-15 (Gandi et al., 2006).

Several published works report the use of a fixed bed adsorptive reactor to carry out some equilibrium limited reactions, such as synthesis of glycerol triacetate by the esterification of glycerol with acetic acid (Gelosa et al., 2003), esterification of acrylic acid with methanol (Ströhlein et al., 2006) and synthesis of ethyl lactate (Pereira et al., 2009).

The common discontinuous operation mode of the fixed bed adsorptive reactor, results in a low efficiency in utilizing the stationary phase inventory and in a large desorbent consumption leading to an excessive dilution of the final products (Lode et al., 2001). These problems can be overcome by transforming the fixed bed adsorptive reactor in a continuous process by applying concepts such rotating annular and simulated moving bed.

2.4.2.2. Continuous rotating annular adsorptive reactor.

In the rotating annular adsorptive reactor, the stationary phase is packed into the annular space formed by two concentric cylinders. The inlets of mobile phase are uniformly distributed along the annular bed entrance; the feed is introduced continuously at a fixed

point at the top of the bed. The components travel through the column with an axial movement due to the gravity, and because of the rotation of the annular bed relatively to the fixed feed inlet, also tangential. As a result of these two effects, the selectively adsorbed species take different helical paths through the annular bed and can be continuously collected at fixed locations (*Figure 2.8*).
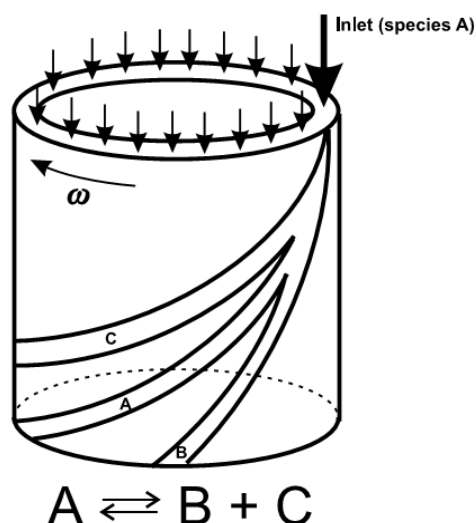
Figure 2.8. Scheme of rotating annular adsorptive reactor.

Martin in 1949 was the first to propose the concept of rotating annular chromatography (Martin, 1949). Several separation problems using the rotating annular chromatography concept have been studied (Bloomingburg et al., 1991, Byers et al., 1990, Reissner et al., 1997)

The application of the rotating annular chromatography concept to reactive systems, showed improvements on the reactants conversion due to the simultaneous reaction and selective separation of the products (Herbsthofer and Bart, 2003).

Sarmidi and Barker (Sarmidi and Barker, 1993) were the first to perform a biochemical reaction in a rotating annular adsorptive reactor. The inversion of sucrose to glucose and fructose using the enzyme invertase was performed. Results showed that for a feed concentration up to 55% w/w of sucrose, a complete conversion could be achieved. The simultaneous inversion and product separation allows overcoming problems associated with substrate inhibition.

However, some drawbacks arise from the use of the rotating annular adsorptive reactor; such as the large amount of desorbent needed to operate the process, which leads to a high dilution of the products, and a poor use of the packed solid phase. The development of continuous countercurrent processes seems to be a good alternative to overcome these drawbacks.

2.4.2.3.Countercurrent True Moving Bed Adsorptive Reactor.

In the countercurrent true moving bed adsorptive reactor operation, liquid and solid phases flow in opposite directions (*Figure 2.9*). Furthermore, liquid and adsorbent streams are continuously recycled: the liquid flowing out of section 4 is recycled to section 1, while the solid phase coming out of section 1 is recycled to section 4. The feed containing reactant A is injected in the middle of the system between section 2 and section 3. Inside the reactor, the reactant A is converted into the products B and C. The product B, the more adsorbed component, is carried by the solid phase and withdrawn from the extract port, and product C, the less adsorbed component, is carried by the liquid phase and is withdrawn from the raffinate port. This countercurrent arrangement maximizes the mass-transfer driving force, leading to a significant reduction in mobile and stationary phases consumptions.
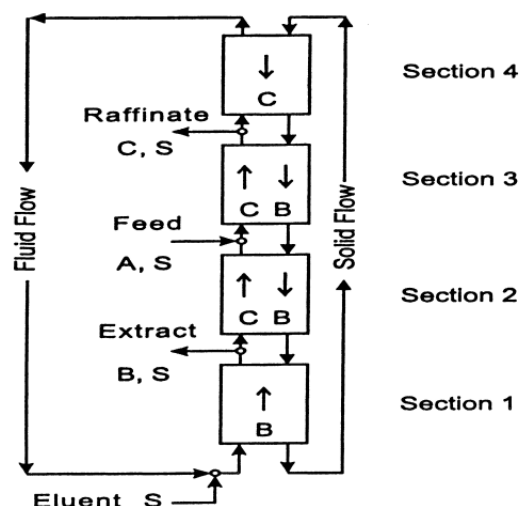
Figure 2.9. True countercurrent adsorptive reactor (Lode et al., 2001)

Petroulas and co-workers investigated theoretical and experimentally a countercurrent moving bed reactor (Petroulas et al., 1985). A reversible heterogeneous reaction (hydrogenation of mesitylene with excess hydrogen over a Pt on alumina catalyst), which takes place on catalyst particles, was considered. The countercurrent contact is promoted by passing the catalyst particles downward through an upcoming gas stream.

An experimental study of the hydrogenation of 1,3,5-trimethylbenzene vapor at 190ºC by Pt supported on 30-50 mesh Al_2O_3, conducted in a countercurrent moving bed reactor, showed that in some cases, the reactant conversion could significantly exceed the equilibrium conversion expected in a tubular reactor at the same temperature and feed conditions (Fish and Carr, 1989).

However, the operation of the countercurrent true moving bed reactor introduces problems concerning the movement of the solid phase. A uniform flow of both solid and liquid is difficult to achieve and also mechanical erosion of the adsorbent phase will occur. The simulated moving bed reactor, where there is no movement of solid phase, is an alternative to overcome these drawbacks.

2.4.2.4. Simulated Moving Bed Adsorptive Reactor

The Simulated moving bed concept allows to overcome the difficulties of the true moving bed reactor concerned with solid movement. In a simulated moving bed system the countercurrent flow of the solid phase is simulated by a periodical switch of the inlet and outlet streams in the direction of the liquid flow. The four sections of the simulated moving bed unit are defined by the position of the inlet (Feed and Eluent) and outlet (Extract and Raffinate) streams (*Figure 2.10*). Each section has different functions in the simulated moving bed reactor. The reactant A is fed to the unit and the reaction occurs in section 2 (between extract and feed streams) and section 3 (between the feed and raffinate streams) forming the products B and C. The more adsorbed product (C) is carried by the solid phase to the extract stream. The less adsorbed product (B) is transported with the liquid phase in the direction of the raffinate stream. In section 1, located between the eluent and extract streams, the solid phase is regenerated by desorption of the more retained product (C). In section 4, placed between the raffinate and eluent streams, the liquid phase is regenerated by adsorption of the less retained product (B).
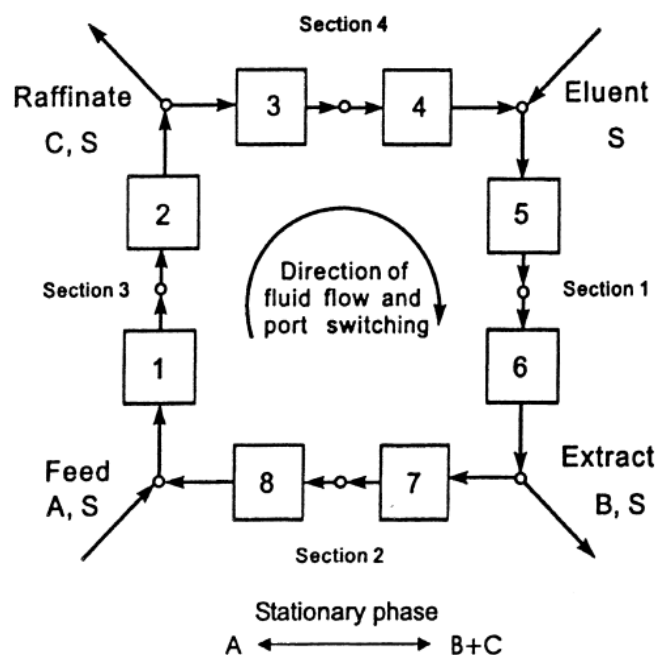
Figure 2.10. Scheme of a Simulated Moving Bed Adsorptive Reactor (Lode et al., 2001).

The simulated moving bed concept is an invention of Universal Oil Products Company and registered for the patent U.S. 2,985,589 (Broughton and Gerhold, 1961). The simulated moving bed technology was originally developed in the areas of petroleum refining and petrochemicals, and was designated as *Sorbex* process (Broughton, 1968, Broughton, 1984). Commercial Sorbex units were used to performe different kinds of separations (*Table 2.5*).

Table 2.5. Comercial Sorbex units (Gattuso et al., 1994).

Process	Separation
Parex	p-Xylene from C8 aromatics
Molex	n-Paraffins from branched and cyclic hydrocabons
Olex	Olefins from Paraffins
Cymex	p- or m-Cymene from cymene isomers
Cresex	p- or m-Cresol from cresol isomers
Sarex	Fructose from corn syrup
Citrex	Citric acid purification

One of the early applications of the simulated moving bed concept to liquid-phase reactive systems was in the production of a higher-fructose syrup, containing more than 50% of fructose, combining the selective adsorption of fructose and an immobilized glucose isomerase reaction (Hashimoto et al., 1983). Further works combining bioreaction and separation were carried out successfully using simulated moving bed adsorptive reactors, such as the inversion of sucrose to glucose and fructose (Azevedo and Rodrigues, 2001, Barker et al., 1992), hydrolysis of lactose and maltose (Shieh and Barker, 1995, Shieh and Barker, 1996) and lactosucrose production (Kawase et al., 2001).

Published works report the use of simulated moving bed reactors in esterification reactions to produce methyl acetate (Yu et al., 2003), ethyl acetate (Mazzotti et al., 1996), β-phenethyl acetate (Kawase et al., 1996), acrylic esters (Ströhlein et al., 2006) and ethyl lactate (Pereira et al., 2009).

In 2009 Rodrigues and Silva patented a novel process for the production of the acetals from the reaction between an alcohol and an aldehyde in a simulated moving bed adsorptive reactor packed with an acid solid catalyst (Rodrigues and Silva, 2009). Previous studies report the use of the simulated moving bed adsorptive reactor to produce the acetals 1,1-diethoxyethane (Silva and Rodrigues, 2005) and 1,1-dimethoxyethane (Pereira et al., 2008).

Recently, a new concept of integrating a simulated moving bed adsorptive reactor with hydrophilic membranes, called *PermSMBR*, was proposed (Silva et al., 2011). The principle of *PermSMBR* can be explained by considering a reversible reaction of the type $A + B \Leftrightarrow C + D$. The reactants A and B are injected into the system through the feed stream. Moreover, the reactant is also used as desorbent. The concept of simulated moving bed is applied by periodically switching the position of the inlet and outlet streams in the direction of liquid flow. Therefore, the less retained product (C) is collected on the raffinate stream and the more retained product (D) on the extract stream. Additionally, the product (D) is also removed by pervaporation (*Figure 2.11*). Simulated results showed that *PemSMBR* could present best performance than SMBR in terms of productivity and desorbent consumption, considering the same purity and conversion criteria.
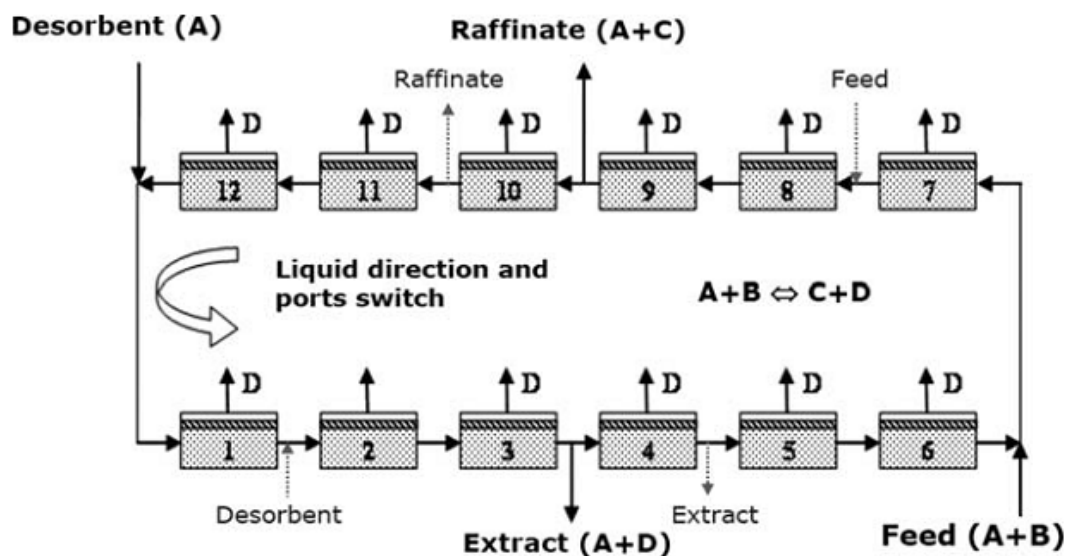
Figure 2.11. Schematic diagram of a PermSMBR unit (Silva et al., 2011).

2.5. Conclusions

This chapter presented some potential applications of the acetals, namely its use as oxygenated additive. Some important aspects of the acetals production were focused, such as the advantage of using heterogeneous catalysis and the use of reactive separation to overcome the limitations of chemical equilibrium on the reaction conversion.

2.6. References

Aizawa T., Nakamura H., Wakabayashi K., Kudo T. and Hasegawa H., "Process for Producing Acetaldehyde Dimethylacetal", U.S. Patent 5,362,918 (1994)

Andrade J., Arntz D., Kraft M. and Prescher G., "Method for Preparation of Acetals", U.S. Patent 4,579,979 (1986)

Azevedo D. C. S. and Rodrigues A. E., "Design methodology and operation of a simulated moving bed reactor for the inversion of sucrose and glucose-fructose separation", Chem. Eng. J., 82(1-3), 95-107 (2001)

Bakhaus A., "Continous process for the manufacture of esters", U.S. Patent 1,400,849 (1921)

Barbara P. and Liguori F., "Ion exchange resins: Catalyst recovery and recycle", Chem. Rev., 109(2), 515-529 (2009)

Barker P. E., Ganetsos G., Ajongwen J. and Akintoye A., "Bioreaction-separation on continuous chromatographic systems", Chem. Eng. J., 50(2), B23-B28 (1992)

Bloomingburg G. F., Bauer J. S., Carta G. and Byers C. H., "Continuous separation of proteins by annular chromatography", Ind. Chem. Eng. Res., 30(5), 1061-1067 (1991)

Bramwyche P. L., Mudgan M. and Satanley H. M., "Manufacture of Diethyl Acetal", U.S. Patent 2,519,540 (1950)

Broughton D. B. and Gerhold C. G., "Continuous Sorption Process Employing Fixed Bed of Sorbent and Moving Inlets and Outlets", U.S. Patent 2,985,589 (1961)

Broughton D. B., "Molex: Case History of a Process", Chem. Eng. Prog., 64(8), 60-65 (1968)

Broughton D. B., "Production-Scale Adsorptive Swparation of Liquid Mixtures by Simulated Moving-Bed Technology", Sep. Sci. Technol., 19(11-12), 723-736 (1984)

Byers C. H., Sisson W. G., DeCarli Ii J. P. and Carta G., "Sugar separations on a pilot scale by continuous annular chromatography", Biotechnol. Progr., 6(1), 13-20 (1990)

Caetano N. S., Loureiro J. M. and Rodrigues A. E., "MTBE synthesis catalysed by acid ion exchange resins: Kinetic studies and modeling of multiphase batch reactors", Chem. Eng. Sci., 49(24 PART A), 4589-4604 (1994)

Capeletti M. R., Balzano L., De La Puente G., Laborde M. and Sedran U., "Synthesis of acetal (1,1-diethoxyethane) from ethanol and acetaldehyde over acidic catalysts", Appl. Catal., A, 198(1-2), L1-L4 (2000)

Chopade S. P. and Sharma M. M., "Alkylation of methyl salicylate with isoamylene and isobutylene: Ion-exchange resins versus acid-treated clay catalysts", React. Funct. Polym., 28(3), 253-261 (1996)

Dürre P., "Biobutanol: An attractive biofuel", Biotechnol. J., 2(12), 1525-1534 (2007)

Egwaw T., Kawaguchi Y., Mogami K. and Shimizu N., "Method of producing a polyvinyl ether compound", U.S. Patent 5,616,812 (1997)

Filliger P. and Schneider J., "Health Costs due to Road Trafic-related Air Pollution", WHO report 1999, avaiable at internet: http://www.airimpacts.org/documents/local/who_pm10.pdf

Fish B. B. and Carr R. W., "An experimental study of the countercurrent moving-bed chromatographic reactor", Chem. Eng. Sci., 44(9), 1773-1783 (1989)

Frevel L. K. and Hedelund J. W., "Acetals and Process for Making the Same", U.S. Patent 2,691,684 (1950)

Frusteri F., Spadaro L., Beatrice C. and Guido C., "Oxygenated additives production for diesel engine emission improvement", Chem. Eng. J., 134(1-3), 239-245 (2007)

Gandi G. K., Silva V. M. T. M. and Rodrigues A. E., "Process development for dimethylacetal synthesis: Thermodynamics and reaction kinetics", Ind. Eng. Chem. Res., 44(19), 7287-7297 (2005)

Gandi G. K., Silva V. M. T. M. and Rodrigues A. E., "Synthesis of 1,1-dimethoxyethane in a fixed bed adsorptive reactor", Ind. Eng. Chem. Res., 45(6), 2032-2039 (2006)

Gandi G. K., Silva V. M. T. M. and Rodrigues A. E., "Acetaldehyde dimethylacetal synthesis with Smopex 101 fibres as catalyst/adsorbent", Chem. Eng. Sci., 62(4), 907-918 (2007)

Gattuso M. J., McCulloch B. and Priegnitz J. W., "Uop Sorbex Simulated Moving Bed Technology. A Cost Effective Route to Chiral Products"",Procinding of Chiral Europe'94, Nice, France, (1994)

Gelosa D., Ramaioli M., Valente G. and Morbidelli M., "Chromatographic Reactors: Esterification of Glycerol with Acetic Acid Using Acidic Polymeric Resins", Ind. Eng. Chem. Res., 42(25), 6536-6544 (2003)

Gomez M. F., Arrúa L. A. and Abello M. C., "Synthesis of 1,1-diethoxyethane using a continuous flow reactor: Catalyst deactivation and effect of feed purity and of solvent addition", J. Chem. Technol. Biotechnol., 79(4), 391-396 (2004)

Guinot H. M., "Process for the Manufacture of Acetal", U.S. Patent 1,850,836 (1932)

Hashimoto K., Adachi S., Noujima H. and Ueda Y., "A new process combining adsorption and enzyme reaction for producing higher-fructose syrup.", Biotech. Bioeng., 25(10), 2371-2393 (1983)

Herbsthofer R. and Bart H. J., "Influence of reaction kinetics on the performance of a chromatographic reactor", Chem. Eng. Technol., 26(8), 874-879 (2003)

Hille M. L., Wittikus H. F., Windhausen B. B., Scholz H. J. A. and Weinelt F. B., "Use of Acetals", U.S. Patent 5,759,963 (1998)

Hille M. L., Weinelt F. B., Wittikus H. and Reimann W., "Environmentally friendly diesel fuel", U.S. Patent 6,013,114 (2000)

Iwasaky H., Kitayama M. and Onishi T., "Process for producing acetals", U.S. Patent 5,792,876 (1998)

Kaufhold M. and El-Chahawi M., "Process for preparing acetaldehyde diethyl acetal", U.S. Patent 5,527,969 (1996)

Kawase M., Suzuki T. B., Inoue K., Yoshimoto K. and Hashimoto K., "Increased esterification conversion by application of the simulated moving-bed reactor", Chem. Eng. Sci., 51(11), 2971-2976 (1996)

Kawase M., Pilgrim A., Araki T. and Hashimoto K., "Lactosucrose production using a simulated moving bed reactor", Chem. Eng. Sci., 56(2), 453-458 (2001)

Kittellson D. B., "Measurement of Engine Exhaust Particle Size presentation", presentation given at University of California, Davis 17 Feveruary 2000, avaiable at internet: http://www.me.umn.edu/centers/mel/reports/dbkucdavis.pdf

Kohlpaintner C., Schulte M., Falbe J., Lappe P. and Weber J., "Aldehydes, aliphatic and araliphatic", in Ullmann's Encyclopedia of Industrial Chemistry,(Wiley-VCH, Weinheim, 1999). Eletronic Release

Kolah A. K., Mahajani S. M. and Sharma M. M., "Acetalization of formaldehyde with methanol in batch and continuous reactive distillation columns", Ind. Eng. Chem. Res., 35(10), 3707-3720 (1996)

Korff J. B., Fermery M. W. and Zimmermann J. W., "Process for the production of acetaldehyde diethyl acetal", U.S. Patent 4,278,819 (1981)

Lilja J., Murzin D. Y., Salmi T., Aumo J., Mäki-Arvela P. and Sundell M., "Esterification of different acids over heterogeneous and homogeneous catalysts and correlation with the taft equation", J. Mol. Catal. A: Chem., 182-183, 555-563 (2002)

Lode F., Houmard M., Migliorini C., Mazzotti M. and Morbidelli M., "Continuous reactive chromatography", Chem. Eng. Sci., 56(2), 269-291 (2001)

Ma Y., Wang Q. L., Yan H., Ji X. and Qiu Q., "Zeolite-catalyzed esterification I. Synthesis of acetates, benzoates and phthalates", Appl. Catal., A, 139(1-2), 51-57 (1996)

Mao W., Wang X., Wang H., Chang H., Zhang X. and Han J., "Thermodynamic and kinetic study of tert-amyl methyl ether (TAME) synthesis", Chem. Eng. Process., 47(5), 761-769 (2008)

Martin A. J. P., "Summarizing paper", Discussions of the Faraday Society, 7, 332-336 (1949)

Mazzotti M., Kruglov A., Neri B., Gelosa D. and Morbidelli M., "A continuous chromatographic reactor: SMBR", Chem. Eng. Sci., 51(10), 1827-1836 (1996)

Mazzotti M., Neri B., Gelosa D. and Morbidelli M., "Dynamics of a Chromatographic Reactor: Esterification Catalyzed by Acidic Resins", Ind. Eng. Chem. Res., 36(8), 3163-3172 (1997)

Mehlman M. A., "Methyl-tertiary-butyl-ether (MTBE) misclassified", Am. J. Ind. Med., 39(5), 505-508 (2001)

Miyamoto N., Ogawa H., Nurun N. M., Obata K. and Arima T., "Smokeless, Low NO, High Thermal Efficiency, and Low Noise Diesel Combustion with Oxygenated Agents as Main Fuel", Society of Automotive Engineers publications SAE-98506, (1998)

Oost C. and Hoffmann U., "The synthesis of tertiary amyl methyl ether (TAME): Microkinetics of the reactions", Chem. Eng. Sci., 51(3), 329-340 (1996)

Oudshoorn O. L., Janissen M., Van Kooten W. E. J., Jansen J. C., Van Bekkum H., Van den Bleek C. M. and Calis H. P. A., "A novel structured catalyst packing for catalytic distillation of ETBE", Chem. Eng. Sci., 54(10), 1413-1418 (1999)

Pereira C. S. M., Gomes P. S., Gandi G. K., Silva V. M. T. M. and Rodrigues A. E., "Multifunctional reactor for the synthesis of dimethylacetal", Ind. Eng. Chem. Res., 47(10), 3515-3524 (2008)

Pereira C. S. M., Silva V. M. T. M. and Rodrigues A. E., "Fixed bed adsorptlve reactor for ethyl lactate synthesis: Experiments, modelling, and simulation", Sep. Sci. Technol., 44(12), 2721-2749 (2009)

Pereira C. S. M., Zabka M., Silva V. M. T. M. and Rodrigues A. E., "A novel process for the ethyl lactate synthesis in a simulated moving bed reactor (SMBR)", Chem. Eng. Sci., 64(14), 3301-3310 (2009)

Petroulas T., Aris R. and Carr Jr R. W., "Analysis and performance of a countercurrent moving-bed chromatographic reactor", Chem. Eng. Sci., 40(12), 2233-2240 (1985)

Ramalinga K., Vijayalakshmi P. and Kaimal T. N. B., "A mild and efficient method for esterification and transesterification catalyzed by iodine", Tetrahedron Lett., 43(5), 879-882 (2002)

Rasa E., Chapman S. W., Bekins B. A., Fogg G. E., Scow K. M. and MacKay D. M., "Role of back diffusion and biodegradation reactions in sustaining an MTBE/TBA plume in alluvial media", J. Contam. Hydrol., 126(3-4), 235-247 (2011)

Reissner K., Prior A., Wolfgang J., Bart H. J. and Byers C. H., "Preparative desalting of bovine serum albumin by continuous annular chromatography", J. Chrom. A., 763(1-2), 49-56 (1997)

Rodrigues A. E. and Silva V. M. T. M., "Industrial Process for Acetals Producing in Simulated Moving Bed Reactor", U.S. Patent 7,488,851 (2009)

Sarmidi M. R. and Barker P. E., "Simultaneous biochemical reaction and separation in a rotating annular chromatograph", Chem. Eng. Sci., 48(14), 2615-2623 (1993)

Shieh M. T. and Barker P. E., "Saccharification of modified starch to maltose in a semi-continuous counter-current chromatographic reactor-separator (SCCR-S)", J. Chem. Technol. Biotechnol., 63(2), 125-134 (1995)

Shieh M. T. and Barker P. E., "Combined bioreaction and separation in a simulated counter-current chromatographic bioreactor-separator for the hydrolysis of lactose", J. Chem. Technol. Biotechnol., 66(3), 265-278 (1996)

Siirola J. J., "An industrial perpective on process synthesis", AIChE. Symp. Ser., 91(304), 222-233 (1995)

Silva V. M. T. M. and Rodrigues A. E., "Synthesis of diethylacetal: Thermodynamic and kinetic studies", Chem. Eng. Sci., 56(4), 1255-1263 (2001)

Silva V. M. T. M. and Rodrigues A. E., "Dynamics of a fixed-bed adsorptive reactor for synthesis of diethylacetal", AIChE J., 48(3), 625-634 (2002)

Silva V. M. T. M. and Rodrigues A. E., "Novel process for diethylacetal synthesis", AIChE Journal, 51(10), 2752-2768 (2005)

Silva V. M. T. M. and Rodrigues A. E., "Kinetic studies in a batch reactor using ion exchange resin catalysts for oxygenates production: Role of mass transfer mechanisms", Chem. Eng. Sci., 61(2), 316-331 (2006)

Silva V. M. T. M., Pereira C. S. M. and Rodrigues A. E., "PermSMBR-A new hybrid technology: Application on green solvent and biofuel production", AlChE J., 57(7), 1840-1851 (2011)

Smith J. A. and Arganbright R. P., "Process for making acetals", U.S. Patent 6,015,875 (2000)

Sneesby M. G., Tadé M. O. and Smith T. N., "Multiplicity and pseudo-multiplicity in MTBE and ETBE reactive distillation", Chem. Eng. Res. Des, 76(A4), 525-531 (1998)

Stankiewicz A., "Reactive separations for process intensification: An industrial perspective", Chem. Eng. Process., 42(3), 137-144 (2003)

Stankiewicz A. I. and Moulijn J. A., "Process intensification: Transforming chemical engineering", Chem. Eng. Prog., 96(1), 22-33 (2000)

Ströhlein G., Assunção Y., Dube N., Bardow A., Mazzotti M. and Morbidelli M., "Esterification of acrylic acid with methanol by reactive chromatography: Experiments and simulations", Chem. Eng. Sci., 61(16), 5296-5306 (2006)

Sundmacher K., Uhde G. and Hoffmann U., "Multiple reactions in catalytic distillation processes for the production of the fuel oxygenates MTBE and TAME: Analysis by rigorous model and experimental validation", Chem. Eng. Sci., 54(13-14), 2839-2847 (1999)

Sundmarcher K. and Kienle A., "Reactive distillation: Status and future directions", Wiley-VCH, Weinheim (2003)

Tanaka K., Yoshikawa R., Ying C., Kita H. and Okamoto K. I., "Application of zeolite T membrane to vapor-permeation-aided esterification of lactic acid with ethanol", Chem. Eng. Sci., 57(9), 1577-1584 (2002)

Taylor R. and Krishna R., "Modelling reactive distillation", Chem. Eng. Sci., 55(22), 5183-5229 (2000)

Umar M., Saleemi A. R. and Qaiser S., "Synthesis of ethyl tert-butyl ether with tert-butyl alcohol and ethanol on various ion exchange resin catalysts", Catal. Commun., 9(5), 721-727 (2008)

Vilarinho Ferreira M. M. and Loureiro J. M., "Synthesis of TAME: Kinetics in batch reactor and thermodynamic study", Chemie-Ingenieur-Technik, 73(6), 684-685 (2001)

Weizmann C., "Process for carrying out condensation reactions", U.S. Patent 2,474,175 (1949)

Yu W., Hidajat K. and Ray A. K., "Modeling, Simulation, and Experimental Study of a Simulated Moving Bed Reactor for the Synthesis of Methyl Acetate Ester", Ind. Eng. Chem. Res., 42(26), 6743-6754 (2003)

Ziyang Z., Hidajat K. and Ray A. K., "Determination of adsorption and kinetic parameters for methyl tert-butyl ether synthesis from tert-butyl alcohol and methanol", J. Catal., 200(2), 209-221 (2001)

3. Thermodynamic Equilibrium and Reaction Kinetics in a Batch Reactor.

The synthesis of 1,1-dibutoxyethane (DBE) or acetaldehyde dibutylacetal was studied in a batch reactor by reacting 1-butanol and acetaldehyde in liquid phase, using Amberlyst-15 as catalyst. The reaction equilibrium constant was experimentally determined in the temperature range 20ºC-40ºC at 6 atm, $K_a=0.00959\exp[1755.3/T(K)]$. The standard properties of reaction at 298.15 K were estimated: $\Delta H^0=-14.59$ kJ mol^{-1}, $\Delta G^0= -3.07$ kJ mol^{-1}, $\Delta S^0=-38.64$ J mol^{-1} K^{-1}. Kinetic experiments were performed in the temperature range 10ºC-50ºC at 6 atm. A two-parameter kinetic law based on a Langmuir-Hinshelwood rate expression, using activity coefficients from the UNIFAC method, was used. The kinetic parameters are $k_c =2.39\times10^9\exp[-6200.9/T(K)]$ (mol g$_{cat}^{-1}$ min^{-1}) and $K_{s,D}=2.25\times10^{-4}\exp[3303.1/T(K)]$. The activation energy of reaction is 51.55 kJ mol^{-1}. This work is an important step for the further implementation of an integrated reaction-separation process, such as simulated moving bed reactor (SMBR).

3.1. Introduction

The acetal 1,1-dibutoxyethane (DBE) is produced by the acid-catalyzed reaction between 1-butanol and acetaldehyde, according to the following stoichiometry:

$$2\ butanol\ (A)\ +\ acetaldehyde\ (B)\ \overset{H^+}{\Leftrightarrow}\ DBE\ (C)\ +\ water\ (D)$$
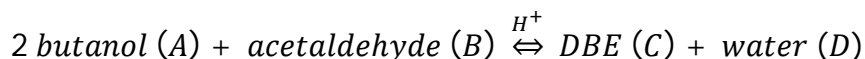
The acetalization reaction involves the formation of a hemiacetal as intermediate compound and water as by-product. This is a reversible reaction; therefore, the conversion of reactants is limited by the chemical equilibrium. In order to displace the equilibrium towards product formation, one of the products from the reaction mixture should be continuously removed.

The synthesis of oxygenated compounds, like acetals, is typically carried out with strong liquid inorganic acid as homogeneous catalysts; however, in spite of his high catalytic activity, the homogenous catalysis presents several drawbacks, such as their corrosive nature, the existence of side reactions, and the fact that the catalyst cannot be easily separated from the reaction mixture (Kolah et al., 2007, Lilja et al., 2002). Therefore, the use of solid-acid catalysts, such as sulfatated zirconia, clays, ion-exchange resins, zeolites and zeotypes appear as a good alternative to homogeneous catalysis (Yadav and Pujari, 1999). Previous works report the use of heterogeneous catalysts for the synthesis of the acetal 1,1-diethoxyethane using Amberlyst-15 and -18 (Silva and Rodrigues, 2001, Silva and Rodrigues, 2005) and the acetal 1,1-dimethoxyethane using Amberlyst-15, a Y-type Zeolite, and SMORPEX 101 fibers (Gandi et al., 2005, Gandi et al., 2007).

Amberlyst-15 proved to be an efficient catalyst for the acetalization of butanol with heptanal (Rat et al., 2008) and formaldehyde (Mahajani et al., 1995); however, it was verified that side reactions are influenced by the type of ion-exchange resins in the esterification of n-butanol with acetic acid at 100-120 °C. The observed side reaction products using Purolite CT 269 (mono-sulfonated) and Amberlyst 48 (bi-sulfonated) were isomers of butene, di-n-butyl ether, sec-butyl-n-butyl ether as well as sec-butanol

and sec-butyl acetate; whereas with Amberlyst-46 (surface-sulfonated) side reactions were almost negligible (Blagov et al., 2006).

In this work, the synthesis of the acetal 1,1-dibutoxyethane from butanol and acetaldehyde by means of a liquid phase reaction catalyzed by Amberlyst-15 is studied in order to obtain thermodynamic and kinetic data for further implementation of the integrated reaction-separation processes, fixed-bed and simulated moving bed reactors (SMBR). Since the reaction is equilibrium-limited; the use of an integrated reaction-separation process, such as SMBR, allows the displacement of chemical equilibrium towards products formation (Silva and Rodrigues, 2005).

3.2. Experimental Section

3.2.1. Experimental Set-Up

The experiments were carried out in a glass-jacketed 1 dm^3 autoclave (Büchi, Switzerland), operating in a batch mode, mechanically stirred, equipped with pressure and temperature sensors and with a blow-off valve. The temperature was controlled by thermostated water (Lauda, Germany) that flows through the jacket. To maintain the reacting mixture in liquid phase over the whole temperature range, the reactor was pressurized with helium *Figure 3.1* shows a schematic representation of the experimental set-up. Dry catalyst is placed in a basket at the top of the stirrer shaft, and falls down in the reactant solution at the beginning of agitation, and therefore the time zero for the reaction is well defined. One of the outlets of the reactor was connected to the liquid sampling valve (Valco, USA), which injects 0.1 µL of pressurized liquid to a gas chromatograph.
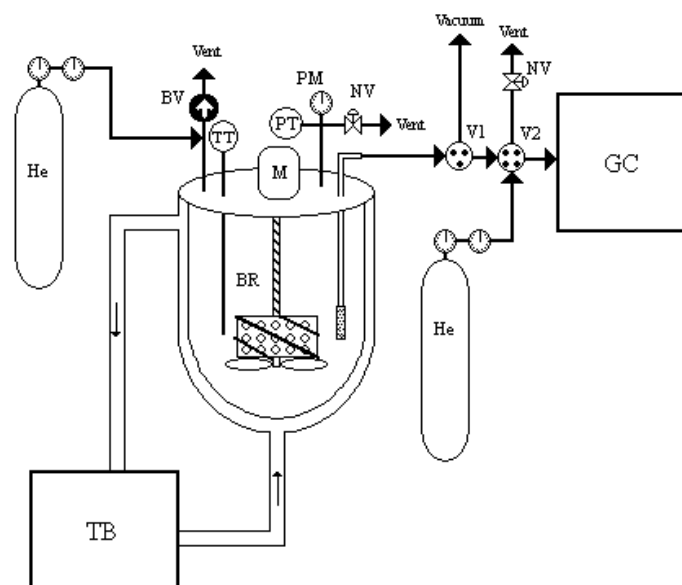
Figure 3.1. . Experimental set-up for kinetic studies. BR-batch reactor; M-motor; TT-temperature sensor; PT-pressure sensor; PM-manometer; BV-blow-off valve; V1-sampling valve; V2-injection valve; NV-needle valve; GC-gas chromatograph; TB-thermostatic bath.

A sampling valve together with a three-way valve controls the sampling, analysis and line cleaning, as shown in *Figure 3.2*.
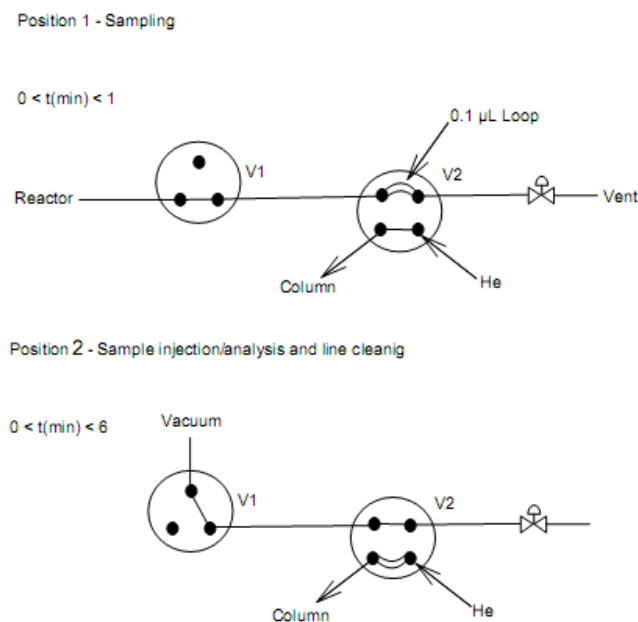
Figure 3.2. Valves scheme for sampling analysis and line cleaning control.

At the beginning of a sampling cycle the reactor line is open and the pressurized liquid flows through the tube (1/16'') until it fills the loop. After 1 minute, to ensure that the loop is completely full, the reactor line is closed and the sampling valve switches the position to inject the sample, the sample is carried with helium to the GC injector, and simultaneously, the sampling line is cleaned by means of vacuum.

3.2.2. Chemicals and Catalyst

The reactants used were 1-butanol (>99.9% pure) and acetaldehyde (>99.5 % pure) (Sigma-Aldrich, UK). The catalyst used was the ion-exchange resin Amberlyst-15 (Rohm and Haas, France). Some of the chemical and physical properties of Amberlyst-15 are presented i *Table 3.1*.

Table 3.1. Chemical and physical properties of Amberlyst 15 resin.

Properties	Amberlyst-15
Moisture content	52-57 %
Shipping weight	770 g/L
Particle size	300-1200 µm
Concentration of acid sites	1.7 meq/mL
Surface area	53 m^2/g
Porosity	0.36
Average pore diameter	24 nm

3.2.3. Analytical Method

The samples were analyzed in a gas chromatograph (Chrompack 9100, Netherlands) and the compounds were separated in a fused silica capillary column (Chrompack CP-Wax 57 CB), 25m x 0.53 mm ID, df=22.0 µm using a thermal conductivity detector (TCD 903 A) for peak detection. The operating conditions for the sample analysis are presented in *Table 3.2*. The column temperature was programmed with a 5 min initial hold at 75ºC, followed by a 25 ºC/min ramp up to 100 ºC and held for 1.5 min. The

carrier gas used was Helium N50. *Figure 3.3* presents a chromatogram obtained at *Table 3.2* conditions.

Table 3.2. Operating conditions used in GC analysis

Injector temperature	150ºC
Detector temperature	250ºC
Column pressure drop	80 kPa
Column flowrate at 50ºC	10.5 mL/min
Make-up flowrate	9.5 mL/min
Reference flowrate	20 mL/min
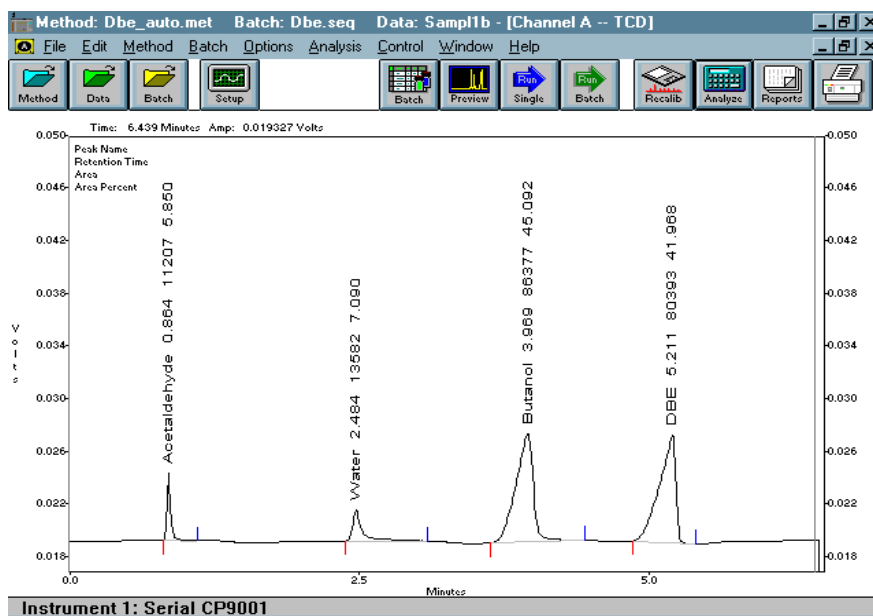
Figure 3.3. Chromatogram obtained at operating conditions of Table 3.2.

The number of moles of component i injected (n_i) is related with peak area of component i (A_i) by the response factor (f_i):

$$n_i = f_i A_i \tag{3.1}$$

It was used reproducibility criteria based on peak area:

$$R.C. (\%) = \frac{\sigma_A}{\bar{A}} \times 100 \ \leq 5\% \tag{3.2}$$

where $\bar{A}$ is the average area and σ_A the standard deviation.

The response factor for each component (*Table 3.3*) was obtained by injecting several volumes of pure component, at given temperature (Appendix B).

Table 3.3. Response factor and retention time

Component	Retention time (min)	Response factor (μmol/u.a.)
Acetaldehyde	0.864	8.4839
Water	2.484	16.629
Butanol	3.969	5.4676
DBE	5.211	2.5029

3.3. Thermodynamic Equilibrium Constant

The equilibrium constants based on activities (Sá Gomes et al., 2007) as shown in *Equation 3.3* were calculated for different temperatures (in the range of 293.15K-323.15K), at 6 atm, at the stoichiometric initial molar ratio of reactants 1-butanol/acetaldehyde ($r_{A/B}$=2.2), the total volume of the reactants was 530 mL and the mass of catalyst 1.8 g. It was ensured that for these conditions, the amount of adsorbed species are negligible and there was only one liquid phase in spite of the fact that water and 1-butanol are only partially miscible; therefore, the equilibrium composition is only

related to thermodynamic reaction equilibrium. Moreover, it were not detected any by-product.

$$K_a = \frac{a_C a_D}{a_A^2 a_B} = \frac{x_C x_D}{x_A^2 x_B} \times \frac{\gamma_C \gamma_D}{\gamma_A^2 \gamma_B} = K_X K_\gamma \tag{3.3}$$

Table 3.4 presents the experimental equilibrium composition and the calculated equilibrium constants.

Table 3.4. Experimental Equilibrium Compositions and Equilibrium Constants.

	T(K)			
	293.15	303.15	313.15	323.15
x_A	0.40720	0.42078	0.43979	0.45274
x_B	0.16090	0.16742	0.17362	0.17915
x_C	0.21595	0.20590	0.19330	0.18406
x_D	0.21595	0.20590	0.19330	0.18406
K_X	1.74794	1.43165	1.11269	0.92256
γ_A	1.07895	1.08250	1.08363	1.08343
γ_B	1.14948	1.14763	1.14400	1.14096
γ_C	1.38198	1.38971	1.40227	1.40939
γ_D	2.11094	2.16536	2.21667	2.27337
K_γ	2.17916	2.23767	2.31391	2.39235
$K_a = K_x.K_\gamma$	3.80905	3.20023	2.57467	2.20709

Experimental conditions: w_{cat}= 1.8 g, V= 530 mL, P= 6 atm, $r_{A/B}$=2.2 and 0.5 <d_p<0.6 mm.

The equilibrium constants were calculated from the experimentally measured equilibrium composition and activity coefficients of species (γ_i) calculated by the

UNIFAC method (Fredenslund et al., 1977). The parameters used are presented in *Table 3.5* and *Table 3.6*.

Table 3.5. Relative Molecular Volume and Surface Parameters of a Pure Species (Reid et al., 1987)

Molecule(i)	Group Identification			$\upsilon_k^{(i)}$	R_k	Q_k
	Name	No. Main	No. Sec			
1-Butanol	CH_3	1	1	1	0.9011	0.848
	CH_2	1	2	3	0.6744	0.540
	OH	5	15	1	1.0000	1.200
Acetaldehyde	CH_3	1	1	1	0.9011	0.848
	CHO	10	21	1	0.9980	0.948
DBE	CH_3	1	1	3	0.9011	0.848
	CH_2	1	2	4	0.6744	0.540
	CH	1	3	1	0.4469	0.228
	CH_2O	13	26	2	0.9183	0.780
Water	H_2O	7	17	1	0.8200	1.400

Table 3.6. Interaction Parameters

$a_{m,n}$	1	5	7	10	13
1	0	986.5	1318	677	251.5
5	156.4	0	353.5	-203.6	28.06
7	300	-229.1	0	-116	540.5
10	505.7	529	480.8	0	304.1
13	83.36	237.7	-314.7	-7.838	0

At equilibrium the standard free energy change is related to the equilibrium constant by:

$$\Delta G^0 = -RT \ln K_a \qquad (3.4)$$

By definition the standard free energy change is related to standard enthalpy and entropy changes by:

$$\Delta G^0 = \Delta H^0 - T\Delta S^0 \qquad (3.5)$$

Therefore, temperature dependency of the equilibrium constant is given by:

$$\ln K_a = \frac{\Delta S^0}{R} - \frac{\Delta H^0}{R}\frac{1}{T} \qquad (3.6)$$

The standard free energy, enthalpy and entropy changes for this reaction can be estimated by fitting experimental values of ln K_a *vs* 1/T (*Figure 3.4*). From the slope, it is concluded that the reaction is slightly exothermic with ΔH^0=-14593.6 J mol⁻¹, and from the intercept ΔS^0=-38.6 J mol⁻¹ K⁻¹; and ΔG^0= -3074.1 J mol⁻¹ calculated from *Equation 3.5*.
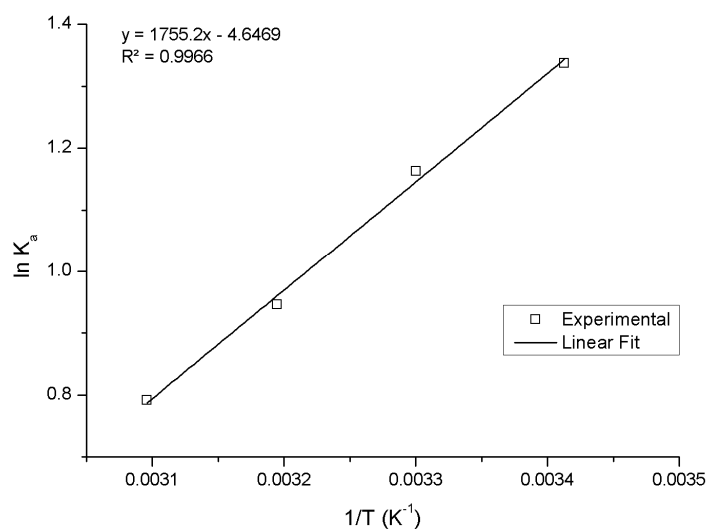
Figure 3.4. Linearization of the experimental equilibrium constants.

3.4. Kinetic Results

The influence of external mass transfer resistance was studied by performing experiments at different stirring speeds. The external mass transfer resistance is eliminated for a stirring speed above 800 rpm. Therefore, all further experiments were carried out at 800 rpm.

3.4.1. Effect of the Particle Size

The determination of concentration of acidic sites of Amberlyst-15 resin for different particle diameters (Xu and Chuang, 1997) shows that the concentration of acid sites is independent of particle size; therefore, any difference in reaction kinetics for different particle sizes can only be attributed to the internal mass transfer resistance.

Experiments carried out with different particle sizes of catalyst show internal diffusion limitations for experiments with particle diameters greater than 0.5 mm (*Figure 3.5*). For diameters of particle below 0.5 mm it is not possible to conclude about internal diffusion limitations. Therefore, the kinetic parameters will be estimated by using a detailed model accounting for intraparticle diffusion.
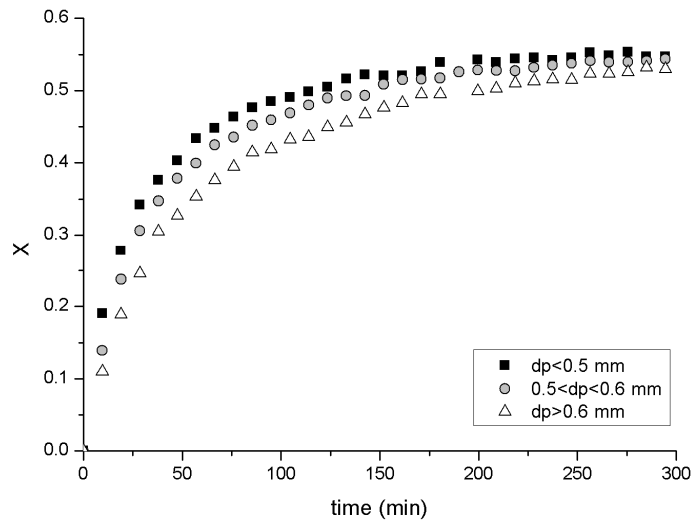
Figure 3.5. Effect of particle size on the conversion of acetaldehyde history: T=293.15 K, P=6 atm, $r_{A/B}$=2.2, w_{cat}=1.8 g, V= 530 mL.

3.4.2. Mass of Catalyst Effect

The conversion increases by increasing the mass of catalyst (*Figure 3.6)* for the same experimental conditions.
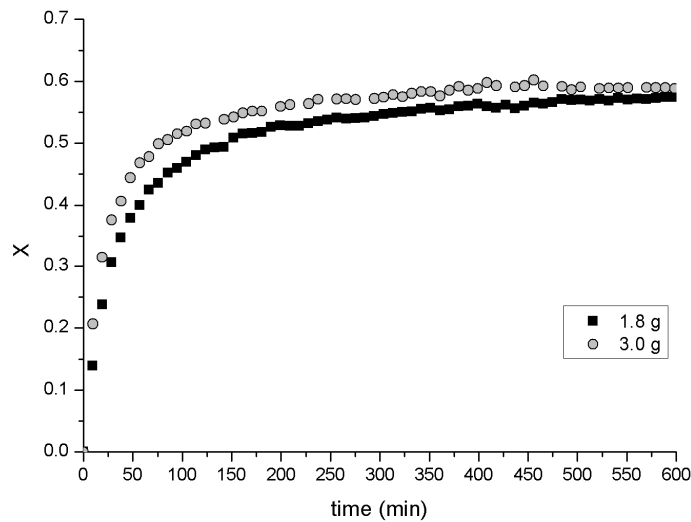
Figure 3.6. Effect of mass of catalyst on the conversion of acetaldehyde history: T=293.15 K, P=6 atm, $r_{A/B=}$2.2, V= 530 mL, 0.5 <d_p<0.6 mm.

The maximum reaction rate occurs at the beginning of the reaction, where the slope of the plot conversion versus time is higher. The initial slopes for catalyst masses of 1,8 and 3.0 g are 0.0176 and 0.0296 min^{-1}, respectively. The ratio between the catalyst mass is 3.0/1.8=1.67, and the ratio between the initial slopes is 0.0296/0.0176=1.68. These results show that the initial reaction rate increased in the same proportion of the mass of catalyst.

3.4.3. Effect of the Temperature

Experiments performed at different temperatures show that the rate of reaction increases with temperature; however, the equilibrium conversion of acetaldehyde decreases due to the exothermic nature of the reaction (*Figure 3.7*).
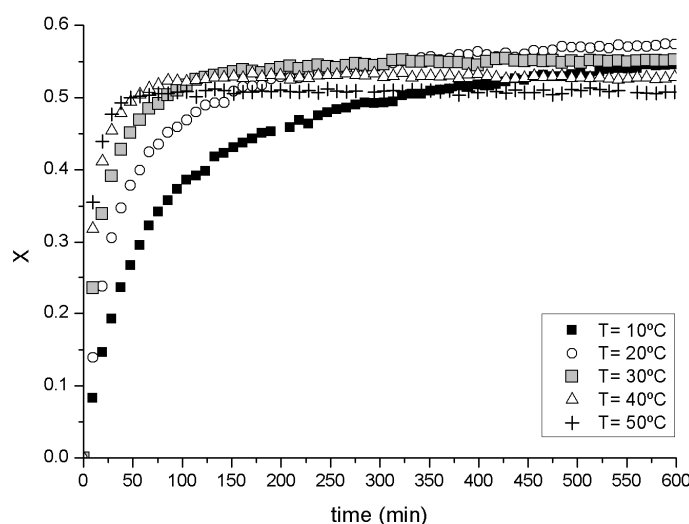
Figure 3.7. Effect of temperature on the conversion of acetaldehyde history: P=6 atm, $r_{A/B}$=2.2, w_{cat}=1.8 g, V= 530 mL, 0.5 <d_p<0.6 mm.

For batch or fixed bed reactors, this could be an issue, since conversion in equilibrium decays from about 57% at 20 ºC to about 48% at 50 ºC. However, in the perspective of process intensification by means of a reactive separation such as the SMBR technology, it is more important to enhance the kinetics of reaction since equilibrium is displaced by products removal, being possible to achieve complete depletion of reactants. At higher temperatures, the mixture viscosity decreases, benefiting also the mass transfer mechanisms and reducing pressure drops in the bed. Moreover, for multicomponent

adsorption equilibria, the effect of temperature on the selectivity of the resin will play a critical role. For the ethyl lactate synthesis, selectivity of water/ethyl lactate decreases by a factor of 3.5 (from 86.7 to 24.8) when increasing the temperature from 20 to 50 ºC (Pereira et al., 2009).

3.4.4. Effect of the Initial Molar Ratio of the Reactants

It is known that one way of increasing conversion is to use excess of one reactant, in order to shift equilibrium towards product formation. However, analyzing the catalyst productivity, for the same catalyst loading (mass of resin per volume of reactants) the maximum quantity of DBE is achieved for the stoichiometric ratio of reactants ($r_{A/B}=2$), as shown in *Figure 3.8*. Moreover, the initial molar ratio ($r_{A/B}$) does not affect significantly the rate of reaction; and therefore, there is no need to operate at molar ratio of reactants far from the stoichiometric one.
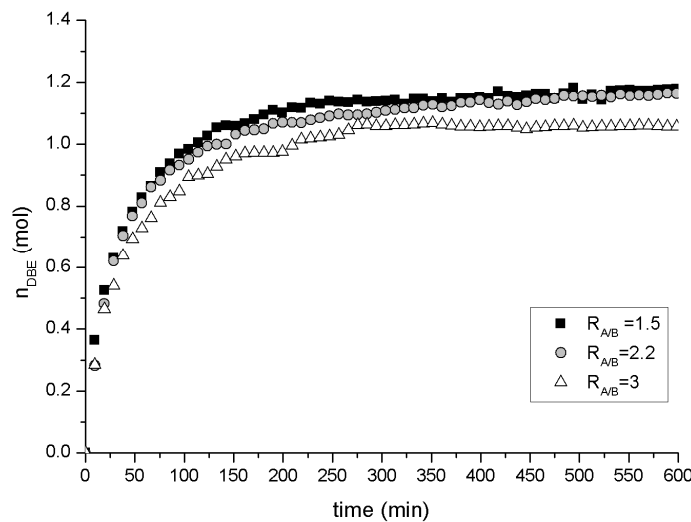
Figure 3.8. Effect of initial molar ratio of reactants on the number of moles of DBE history: T=293.15 K, P=6 atm, w_{cat}=1.8 g, V= 530 mL, 0.5 <d_p<0.6 mm.

3.5. Batch Reactor Model

As shown in *Figure 3.5* for particle diameters greater than 0.5 mm the kinetics of reaction is affected by internal mass transfer resistances; for smaller diameters particles it is not possible to conclude about internal mass transfer resistances. Therefore, it will

be used an isothermally operated batch reactor model that considers diffusion of components inside the catalyst particle (Silva and Rodrigues, 2005). In this work surface diffusion was neglected; however, Dogu et al. (Dogu et al., 2003) showed that although molecular diffusion is the main transport mechanism in macropores, surface diffusion could also have a significant contribution. From our knowledge, this behaviour was not reported or noticed for esterification or acetalization reactions. Therefore, surface diffusion was not considered in this work.

Mass balance in the bulk fluid:

$$\frac{dC_{b,j}}{dt} = -\frac{A_p}{V_{liq}} D_j \left.\frac{\partial C_{p,j}}{\partial r}\right|_{r=r_p} \qquad (j = A, B, C \text{ and } D) \qquad (3.7)$$

with,

$$A_p = \frac{3}{r_p} V_p \qquad (3.8)$$

where $C_{b,j}$ is the bulk concentration of component j, $C_{p,j}$ is the concentration of component j inside particle pores, A_p is the external area between fluid and particle, V_{liq} is the volume of liquid inside the reactor, r_p is the particle radius, V_p is the total volume of particles, r is the particle radial position and t the time coordinate. The effective diffusivity D_j of the compound j is given by:

$$D_j = \frac{\varepsilon_p D_{j,m}}{\tau_p} \qquad (3.9)$$

where $D_{j,m}$ is the molecular diffusivity of compound j in the multicomponent mixture and τ_p is the tortuosity of ion exchange resin. The coefficients $D_{j,m}$ were estimated

similar way as performed to the system of ethyl lactate synthesis, once one reactant (lactic acid solution) has high viscosity, similarly to this case, where butanol is very viscous too (Pereira et al., 2009). Different values of τ_p, such as 1.3 (Yu et al., 2004), 2 (Silva, 2003) and 4.9 (Oktar et al., 1999) are reported in literature for the calculation of effective diffusivity in Amberlyst-15. Estimations of tortuosity were made using the correlations given by Wakao and Smith (Wakao and Smith, 1962) ($\tau_p = 1/\varepsilon_p$) and Suzuki and Smith (Suzuki and Smith, 1972) ($\tau_p = \varepsilon_p + 1.5(1 - \varepsilon_p)$); the values obtained $\varepsilon_p = 0.36$ were 2.78 and 1.32, respectively. In this work the tortuosity used was 2, i.e., the mean between the estimated values.

The infinite dilution molecular diffusivities were estimated by the Scheibel correlation which modified the Wilke-Chang equation in order to eliminate its association factor (Scheibel, 1954):

$$D_{j,i}^0 = \frac{8.2 \times 10^{-8}}{\eta_i V_j^{1/3}} \left[1 + \left(\frac{3V_i}{V_j} \right)^{2/3} \right] \tag{3.10}$$

where $D_{j,i}^0$ is the diffusion coefficient for a dilute solute j into a solvent i, V_j is the molar volume of the component *j*, η_i is the viscosity of solvent i. *Table 3.7* presents the liquid molar volume and viscosity for the pure components.

Table 3.7. Pure-Component Liquid Molar Volume and Viscosity for Different Temperatures (Rowley et al., 2002).

T(K)	Liquid molar volume (mL mol⁻¹)					Viscosity (cP)			
	V_A	V_B	V_C	V_D		η_A	η_B	η_C	η_D
293.15	91.57	56.48	208.51	18.05		2.899	0.228	1.183	0.996
303.15	92.42	57.45	213.15	18.09		2.249	0.223	0.988	0.787
313.15	93.31	58.48	217.79	18.16		1.780	0.220	0.820	0.645
323.15	94.24	59.60	222.43	18.23		1.411	0.214	0.679	0.544

For concentrated multicomponent system was used the Perkins and Geankoplis method (Perkins and Geankoplis, 1969):

$$D_{j,m}\eta_m^{0.8} = \sum_{\substack{i=1 \\ i \neq j}}^{n} x_i D_{j,i}^0 \eta_i^{0.8}$$

(3.11)

The viscosity of the liquid mixture was calculated by the Grunberg-Nissan approach (Grunberg and Nissan, 1949):

$$ln(\eta_m) = x_1 ln(\eta_1) + x_2 ln(\eta_2) + x_1 x_2 G_{1,2}$$

(3.12)

where $G_{1,2}$ is an empirical interaction parameter adjusted by experimental data. The liquid mixture viscosity and the molar diffusivities for equilibrium are presented in *Table 3.8.*

Table 3.8. Liquid Mixture Viscosity and Molecular Diffusivities Calculated Based on the Equilibrium Composition (Table 3.4)

T(K)	Liquid mixture Viscosity (cP)	Molecular Diffusivity (cm^2/s) $\times 10^5$			
	η_m	$D_{A,m}$	$D_{B,m}$	$D_{C,m}$	$D_{D,m}$
293.15	0.923	1.654	2.191	0.490	6.930
303.15	0.796	1.994	2.704	0.566	8.538
313.15	0.695	2.386	3.321	0.639	10.468
323.15	0.601	2.871	4.060	0.736	12.844

Mass balance in the particle:

$$\varepsilon_p \frac{\partial C_{p,j}}{\partial t} = \frac{1}{r^2} \frac{\partial}{\partial r} \left[D_j r^2 \frac{\partial C_{p,j}}{\partial r} \right] + (1 - \varepsilon_p) v_j \rho_s \Re^p \tag{3.13}$$

where ε_p is the particle porosity, v_j is the stoichiometric coefficient of the component j, ρ_s is the true density of resin and $\Re^p$ is the reaction rate relative to the local concentration (in mol g_{cat}^{-1} min^{-1}).

Initial conditions:

$$t = 0, \quad C_{b,j} = C_{b0,j}; \quad C_{p,j} = C_{p0,j} \tag{3.14}$$

Considering the external mass transfer resistance as negligible, the boundary conditions are:

$$r = 0, \quad \frac{\partial C_{p,j}}{\partial r} = 0 \tag{3.15}$$

$$r = r_p, \quad C_{b,j} = C_{p,j}\big|_{r=r_p} \tag{3.16}$$

Introducing the dimensionless space variable $\rho = r/r_p$, the model equations become:

$$\frac{dC_{b,j}}{dt} = -\frac{3}{r_p^2} \frac{1 - \varepsilon_b}{\varepsilon_b} D_j \frac{\partial C_{p,j}}{\partial \rho}\bigg|_{\rho=1} \tag{3.17}$$

where ε_b is the bulk porosity.

$$\frac{\partial C_{p,j}}{\partial t} = \frac{D_j}{r_p^2} \frac{1}{\rho^2} \frac{\partial}{\partial \rho} \left[\rho^2 \frac{\partial C_{p,j}}{\partial \rho} \right] + \frac{1 - \varepsilon_p}{\varepsilon_p} v_j \rho_s \Re^p \tag{3.18}$$

Boundary conditions:

$$\rho = 0 , \quad \frac{\partial C_{p,j}}{\partial \rho} = 0 \tag{3.19}$$

$$\rho = 1 , \quad C_{b,j} = C_{p,j}\big|_{\rho=1} \tag{3.20}$$

3.5.1. Kinetic Model

In this work was considered the Langmuir-Hinshelwood model *Equation 3.21*, following previous experience in our laboratory with the acetals 1,1-diethoxyethane and 1,1-dimethoxyethane synthesis (Gandi et al., 2005, Silva and Rodrigues, 2001). The reaction rate is:

$$\Re = k_c \frac{a_A a_B - \dfrac{a_C a_D}{K_a a_A}}{(1 + K_{s,A} a_A + K_{s,B} a_B + K_{I_1} a_A a_B + K_{I_2} \dfrac{a_C}{a_A} + K_{s,C} a_C + K_{s,D} a_D)^2} \tag{3.21}$$

This model is based on the adsorption of the reactants species (1-butanol and acetaldehyde), reaction between adsorbed reactants on the catalyst surface and desorption of reaction products (water and DBE). The surface reaction involves three steps:

- Surface reaction between the adsorbed species of butanol (A) and acetaldehyde (B) to give adsorbed hemi-acetal, I_1S:

$$AS + BS \overset{K_1}{\Leftrightarrow} I_1S + S$$
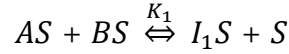
- Surface reaction to obtain adsorbed water, DS:

$$I_1S + S \overset{K_2}{\Leftrightarrow} I_2S + DS$$
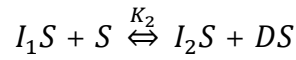
- Surface reaction to obtain adsorbed acetal, CS:

$$I_2S + AS \overset{K_3}{\Leftrightarrow} CS + S$$
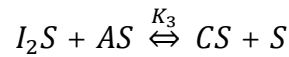
The reaction where water is formed (step 2) was assumed to be the rate controlling step, since the formation of the intermediate I2 from the protonated hemiacetal is the rate determining step for acetalizations (Morrison and Boyd, 1983, Rabindran Jermy and Pandurangan, 2006). Due to the acidic property of Amberlyst-15, the water will be the more adsorbed component; therefore, neglecting the other adsorption constants, the kinetic model can be reduced to a three parameters equation (see *Equation 3.22*).

$$\Re = k_c \frac{a_A a_B - \dfrac{a_C a_D}{K_a a_A}}{(1 + K_{s,D} a_D)^2} \tag{3.22}$$

3.6. Numerical Solution

The model equations were solved using the commercial software gPROMS (general PROcess Modeling System) version 3.1.5. The batch reactor model is defined by a set of partial differential equations (PDE's). The radial domain was discretized using the second order orthogonal collocation in finite elements method (OCFEM). The system of ordinary differential equations (ODE's), resulting from radial discretization was integrated over time using DASOLV integrator implementation in gPROMS. For radial discretization were used ten finite elements with two collocation points in each element. For all simulations was fixed a tolerance equal to 10^{-5}.

3.6.1. Parameter Estimation

In order to determine the parameters of the reaction rate model proposed it is necessary to find a combination of these parameters that provide the best fit of the batch reactor model results with experimental measurements.

The parameter estimation was performed in gPROMS software providing the best fit of measured and predicted data using the maximum likelihood method.

The objective function associated with parameter estimation is described by the following equation:

$$\Phi = \frac{N}{2}\ln(2\pi) + \frac{1}{2}\min_{\theta}\left\{\sum_{i=1}^{NE}\sum_{j=1}^{NV_i}\sum_{k=1}^{NM_{ij}}\left[\ln(\sigma_{ijk}^2) + \frac{(\tilde{z}_{ijk} - z_{ijk})^2}{\sigma_{ijk}^2}\right]\right\} \qquad (3.23)$$

where $\tilde{z}_{ijk}$ and z_{ijk} are the measured and predicted data respectively, N is the total number of measurements taken during the experiments, θ is the set of parameters to be estimated (k_c and $K_{s,D}$), NE is the number of experiments performed, NV_i is the number of variables measured in the ith experiment, NM_{ij} is the number of measurements of jth variable, σ_{ijk}^2 is the variance of the kth measurement of variable j in experiment i.

The results of parameter estimation for different temperatures are presented in *Table 3.9.*

Table 3.9. Estimated Model Parameters

	T(K)		
	293.15	303.15	313.15
k_c (mol g^{-1} min)	1.58	3.04	6.09
$K_{s,D}$	16.77	12.34	8.65

The temperature dependence of the estimated parameters is given by the Arrhenius equation:

$$k_c = k_{0,c} exp\left(-\frac{E_{a,c}}{RT}\right)$$

(3.24)

$$K_{s,D} = K_{0,S} exp\left(-\frac{\Delta H_s}{RT}\right)$$

(3.25)

The predicted values of k_c and $K_{s,D}$ are represented as function of temperature in *Figure 3.9*. By fitting the predicted values by *Equation 3.24* and *Equation 3.25*, it is obtained $E_{a,c}$ = 51.55 kJ mol^{-1} and ΔH_s =-27.5 kJ mol^{-1}.
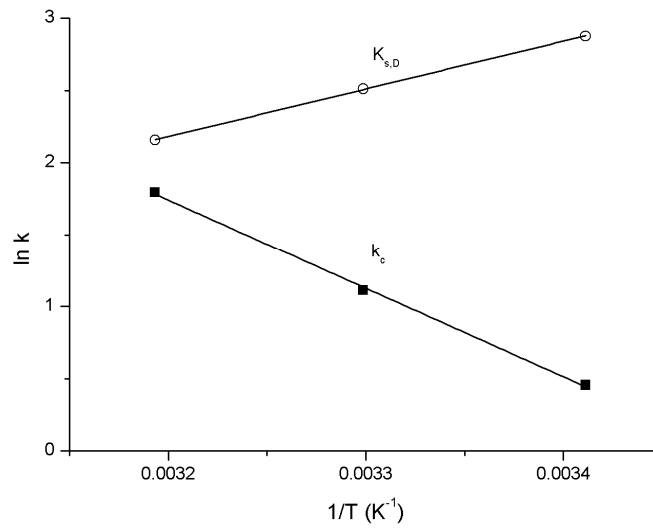
Figure 3.9. Representation of experimental values of kc and $K_{s,D}$ as function of 1/T and linear fitting.

3.7. Model Results

The kinetic law and the parameters of the Batch reactor model considered in the following simulations are presented in *Table 3.10*.

Table 3.10. Kinetic law and parameters used in batch reactor model simulations.

Kinetic law	$\Re = k_c \dfrac{a_A a_B - a_C a_D / K_a a_A}{\left(1 + K_{s,D} a_D\right)^2}$
Equilibrium constant (dimensionless)	$K_a = 9.59 \times 10^{-3} exp\left(\dfrac{1755.3}{T(K)}\right)$
Kinetic constant (mol g_{cat}^{-1} min^{-1})	$k_c = 2.39 \times 10^9 exp\left(-\dfrac{6200.9}{T(K)}\right)$
Water adsorption constant (dimensionless)	$K_{s,D} = 2.25 \times 10^{-4} exp\left(\dfrac{3303.1}{T(K)}\right)$

Figure 3.10a and *Figure 3.10b* show the time evolution of the amount (moles) of reactants (1-butanol and acetaldehyde) and products (DBE and water) at two different temperatures (293.15 K and 313.15 K); comparison between experimental and simulated results is also presented.
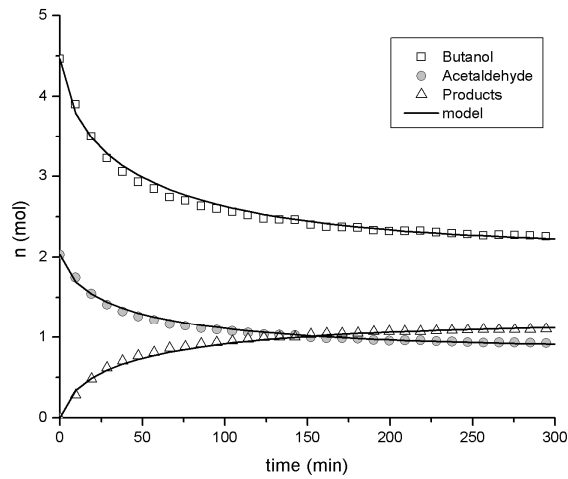
(a)
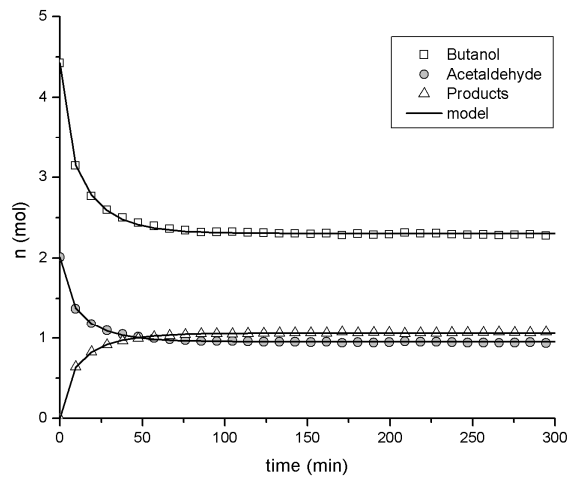
(b)

Figure 3.10. Experimental and simulated kinetic curves: P= 6 atm, w_{cat}=1.8 g, d_p= 0.550 mm, $r_{A/B}$=2.2, (a) 293.15 K, (b) 313.15 K.

In order to validate the estimation of mass transfer parameters, experiments for different particle diameters were performed. *Figure 3.11a* and *Figure 3.11b* show that the model gives a good prediction of the batch reaction for both experiments and, therefore, the good agreement between experimental and simulated results leads us to conclude that the model gives a good prediction of the effect of the internal mass transfer resistance.
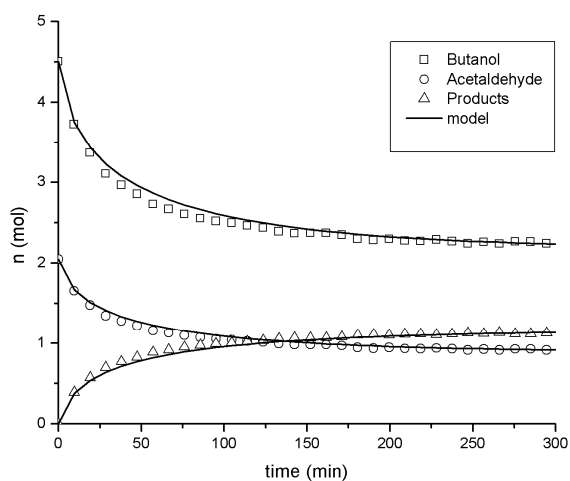
(a)
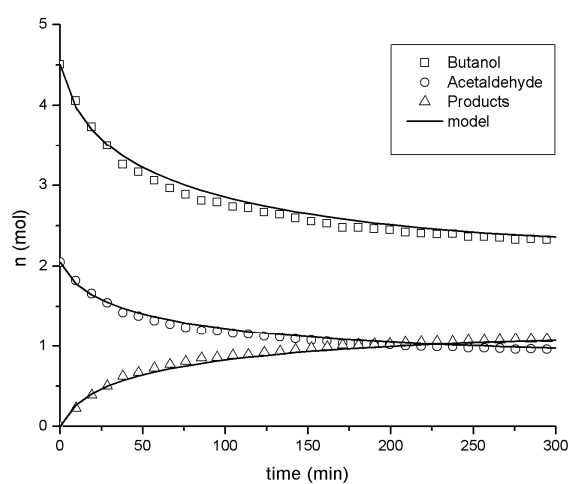
(b)

Figure 3.11. Experimental and simulated kinetic curves: T = 293.15 K, P= 6 atm, w_{cat}=1.8 g, $r_{A/B}$=2.2, (a) d_p= 0.428 mm, (b) d_p=0.890 mm.

By simulation it is possible to observe the effect of the particle diameter on the internal concentration profile. *Figure 3.12* shows the internal concentration profile of 1-butanol for three particle diameters. The presence of a concentration gradient between the surface and the center of catalyst indicates the presence on internal mass transfer resistances. The internal concentration profile is more abrupt for greater particle diameter indicating that internal mass transfer resistance increases with particle diameter as it was expected.
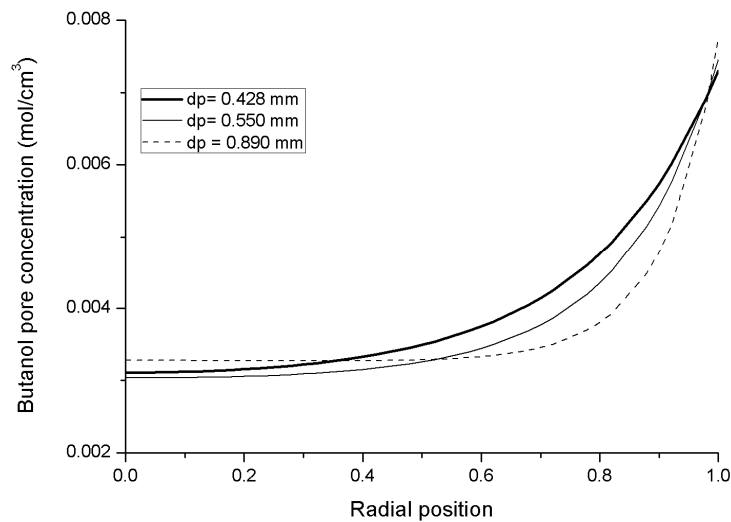
Figure 3.12. Internal concentration profile of butanol for t= 9.5 min.

In order to evaluate how much is the internal mass transfer controlling the kinetic experiments, it is possible to calculate the catalyst effectiveness factor for each experiment, which is defined by the following expression:

$$\eta = \frac{\langle \mathfrak{R} \rangle}{\mathfrak{R}_s} = 3 \frac{\int_0^1 \rho^2 \mathfrak{R} d\rho}{\mathfrak{R}_s} \tag{3.26}$$

where $\mathfrak{R}_s$ is the reaction rate at surface conditions and $\langle \mathfrak{R} \rangle$ is the average reaction rate

defined as:

$$\langle \mathfrak{R} \rangle = \frac{\int_0^{r_p} r^2 \mathfrak{R} dr}{\int_0^{r_p} r^2 dr} = 3 \int_0^1 \rho^2 \mathfrak{R} \, d\rho \tag{3.27}$$

The highest effectiveness factor of about 69% at equilibrium was obtained using a

catalyst with an average diameter of 428 μm (*Figure 3.13*).
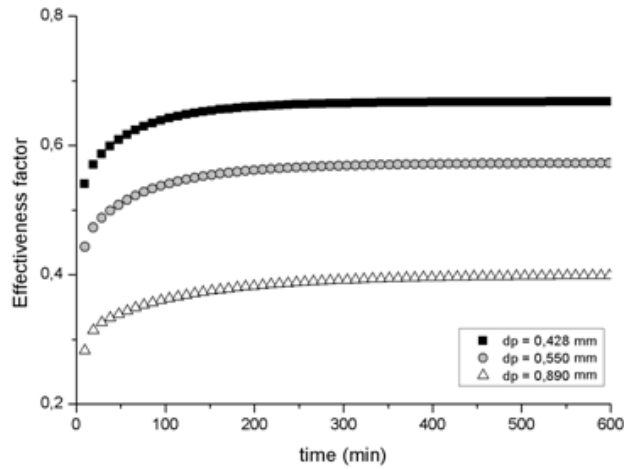
Figure 3.13. Effectiveness factor time evolution.

For the largest particle diameter of 890 μm, the effectiveness factor is about 42% at

equilibrium. From this it is possible to conclude that all experiments were performed

under diffusion-controlled regime. In order to operate under chemical reaction-

controlled regime (effectiveness factor about 1), it would be necessary to use a particle diameter lower than 175 μm which is not commercially available, and it is not possible to grind the resin without affecting its catalytic properties (Pöpken et al., 2000)

In *Table 3.11* acetalization reactions of acetaldehyde with methanol (Gandi et al., 2005), ethanol (Silva and Rodrigues, 2006) and 1-butanol are compared with terms of equilibrium conversion, reaction half-life, effectiveness factors and activation energy. These results show that both equilibrium conversion and reaction rate decreases with the increase of the chain length of the alcohol.

Table 3.11. Acetalization reaction of acetaldehyde with methanol (reaction 1), ethanol (reaction 2) and 1-butanol (reaction 3).

	X_{eq}	$t_{1/2}$ (min)	η	$E_{a,c}$ (kJ/mol)
Reaction 1	0.63	40	0.16	72.4
Reaction 2	0.56	180	0.36	65.1
Reaction 3	0.53	764	0.61	51.6

P= 6 atm, w_{cat}=0.5 g, d_p= 0.550 mm, $r_{A/B}$=2, T= 293.15 K.

3.8. Conclusions

The 1,1- dibutoxyethane (DBE) synthesis in liquid phase reaction catalyzed by Amberlyst-15 was studied in a laboratory-scale batch reactor. The thermodynamic equilibrium constant was calculated based on the equilibrium compositions in the temperature range of 293.15-323.15 K and is given by the expression K_a=0.00959exp [1755.3/T (K)]. The reaction is exothermic and the standard properties of reaction at 298.15 are ΔH^0=-14593.6 J mol^{-1}, ΔS^0=-38.6 J mol^{-1} K^{-1} and ΔG^0= -3074.1 J mol^{-1}.

Kinetic experiments showed that the rate of reaction increases with temperature, however, the equilibrium conversion decreases with temperature due the exothermic nature of the reaction. Experiments performed at different particle diameters have

shown the existence of internal mass transfer resistances for particle diameters greater than 0.5 mm.

Due to the strong non-ideality of liquid reaction mixture, both equilibrium constant and kinetic law were expressed in terms of activities. The activation energy of 51.55 KJ mol^{-1} was calculated by fitting the estimated kinetic parameters at different temperatures to the Arrhenius equation.

The comparison between experimental and simulated results shows that the model gives a good representation of the batch reactor performance for different temperatures and particle of catalyst diameters. The simulated results of catalyst internal concentration profiles showed a concentration gradient between the surface and the center of catalyst due the presence of internal mass transfer resistances. The time evolution of effectiveness factor, for different particle diameter, shows that the controlling mechanism is the internal diffusion.

This work is an important step for the further implementation of an integrated reaction-separation process, such as simulated moving bed reactor (SMBR), in order to enhance the conversion of reaction limited by the chemical equilibrium.

3.9.Notation

a   liquid phase activity

A_p external exchange area between the bulk and the particles

C_i concentration, mol cm^{-3}

C_b bulk concentration, mol cm^{-3}

C_p concentration inside the particle, mol dm^{-3}

d_p average particle diameter, mm

D_j effective diffusivity, cm^2 min^{-1}

$D_{j,m}$ molecular diffusivity coefficient of a solute in a mixture, cm^2 min^{-1}

$E_{a,c}$ reaction activation energy, kJ mol^{-1}

ΔG^0 standard Gibbs free energy, J mol^{-1}

ΔH^0 standard enthalpy, J mol^{-1}

ΔH_s enthalpy of adsorption, J mol^{-1}

k_c kinetic constant, mol g$_{cat}^{-1}$ min

$k_{0,c}$ Arrhenius constant for eq (18), mol g$_{cat}^{-1}$ min

$k_{0,S}$ Arrhenius constant for eq (19), mol g$_{cat}^{-1}$ min

K_a equilibrium constant based on activities

K_x equilibrium constant based on molar fraction

K_γ equilibrium constant based on activity coefficients

K_s equilibrium adsorption constant

n numbe of moles, mol

P pressure, atm

R gas constant, J mol^{-1} K^{-1}

r radial position, cm

r_p particle radius, mm

$r_{A/B}$ initial molar ratio of reactants

ΔS^0 standard entropy, J mol^{-1} K^{-1}

$\mathfrak{R}$ reaction rate, mol g$_{cat}^{-1}$ min

$\mathfrak{R}_s$ reaction rate at surface conditions, mol g$_{cat}^{-1}$ min

$\langle\mathfrak{R}\rangle$ average reaction rate, mol g$_{cat}^{-1}$ min

$\mathfrak{R}^p$ reaction rate relative to the local pore concentration, mol g$_{cat}^{-1}$ min

t time coordinate, min

T temperature, K

x molar fraction

X conversion of the limiting reactant

V volume of solution, cm^3

V_{liq} total volume of reactant mixture, cm^3

V_p total volume of the particles, cm^3

w_{cat} mass of dry catalyst, g

Greek letters

γ activity coefficient

ε_b bulk porosity

ε_p particle porosity

η effectiveness factor

ρ dimensionless radial coordinate

ρ_p particle density, $g\ cm^{-3}$

υ stoichiometric coefficient

τ_p tortuosity factor

Subscripts

A   butanol

B   acetaldehyde

C   DBE

D   water

i   relative to component i

liq   liquid phase

p   relative to the particle

s   relative to the surface of particle

3.9. References

Blagov S., Parada S., Bailer O., Moritz P., Lam D., Weinand R. and Hasse H., "Influence of ion-exchange resin catalysts on side reactions of the esterification of n-Butanol with acetic acid", Chem. Eng. Sci., 61(2), 753-765 (2006)

Dogu T., Aydin E., Boz N., Murtezaoglu K. and Dogu G., "Diffusion resistances and contribution of surface diffusion in TAME and TAEE production using amberlyst-15", Int. J. Chem. React. Eng., 1(A6), (2003)

Fredenslund A., Gmehling J. and Rasmussen P., "Vapor-Liquid Equilibria Using UNIFAC", Elsevier, Amsterdam (1977)

Gandi G. K., Silva V. M. T. M. and Rodrigues A. E., "Process development for dimethylacetal synthesis: Thermodynamics and reaction kinetics", Ind. Eng. Chem. Res, 44(19), 7287-7297 (2005)

Gandi G. K., Silva V. M. T. M. and Rodrigues A. E., "Process development for dimethylacetal synthesis: Thermodynamics and reaction kinetics", Ind. Eng. Chem. Res., 44(19), 7287-7297 (2005)

Gandi G. K., Silva V. M. T. M. and Rodrigues A. E., "Acetaldehyde dimethylacetal synthesis with Smopex 101 fibres as catalyst/adsorbent", Chem. Eng. Sci., 62(4), 907-918 (2007)

Grunberg L. and Nissan A. H., "Mixture law for viscosity [21]", Nature, 164(4175), 799-800 (1949)

Kolah A. K., Asthana N. S., Vu D. T., Lira C. T. and Miller D. J., "Reaction kinetics of the catalytic esterification of citric acid with ethanol", Ind. Eng. Chem. Res., 46(10), 3180-3187 (2007)

Lilja J., Murzin D. Y., Salmi T., Aumo J., Mäki-Arvela P. and Sundell M., "Esterification of different acids over heterogeneous and homogeneous catalysts and correlation with the taft equation", J. Mol. Catal. A: Chem., 182-183, 555-563 (2002)

Mahajani S. M., Kolah A. K. and Sharma M. M., "Extractive reactions with cationic exchange resins as catalysts (acetalization of aldehydes with alcohols)", React. Funct. Polym., 28(1), 29-38 (1995)

Morrison R. T. and Boyd R. N., "Organic Chemistry", Allyn and Bacon, Boston (1983)

Oktar N., Mürtezaoǧlu K., Doǧu T. and Doǧu G., "Dynamic analysis of adsorption equilibrium and rate parameters of reactants and products in MTBE, ETBE and TAME production", Can. J. Chem. Eng., 77(2), 406-412 (1999)

Pereira C. S. M., Silva V. M. T. M. and Rodrigues A. E., "Fixed bed adsorptlve reactor for ethyl lactate synthesis: Experiments, modelling, and simulation", Sep. Sci. Technol., 44(12), 2721-2749 (2009)

Perkins L. R. and Geankoplis C. J., "Molecular diffusion in a ternary liquid system with the diffusing component dilute", Chem. Eng. Sci., 24(7), 1035-1042 (1969)

Pöpken T., Götze L. and Gmehling J., "Reaction kinetics and chemical equilibrium of homogeneously and heterogeneously catalyzed acetic acid esterification with methanol and methyl acetate hydrolysis", Ind. Chem. Eng. Res., 39(7), 2601-2611 (2000)

Rabindran Jermy B. and Pandurangan A., "Al-MCM-41 as an efficient heterogeneous catalyst in the acetalization of cyclohexanone with methanol, ethylene glycol and pentaerythritol", J. Mol. Cat. A: Chem., 256(1-2), 184-192 (2006)

Rat M., Zahedi-Niaki M. H., Kaliaguine S. and Do T. O., "Sulfonic acid functionalized periodic mesoporous organosilicas as acetalization catalysts", Microporous Mesoporous Mater., 112(1-3), 26-31 (2008)

Reid R. C., Prausnitz J. M. and Poling B. E., "The Properties of Gases and Liquids", McGraw-Hill, New York (1987)

Rowley R. L., Wilding W. V., Oscarson J. L., Zundel N. A., Marshall T. L., Daubert T. E. and Danner R. P., "DIPPR Data Compilation of Pure Compound Properties", AIChE, New York (2002)

Sá Gomes P., Leão C. P. and Rodrigues A. E., "Simulation of true moving bed adsorptive reactor: Detailed particle model and linear driving force approximations", Chem. Eng. Sci., 62(4), 1026-1041 (2007)

Scheibel E. G., "Liquid diffusivities", Ind. Eng. Chem., 46(9), 2007-2008 (1954)

Silva V. M. T. M. and Rodrigues A. E., "Synthesis of diethylacetal: Thermodynamic and kinetic studies", Chem. Eng. Sci., 56(4), 1255-1263 (2001)

Silva V. M. T. M., "Diethylacetal synthesis in simulated moving bed reactor", Journal, Ph.D Thesis(Issue), (2003)

Silva V. M. T. M. and Rodrigues A. E., "Novel process for diethylacetal synthesis", AIChE Journal, 51(10), 2752-2768 (2005)

Silva V. M. T. M. and Rodrigues A. E., "Kinetic studies in a batch reactor using ion exchange resin catalysts for oxygenates production: Role of mass transfer mechanisms", Chem. Eng. Sci., 61(2), 316-331 (2006)

Suzuki M. and Smith J. M., "Axial dispersion in beds of small particles", Chem. Eng. J., 3(C), 256-264 (1972)

Wakao N. and Smith J. M., "Diffusion in catalyst pellets", Chem. Eng. Sci., 17(11), 825-834 (1962)

Xu Z. P. and Chuang K. T., "Effect of internal diffusion on heterogeneous catalytic esterification of acetic acid", Chem. Eng. Sci., 52(17), 3011-3017 (1997)

Yadav G. D. and Pujari A. A., "Kinetics of acetalization of perfumery aldehydes with alkanols over solid acid catalysts", Can. J. Chem. Eng., 77(3), 489-496 (1999)

Yu W., Hidajat K. and Ray A. K., "Determination of adsorption and kinetic parameters for methyl acetate esterification and hydrolysis reaction catalyzed by Amberlyst 15", Appl. Catal., A, 260(2), 191-205 (2004)

4. Fixed Bed Adsorptive Reactor

The synthesis of 1,1-dibutoxyethane in a fixed-bed adsorptive reactor using Amberlyst-15 was studied for the first time. The adsorption of non-reactive pairs was investigated experimentally, at 25 ºC, by frontal chromatography in a fixed-bed adsorber. In order to avoid the immiscibility of liquid phase, the liquid-liquid equilibrium for the mixture 1-butanol/water was studied. The multicomponent equilibrium adsorption data was assumed to follow the modified Langmuir type isotherm. Reaction experiments of 1,1-dibutoxyethane production and column regeneration were performed in the fixed-bed adsorptive reactor. This work will enable further developments in chromatographic reactors aiming at the synthesis of 1,1- dibutoxyethane process intensification.

4.1. Introduction

One important trend on chemical engineering and process technology is the process intensification, which consists in the development of innovative frameworks and techniques that improve the chemical manufacturing and processing, reducing equipment volume, energy consumption, or waste formation, leading to cheaper, safer and sustainable technologies (Stankiewicz and Moulijn, 2000). One of the basic components of process intensification is the multifunctional reactors, which combines reaction and separation in a single unit (Stankiewicz, 2003). Using independent equipments for reaction and separation processes, equipment and energy costs are usually higher. Therefore, the integrated reaction and separation process seems to be a better alternative to the conventional process leading to reduced investment costs and significant energy recovery and savings. These reactive separation techniques, such as chromatographic reactors (Mazzotti et al., 1997) and reactive distillation (Taylor and Krishna, 2000), are widely used for reversible reactions, where conversion can exceed its equilibrium value; and for consecutive-competitive or parallel reactions, where reaction yield and product selectivity can be largely enhanced.

By following this process intensification strategy, it is possible to develop competitive, efficient and environmentally friendly processes based on equilibrium limited reactions, as for example the use of reactive chromatography (SMBR) for continuous production of acetals (Pereira et al., 2008, Rodrigues and Silva, 2009) and esters (Pereira et al., 2009).

Acetals can be produced by the acid-catalyzed addition of 2 mol of a monohydric alcohol and 1 mol of an aldehyde (Guinot, 1932). The synthesis of oxygenated compounds, like acetals, is typically carried out with a strong liquid inorganic acid as homogenous catalyst; however, in spite of the high catalytic activity of homogeneous catalysis, they suffer from several drawbacks, such as their corrosive nature, the existence of side reactions, and the fact that the catalyst cannot be easily separated from the reaction mixture (Lilja et al., 2002). The use of solid acid catalysts, such as sulfatated zirconia, clays, ion-exchange resins, zeolites and zeotypes appears as a good alternative to the homogenous catalysis (Yadav and Pujari, 1999). Previous works report the use of ion-exchange resins for acetalization (Gandi et al., 2007, Silva and Rodrigues, 2006) and esterification reactions (Pereira et al., 2008, Sanz et al., 2004).

The objective of the present work is the study of the dynamic behavior of fixed-bed adsorptive reactor for the synthesis of 1,1-dibutoxyethane (DBE), using the acid resin catalyst Amberlyst-15. The multicomponent Langmuir isotherm parameters are obtained by performing binary adsorptive experiments in absence of reaction. The liquid-liquid equilibrium zone for the binary mixture 1-butanol/water was determined in order to avoid the immiscibility of the liquid phase during adsorption experiments. The mathematical model, that includes the interstitial fluid velocity variation, is validated by comparison with experimental reaction/regeneration experiments. The results obtained in this work provide new information about the adsorption and reaction dynamics for the synthesis of 1,1-dibutoxyethane in a fixed-bed reactor, that is very important in the future implementation of the process in a simulated moving-bed reactor (SMBR).

4.2. Experimental Section

4.2.1. Experimental Setup

The experimental work was performed in a laboratory-scale jacketed glass column, packed with the sulfonic acid ion-exchange resin Amberlyst-15 (Silva and Rodrigues, 2002). A schematic representation of the process is presented in *Figure 4.1*.
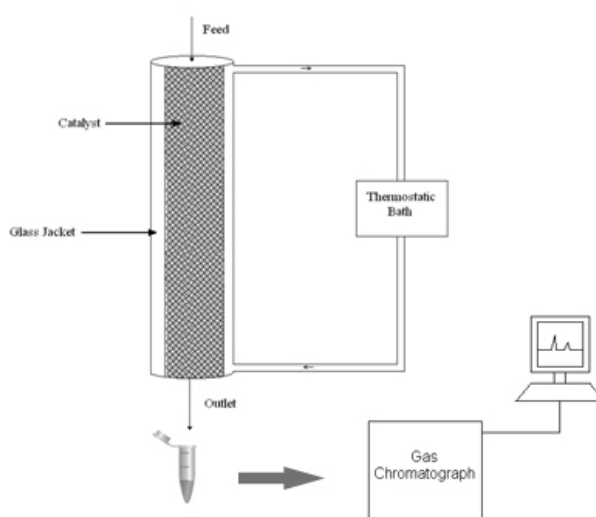
Figure 4.1. Schematic representation of fixed-bed adsorptive reactor.

During the experiments, the column was maintained at constant temperature, through a thermostatic bath at 25ºC. The experimental results were obtained by gas chromatography analysis of small samples withdrawn, at different times, at the column outlet.

The characteristics of the fixed-bed reactor are presented in *Table 4.1.*

Table 4.1. Characteristics of the Fixed-Bed Column

Solid weight	25 g
Length of the bed	12 cm
Internal diameter	2.6 cm
Radius of the particle	375 μm
Bed porosity	0.36
Bulk density	390 kg/m^3

4.2.2. Chemicals and Catalyst

The reactants used were butanol (>99.9% pure) and acetaldehyde (>99.5 % pure) (Sigma-Aldrich, UK). The catalyst used was the ion-exchange resin Amberlyst-15 (Rohm and Haas, France). The ion-exchange capacity is 4.7 meq/g of dry resin and the surface area is 53 m^2/g. Ion exchange resins are produced by copolymerization with styrene and divinyl-benzene used as cross-linking agent. The functional groups are attached to the polymeric matrix developed in the gel phase by long polystyrene chains fixed by bridges of divinil-benzene, leading to a stable and rigid structure (Quinta Ferreira et al., 1996). When the dry resin contacts a fluid, it swells, and the swelling ratio depends on the interactions between the fluid and the resin and on the amount of the cross-links (Sainio et al., 2004). For the Amberlyst-15 the swelling ratio for n-butanol, methanol, methyl acetate, and n-butyl acetate is, respectively, 1.59, 1.58, 1.45 and 1.43 (Bozek-Winkler and Gmehling, 2006).

4.3. Mathematical Model

The multicomponent Langmuir isotherm was considered in this work in order to describe the adsorption equilibrium.

$$q_i = \frac{Q_i K_i C_{p,i}}{1 + \sum_{j=1}^{NC} K_j C_{p,j}} \tag{4.1}$$

where Q_i and K_i represent the total molar capacity per volume of resin and the equilibrium constant for component i, respectively. The thermodynamic consistency of Langmuir isotherm requires that the total molar capacity should be the same for all the components. However, experimental determination of capacity expressed in terms of volumes, masses and moles of a component per gram of A15 showed that the assumption of a constant amount adsorbed is not suitable (Pöpken et al., 2000). Therefore, the Langmuir model is not a rigorous description of the physical phenomena of adsorption; however, previous works showed that Langmuir model can represent satisfactorily the experimental adsorption data on ion-exchange resins. (Gandi et al., 2007, Silva and Rodrigues, 2002). In order to better describe the adsorption on the swollen resin, an appropriate model, such as the modified Flory-Huggins model, should be used to predict the resin phase activities. However, for resins with a high degree of functionalization, such as A15, this model does not yield consistent results (Mazzotti et al., 1997, Pöpken et al., 2000).

The dynamic behaviour of the fixed-bed reactor used for the DBE production will be described by the mathematical model that considers the following assumptions and mass balances:

- Isothermal operation;

- The axial dispersed plug flow model is used to describe the flow pattern;

- The external and internal mass-transfer resistances for adsorbable species are combined in a global resistance;

- Constant column length and packing porosity;

- Velocity variations due the changes in bulk composition.

Bulk fluid mass balance to component i:

$$\frac{\partial C_i}{\partial t} + \frac{\partial (u C_i)}{\partial z} + \frac{(1-\varepsilon)}{\varepsilon}\frac{3}{r_p} K_{L,i}\left(C_i - \bar{C}_{p,i}\right) = D_{ax}\frac{\partial^2 C_i}{\partial z^2} \tag{4.2}$$

Pellet mass balance to component i:

$$\frac{3}{r_p} K_{L,i}\left(C_i - \bar{C}_{p,i}\right) = \varepsilon_p \frac{\partial \bar{C}_{p,i}}{\partial t} + \left(1-\varepsilon_p\right)\frac{\partial \bar{q}_i}{\partial t} - v_i \rho_p r\left(\bar{C}_{p,i}\right) \tag{4.3}$$

The mathematical model is constituted by a system of second-order partial differential equations related to bulk concentration C (*Equation 4.2*); a system of ordinary differential equations related to the average particle pores concentration $\bar{C}_{p,i}$ (*Equation 4.3*); a system of algebraic equations regarding the multicomponente adsorption equilibrium between $\bar{q}_i$ and concentration $\bar{C}_{p,i}$; together with the initial and Danckwerts boundary conditions:

$$t = 0 \qquad C_i = \bar{C}_{p,i} = C_{i,0} \tag{4.4}$$

$$z = 0 \qquad u C_i - D_{ax}\frac{\partial C_i}{\partial z}\bigg|_{z=0} = u C_{i,F} \tag{4.5}$$

$$z = L \qquad \frac{\partial C_i}{\partial z}\bigg|_{z=L_c} = 0 \tag{4.6}$$

The subscripts F and 0 refer to the feed and initial states, respectively, u is the interstitial velocity, $K_{L,i}$ is the global mass transfer resistance coefficient of the component i, D_{ax} is the axial dispersion coefficient, t is the time variable, z is the axial coordinate, v_i is the stoichiometric coefficient of component i, ρ_b is the bulk density, and r is the rate of the chemical reaction given by:

$$r = k_c \frac{a_A a_B - \dfrac{a_C a_D}{K_{eq} a_A}}{\left(1 + K_{s,D} a_D\right)^2} \qquad (4.7)$$

where the activities of the components, a_i, are calculated based on the average concentration into the particle pores. The activity coefficients were calculated using the UNIFAC method (Fredenslund et al., 1977). The equilibrium constant and the kinetic parameters were determined in a previous work (Graça et al., 2010) and are given by:

$$K_{eq} = 9.59 \times 10^{-3} exp\left(\frac{1755.3}{T(K)}\right) \qquad (4.8)$$

$$k_c = 2.39 \times 10^9 exp\left(-\frac{6200.9}{T(K)}\right) \qquad (4.9)$$

$$K_{s,D} = 2.25 \times 10^{-4} exp\left(\frac{3303.1}{T(K)}\right) \qquad (4.10)$$

Moreover, the interstitial fluid velocity variation was calculated using the total mass balance assuming ideal liquid volumes additivity (Lode et al., 2001):

$$\frac{du}{dz} = -\frac{(1-\varepsilon)}{\varepsilon}\frac{3}{r_p}\sum_{i=1}^{NC} K_{L,i} V_{mol,i}\left(C_i - \bar{C}_{p,i}\right) \qquad (4.11)$$

where $V_{mol,i}$ is the molar volume of component i.

The axial dispersion coefficient D_{ax} was estimated experimentally from the Peclet number:

$$Pe = \frac{uL_c}{D_{ax}} \tag{4.12}$$

The global mass transfer coefficient was defined as:

$$\frac{1}{K_L} = \frac{1}{k_e} + \frac{1}{\varepsilon_p k_i} \tag{4.13}$$

The internal mass transfer coefficient was estimated by the fowling expression (Glueckauf, 1955):

$$k_i = \frac{5D_m/\tau}{r_p} \tag{4.14}$$

The external mass transfer coefficient was estimated by the Wilson and Geankopolis correlation (Ruthven, 1984)

$$Sh_p = \frac{1.09}{\varepsilon}\left(Re_p Sc\right)^{0.33} \qquad 0.0015 < Re_p < 55 \tag{4.15}$$

where $Sh_p = k_e d_p/D_m$ and $Re_p = \rho d_p u_0/\eta$ are, respectively, the Sherwood and Reynolds numbers, relative to particle and $Sc = \eta/\rho D_m$ is the Schmidt number.

The infinite dilution diffusivities were estimated by Scheibel correlation (Scheibel, 1954)

$$D_{A,B}^0 (cm^2/s) = \frac{8.2 \times 10^{-8} T}{\eta_B V_{mol,A}^{\frac{1}{3}}} \left[1 + \left(\frac{3 V_{mol,B}}{V_{mol,A}} \right)^{\frac{2}{3}} \right] \tag{4.16}$$

where $D_{A,B}^0$ is the diffusion coefficient for a dilute solute A into a solvent B, T is the temperature, $V_{mol,i}$ is the molar volume of component i, and η_B is the viscosity of solvent B.

For binary systems, the diffusion coefficient in concentrated solutions, $D_{A,B}$, was calculated using the Vignes equation (Vignes, 1966)

$$D_{2,1} = D_{1,2} = \left(D_{1,2}^0 \right)^{x_2} \left(D_{2,1}^0 \right)^{x_1} \tag{4.17}$$

For multicomponent concentrated solutions the Perkins and Geankopolis mixing rule was used (Perkins and Geankoplis, 1969):

$$D_{A,m} \eta_m^{0.8} = \sum_{\substack{i=1 \\ i \neq A/}}^{n} x_i D_{A,i}^0 \eta_i^{0.8} \tag{4.18}$$

where η_i is the viscosity of pure component i and η_m is the viscosity of the mixture. The mixture viscosity and components diffusivities were calculated at each time at every axial position.

The model equations were solved using the commercial software gPROMS (general PROcess Modeling System) version 3.1.5. The mathematical model involves a system of partial and algebraic equations (PDAEs). The axial co-ordinate was discretized using the third order orthogonal collocation in finite elements method (OCFEM). The system of ordinary differential equations (ODE's), resulting from the axial discretization, was

integrated over the time using the DASOLV integrator implementation in gPROMS. For axial discretization were used thirty finite elements. All simulations used a fixed tolerance equal to 10^{-7}.

4.4. Hydrodynamic Study of the Fixed-Bed Column

In order to determine the Peclet number and the bed porosity, tracer experiments were performed using a blue dextran solution (5 kg/m^3). Samples of 0.2 cm^3 were injected under different flow rates and the column response was monitored using a UV-VIS detector at 300 nm. The bed porosity was calculated from the stoichiometric time of the experimental curves. The Peclet number, using axial dispersion model, was obtained by calculating the second moment of the experimental curves ($\sigma^2 = 2t_{st}^2/Pe$). *Figure 4.2* shows the experimental and simulated curves (Levenspiel and Smith, 1995) of the tracer experiments and the estimated values for bed porosity and Peclet number are presented in *Table 4.2*.
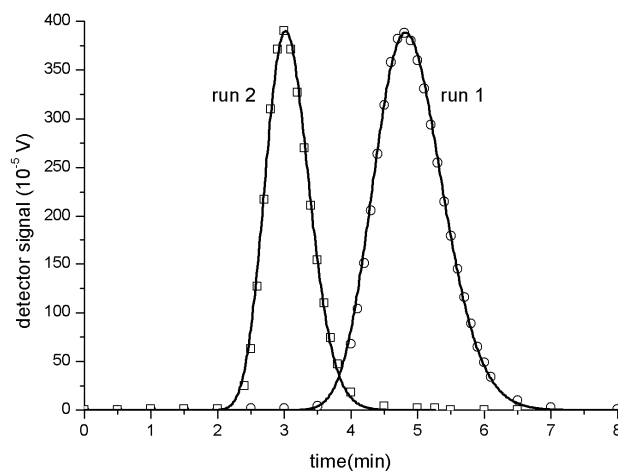
Figure 4.2. . Tracer experiments using blue dextran solution. Points are experimental values and lines are simulated curves.

Table 4.2. Results obtained from tracer experiments.

	Q(mL/min)	t_{st} (min)	ε	σ^2(min^2)	Pe
run 1	5	4.87	0.357	0.273	173.5
run 2	8	3.05	0.358	0.108	173.0

4.5. Adsorption/Desorption experiments with non-reactive pairs.

The adsorption/desorption experiments were performed in a fixed-bed column. Before the beginning of each run, the column is previously saturated with pure 1-butanol.Then, the feed is changed to a binary mixture of 1-butanol/water or DBE/water, and the time evolution of the column outlet composition is evaluated until saturation with the new feed is achieved. After saturation, the column is regenerated with pure 1-butanol.

For the binary mixture 1-butanol/water we must avoid the formation of two liquid phases, depending on the temperature and composition conditions. The formation of two liquid phases with different densities can lead to backmixing problems during the fixed-bed operation; so, the knowledge of liquid-liquid equilibrium for the mixture 1-butanol/water is of utmost importance in the study of fixed-bed adsorption.

Figure 4.3 shows the predicted liquid-liquid equilibrium zone for the binary mixture of 1-butanol/water using UNIFAC and UNIQUAC (Winkelman et al., 2009) for liquid phase activity coefficients (Appendix C).
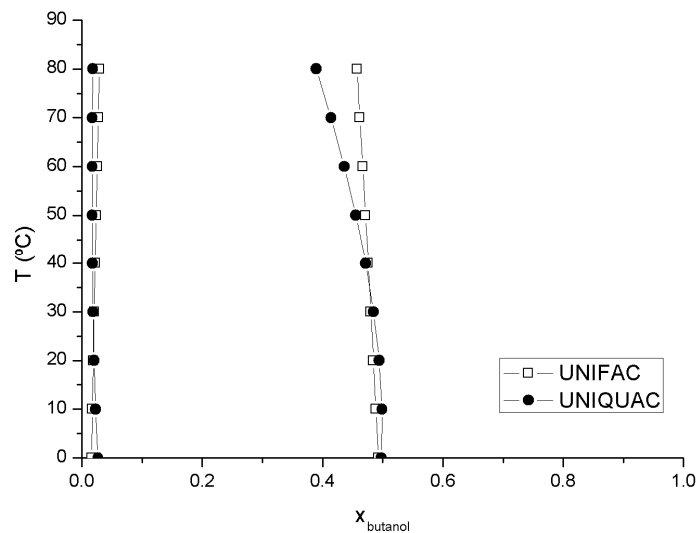
Figure 4.3. Liquid-Liquid equilibrium phase diagram.

Taking into account these results, the adsorption/desorption experiments with 1-butanol/water binary mixtures were performed at 25ºC, using 1-butanol molar fraction above 0.5, in order to avoid the formation of two liquid phases.*Table 4.3* presents the experimental conditions for the adsorption/desorption experiments with binary mixtures of 1-butanol/water and 1-butanol/DBE.

Table 4.3. Experimental conditions for adsorption/desorption with 1-butanol/water and 1-butanol/DBE at 25ºC.

Run	1-butanol/DBE						1-butanol/water			
	S1	R1	S2	R2	S3	R3	S4	R4	S5	R5
Q (mL/min)	9.0	9.0	8.0	8.0	8.0	8.0	8.0	8.0	9.0	9.0
$C_{0,A}$ (mol/L)	10.87	7.0	10.87	7.46	10.87	6.16	10.87	9.69	10.87	9.39
$C_{0,B}$ (mol/L)	0	1.69	0	1.49	0	2.07	0	5.98	0	7.53
$C_{F,A}$ (mol/L)	7.0	10.87	7.46	10.87	6.16	10.87	9.69	10.87	9.39	10.87
$C_{F,B}$ (mol/L)	1.69	0	1.49	0	2.06	0	6.0	0	7.54	0

The difference of densities between adsorbed and desorbed components can lead to hydrodynamic problems, which were overcome by using a Top-Down configuration, when the desorbed component is denser than the adsorbed component; and a Bottom-Top configuration, when the desorbed component is less dense than the adsorbed component.

Based on the experimental outlet column concentrations as function of time, the total amount of species retained/leaving the column (amount in interparticle space + amount in particle pores + amount adsorbed in the solid phase) are calculated by *Equation 4.19*

and *Equation 4.20*, respectively, which are theoretically described by *Equation 4.21* and *Equation 4.22*, respectively.

$$n_{exp}^{ads} = Q \int_0^\infty [C_F - C_{out}(t)]dt \tag{4.19}$$

$$n_{exp}^{des} = Q \int_0^\infty [C_{out}(t) - C_F]dt \tag{4.20}$$

$$n_{theo}^{ads} = \{[\varepsilon + (1-\varepsilon)\varepsilon_p](C_F - C_0) + (1-\varepsilon)(1-\varepsilon_p)[q(C_F) - q(C_0)]\}V_c \tag{4.21}$$

$$n_{theo}^{des} = \{[\varepsilon + (1-\varepsilon)\varepsilon_p](C_0 - C_F) + (1-\varepsilon)(1-\varepsilon_p)[q(C_0) - q(C_F)]\}V_c \tag{4.22}$$

The adsorption parameters were optimized by minimizing the difference between experimental and theoretical values of number of moles adsorbed/desorbed. *Table 4.4* presents the experimental and theoretical number of moles adsorbed calculated in each experiment. In order to close the mass balance in each adsorption/desorption experiment, the amount of a component desorbed during the desorption step has to be the same that was adsorbed during the adsorption step. For the experiments presented in *Table 4.4,* the mass balance closes with an error lower than 5%.

Breakthrough experiments with acetaldehyde were not performed, because acetaldehyde reacts with itself to give an acetaldehyde trimer. Therefore, the adsorption parameters of acetaldehyde were determined by optimization of reaction data. The value of τ used in this work was 2.5, found by a "best fit" procedure to the adsorption experimental data.

The Langmuir isotherm parameters estimated by optimization are presented in *Table 4.5*.

Table 4.4. Experimental and theoretical values for the number of moles adsorbed/desorbed.

Run	1-butanol/DBE						1-butanol/water			
	S1	R1	S2	R2	S3	R3	S4	R4	S5	R5
$n_{exp,A}$ (mol)	-0.148	0.154	-0.132	0.138	-0.186	0.180	-0.150	0.150	-0.176	0.176
$n_{exp,B}$ (mol)	0.065	-0.067	0.058	-0.060	0.081	-0.079	0.765	-0.759	0.897	-0.895
$n_{theo,A}$ (mol)	-0.150	0.150	-0.132	0.132	-0.182	0.184	-0.153	0.153	-0.179	0.179
$n_{theo,B}$ (mol)	0.065	-0.065	0.057	-0.057	0.080	-0.080	0.807	-0.805	0.941	-0.940
Δn_A (%)	-0.81	3.08	0.41	4.88	1.68	-2.28	-1.96	-1.74	-1.37	-1.71
Δn_B (%)	0.91	2.98	0.31	4.79	1.57	-2.40	-5.49	-6.07	-4.78	-5.12

Table 4.5. Multicomponent Langmuir isotherm parameters.

Component	Q (mol/L_{solid})	K (L/mol)
1-Butanol	8.5	7.5
Acetaldehyde	15.1	0.5
Water	44.9	12.1
DBE	5.8	0.4

The experimental and simulated adsorption/desorption results for the binary pair 1-butanol/DBE are presented in *Figure 4.4.*
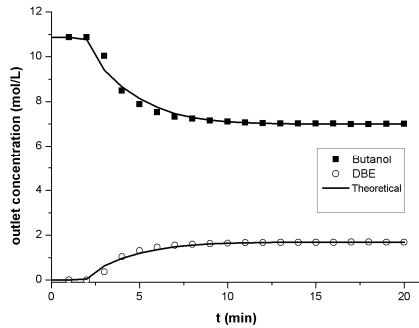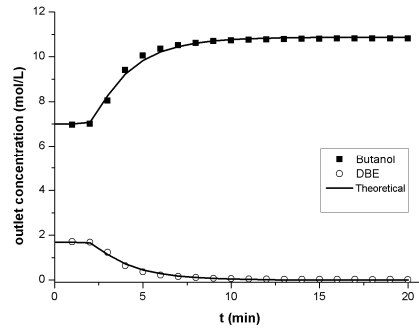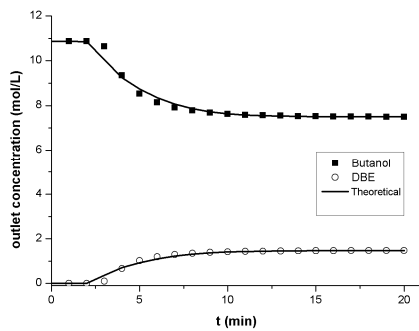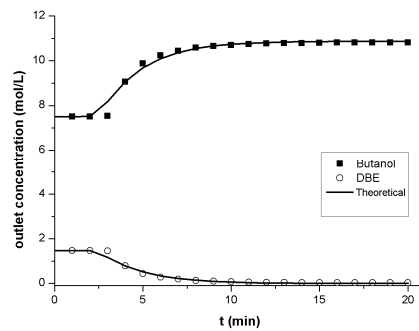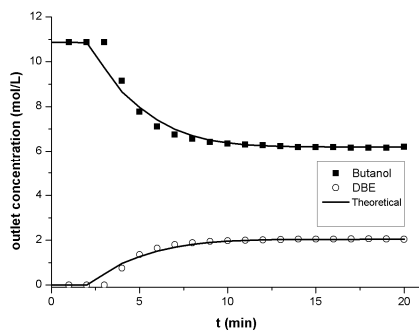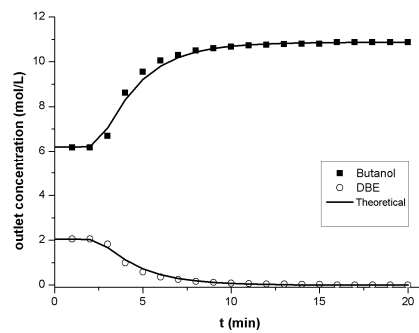
Figure 4.4. Adsorption/desorption experiments with 1-butanol/DBE

The experimental and simulated adsorption/desorption results for the binary pair 1-butanol/water are presented in *Figure 4.5*.
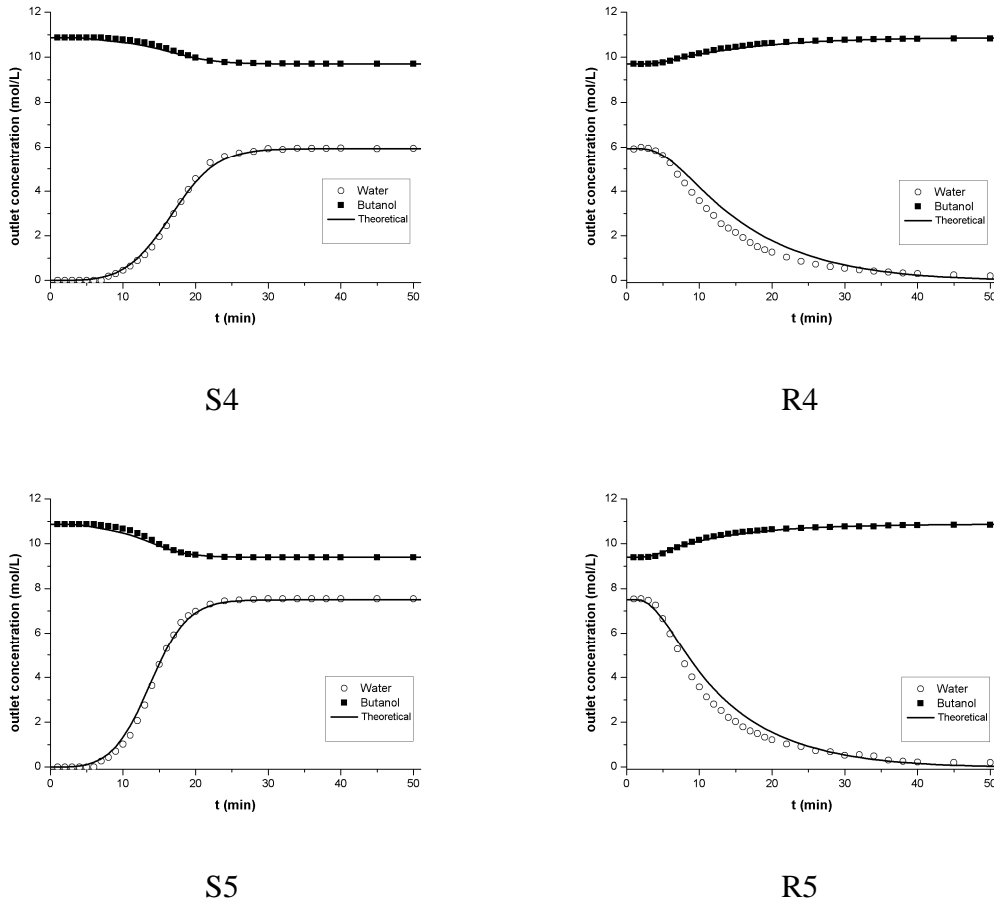
Figure 4.5. Adsorption/desorption experiments with 1-butanol/water

4.6. Adsorptive Reactor

Reaction experiments were performed in a fixed-bed column; a binary mixture of 1-butanol/acetaldehyde was fed to the column previous saturated with 1-butanol, and the composition of reactants and products was measured at the column outlet at different times. After each reaction experiment, the column was regenerated with pure 1-butanol. In the reaction experiments, since the feed mixture is less dense than 1-butanol, the direction flow adopted was from the top to bottom. In the regeneration step, since the reaction mixture is heavier than pure 1-butanol, the direction flow adopted was from the top to the bottom.

Figure 4.6 shows the time evolution of concentration in the column outlet during a reaction experiment. The reaction occurs inside the column between adsorbed 1-butanol and acetaldehyde; water and DBE are formed as products. However, water is preferentially adsorbed by the resin, whereas the DBE is soon desorbed and carried by the fluid phase along the column. The acetaldehyde is consumed above equilibrium conversion in the transient zone that corresponds to the reactive front that travels along the column (*Figure 4.7*), and leaves the column between 12 and 25 minutes (*Figure 4.6*). In *Figure 4.7* (at t=10 min and x>10 cm) it can be seen that the acetaldehyde is completely consumed. When the resin becomes saturated by the water, the selective separation between water and DBE is not possible anymore and the steady state is reached. In *Figure 4.6*, the outlet column composition is constant and corresponds to the equilibrium composition for the conditions of the experiment ($C_{A,F}$=8.44 mol/l, $C_{B,F}$=3.92 mol/l, T=25 ℃). In general, the steady state outlet composition, for different operating conditions will depend not only on the chemical equilibrium, but also on the residence time, the reaction rate and mass transfer rates.
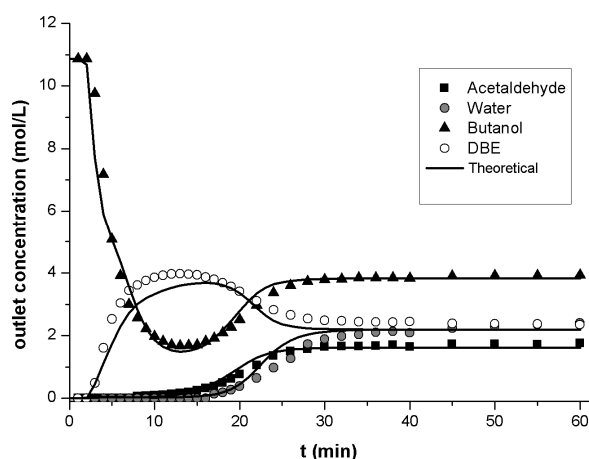
Figure 4.6. Concentration histories in a fixed-bed adsorptive reactor, initially saturated with 1-butanol and then fed with 1-butanol and acetaldehyde. Experimental conditions: Q= 8 mL/min, $C_{F,A}$=8.44 mol/L and $C_{F,B}$=3.92 mol/L

By simulation is possible to obtain concentration profiles inside the column during the reaction experiments (*Figure 4.7*).

t= 3 min

t= 10 min

t= 20 min

t= 30 min
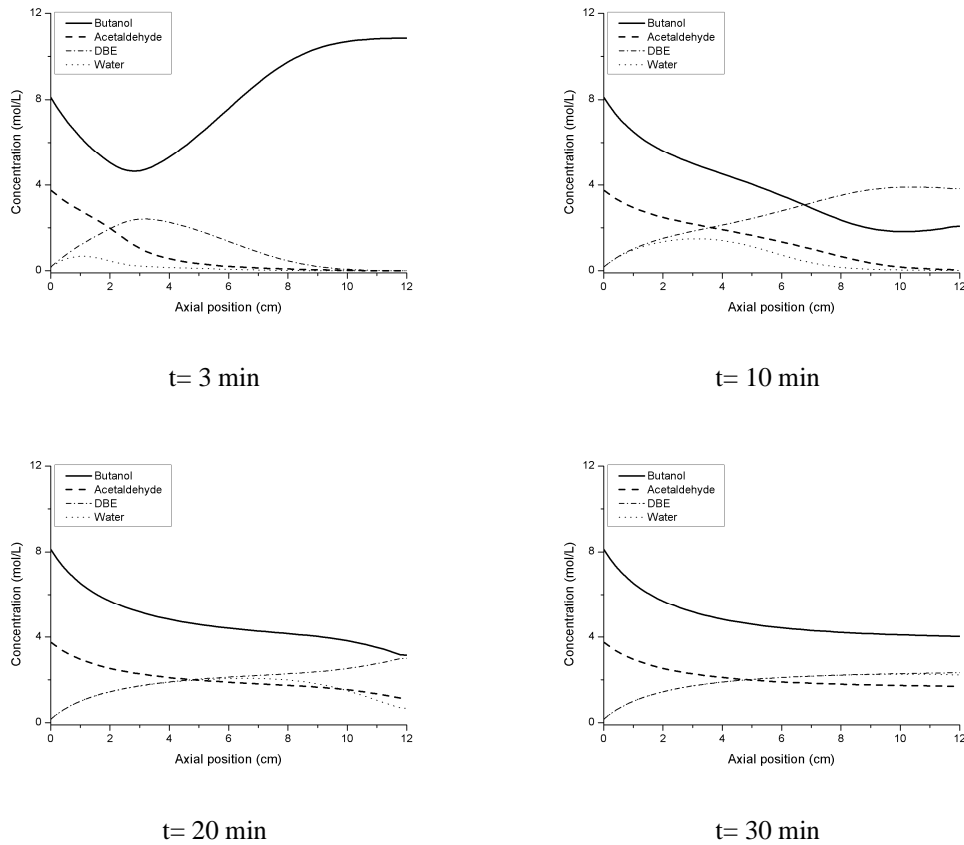
Figure 4.7. Internal concentration profiles of all species in fluid phase inside the column, during the reaction experiment of Figure 4.6.

After the steady-state is reached, the column is regenerated with pure 1-butanol in order to remove the adsorbed species. *Figure 4.8* and *Figure 4.9* show the concentration time evolution in the column outlet during reaction/regeneration experiments. In the regeneration experiments, DBE and acetaldehyde, due to their weak affinity with the resin, are easily removed. On the other hand, water is strongly adsorbed and, therefore, a large amount of 1-butanol is needed in order to totally remove water.
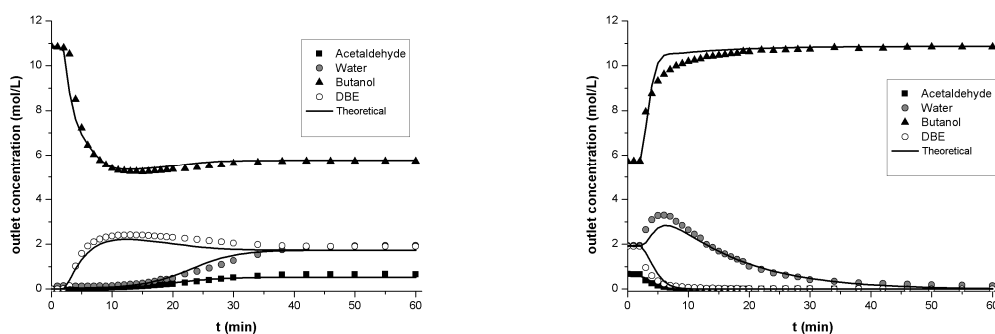
Figure 4.8. Concentration histories in a fixed-bed adsorptive reactor, reaction (left) and regeneration (right) experiments. Experimental conditions: Q= 9 mL/min, $C_{F,A}$=9.43 mol/L and $C_{F,B}$=2.31 mol/L
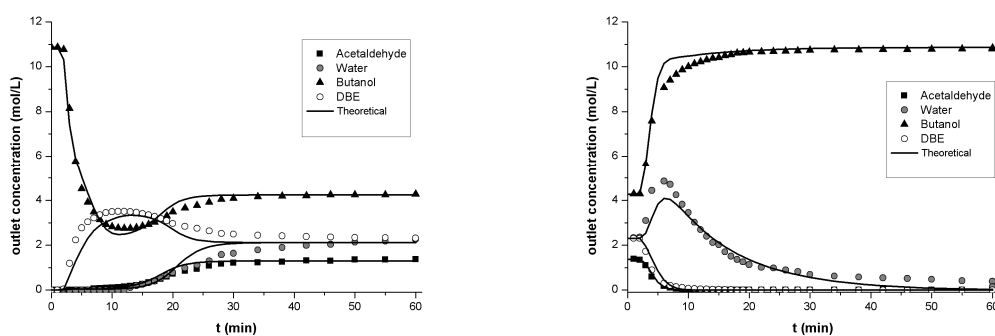
Figure 4.9. Concentration histories in a fixed-bed adsorptive reactor, reaction and regeneration experiments. Experimental conditions: Q= 9 mL/min, $C_{F,A}$=8.7 mol/L and $C_{F,B}$=3.51 mol/L

4.7. Conclusions

Adsorption/desorption experiments in absence of reaction were carried out in a fixed-bed column with the non-reactive binary mixtures of 1-butanol/water and 1-butanol/DBE, at 25°C. For the experiments with 1-butanol/water, it was necessary to study the liquid-liquid equilibrium in order to measure adsorption data in conditions of full miscibility. It was concluded that, for a fixed-bed operation at 25°C, the molar fraction of 1-butanol should be higher than 50% in order to prevent the formation of two liquid phases. The adsorption parameters were estimated by minimizing the error between experimental and theoretical number of moles adsorbed/desorbed for all adsorption/desorption experiments.

For the chromatographic reactor, the mathematical model was derived assuming axial dispersion, isothermal operation, external and internal mass transfer resistances, multicomponent Langmuir isotherm and fluid velocity variations with the composition. The model equations were solved using the commercial software gProms. Reaction experiments were performed by feeding 1-butanol/acetaldehyde mixtures to the column initially saturated with 1-butanol. It was observed a good agreement between model predictions an experimental data. Experimental and simulated results of adsorptive reactor show a selective separation between water and DBE over the resin, where DBE is the less retained component and easily displaced by water, the more retained component. In view of these results, an integrated process of separation and reaction can be designed in order to enhance the conversion of this reaction. In fact, the removal of one product from the reaction medium will displace the chemical reaction towards more products formation.

4.8. Notation

a liquid phase activity

$\bar{C}_{p,i}$ average particle pore concentration, mol dm^{-3}

C_i concentration, mol dm^{-3}

D_j effective diffusivity, dm^2 min^{-1}

$D_{j,m}$ molecular diffusivity coefficient of a solute in a mixture, dm^2 min^{-1}

d_p particle diameter, dm

K adsorption constant, mol dm^{-3}

k_c kinetic constant, mol g$_{cat}^{-1}$ min

k_e external mass-transfer coefficient, dm min^{-1}

K_{eq} equilibrium constant

k_i internal mass-transfer coefficient, dm min^{-1}

K_L global mass-transfer coefficient, dm min^{-1}

K_s equilibrium adsorption constant

n   number of moles, mol

Q   adsorption capacity, $mol\ dm^{-3}$

q   solid phase concentration, $mol\ dm^{-3}$

r   reaction rate, $mol\ g_{cat}^{-1}\ min$

r_p particle radius, mm

t   time coordinate, min

T   temperature, ºC

t_{st} stoichiometric time, min

u   interstitial velocity, $dm\ min^{-1}$

u_0 superficial velocity, $dm\ min^{-1}$

V   volume of solution, dm^3

V_{mol} molar volume, $dm^3\ mol^{-1}$

V_p total volume of the particles, dm^3

X   conversion of the limiting reactant

x   molar fraction

z   axial position, dm

Greek letters

γ   activity coefficient

ε   bed porosity

ε_p particle porosity

η   fluid viscosity, $g\ dm^{-1}\ min^{-1}$

ρ_p particle density, $g\ dm^{-3}$

τ   tortuosity factor

υ   stoichiometric coefficient

Subscripts

A   butanol

B   acetaldehyde

C   DBE

D   water

i   relative to component i

p   relative to the particle

4.9. References

Bozek-Winkler E. and Gmehling J., "Transesterification of methyl acetate and n-butanol catalyzed by Amberlyst 15", Ind. Eng. Chem. Res., 45(20), 6648-6654 (2006)

Fredenslund A., Gmehling J. and Rasmussen P., "Vapor-Liquid Equilibria Using UNIFAC", Elsevier, Amsterdam (1977)

Gandi G. K., Silva V. M. T. M. and Rodrigues A. E., "Acetaldehyde dimethylacetal synthesis with Smopex 101 fibres as catalyst/adsorbent", Chem. Eng. Sci., 62(4), 907-918 (2007)

Glueckauf E., "Theory of chromatography: Part 10. - Formula for diffusion into spheres and their application to chromatography", Trans. Faraday Soc., 51, 1540-1551 (1955)

Graça N. S., Pais L. S., Silva V. M. T. M. and Rodrigues A. E., "Oxygenated biofuels from butanol for diesel blends: Synthesis of the acetal 1,1-dibutoxyethane catalyzed by amberlyst-15 ion-exchange resin", Ind. Eng. Chem. Res., 49(15), 6763-6771 (2010)

Guinot H. M., "Process for the Manufacture of Acetal", U.S. Patent 1,850,836 (1932)

Levenspiel O. and Smith W. K., "Notes on the diffusion-type model for the longitudinal mixing of fluids in flow", Chem. Eng. Sci., 50(24), 3891-3896 (1995)

Lilja J., Murzin D. Y., Salmi T., Aumo J., Mäki-Arvela P. and Sundell M., "Esterification of different acids over heterogeneous and homogeneous catalysts and correlation with the taft equation", J. Mol. Catal. A: Chem., 182-183, 555-563 (2002)

Lode F., Houmard M., Migliorini C., Mazzotti M. and Morbidelli M., "Continuous reactive chromatography", Chem. Eng. Sci., 56(2), 269-291 (2001)

Mazzotti M., Neri B., Gelosa D., Kruglov A. and Morbidelli M., "Kinetics of Liquid-Phase Esterification Catalyzed by Acidic Resins", Ind. Eng. Chem. Res., 36(1), 3-10 (1997)

Mazzotti M., Neri B., Gelosa D. and Morbidelli M., "Dynamics of a Chromatographic Reactor: Esterification Catalyzed by Acidic Resins", Ind. Eng. Chem. Res., 36(8), 3163-3172 (1997)

Pereira C. S. M., Gomes P. S., Gandi G. K., Silva V. M. T. M. and Rodrigues A. E., "Multifunctional reactor for the synthesis of dimethylacetal", Ind. Eng. Chem. Res., 47(10), 3515-3524 (2008)

Pereira C. S. M., Pinho S. P., Silva V. M. T. M. and Rodrigues A. E., "Thermodynamic equilibrium and reaction kinetics for the esterification of lactic acid with ethanol catalyzed by acid ion-exchange resin", Ind. Chem. Eng. Res., 47(5), 1453-1463 (2008)

Pereira C. S. M., Silva V. M. T. M. and Rodrigues A. E., "Fixed bed adsorptlve reactor for ethyl lactate synthesis: Experiments, modelling, and simulation", Sep. Sci. Technol., 44(12), 2721-2749 (2009)

Perkins L. R. and Geankoplis C. J., "Molecular diffusion in a ternary liquid system with the diffusing component dilute", Chem. Eng. Sci., 24(7), 1035-1042 (1969)

Pöpken T., Götze L. and Gmehling J., "Reaction kinetics and chemical equilibrium of homogeneously and heterogeneously catalyzed acetic acid esterification with methanol and methyl acetate hydrolysis", Ind. Chem. Eng. Res., 39(7), 2601-2611 (2000)

Quinta Ferreira R. M., Almeida-Costa C. A. and Rodrigues A. E., "Heterogeneous models of tubular reactors packed with ion-exchange resins: Simulation of the MTBE synthesis", Ind. Eng. Chem. Res., 35(11), 3827-3841 (1996)

Rodrigues A. E. and Silva V. M. T. M., "Industrial Process for Acetals Producing in Simulated Moving Bed Reactor", U.S. Patent 7,488,851 (2009)

Ruthven D. M., "Principles of Adsorption and Adsorption Processes", Wiley, New York (1984)

Sainio T., Laatikainen M. and Paatero E., "Phase equilibria in solvent mixture-ion exchange resin catalyst systems", Fluid Phase Equilibr., 218(2), 269-283 (2004)

Sanz M. T., Murga R., Beltrán S., Cabezas J. L. and Coca J., "Kinetic Study for the Reactive System of Lactic Acid Esterification with Methanol: Methyl Lactate Hydrolysis Reaction", Ind. Chem. Eng. Res., 43(9), 2049-2053 (2004)

Scheibel E. G., "Liquid diffusivities", Ind. Eng. Chem., 46(9), 2007-2008 (1954)

Silva V. M. T. M. and Rodrigues A. E., "Dynamics of a fixed-bed adsorptive reactor for synthesis of diethylacetal", AIChE J., 48(3), 625-634 (2002)

Silva V. M. T. M. and Rodrigues A. E., "Kinetic studies in a batch reactor using ion exchange resin catalysts for oxygenates production: Role of mass transfer mechanisms", Chem. Eng. Sci., 61(2), 316-331 (2006)

Stankiewicz A., "Reactive separations for process intensification: An industrial perspective", Chem. Eng. Process., 42(3), 137-144 (2003)

Stankiewicz A. I. and Moulijn J. A., "Process intensification: Transforming chemical engineering", Chem. Eng. Prog., 96(1), 22-33 (2000)

Taylor R. and Krishna R., "Modelling reactive distillation", Chem. Eng. Sci., 55(22), 5183-5229 (2000)

Vignes A., "Diffusion in binary solutions: Variation of diffusion coefficient with composition", Ind. Eng. Chem. Fundam., 5(2), 189-199 (1966)

Winkelman J. G. M., Kraai G. N. and Heeres H. J., "Binary, ternary and quaternary liquid-liquid equilibria in 1-butanol, oleic acid, water and n-heptane mixtures", Fluid Phase Equilibria, 284(2), 71-79 (2009)

Yadav G. D. and Pujari A. A., "Kinetics of acetalization of perfumery aldehydes with alkanols over solid acid catalysts", Canadian Journal of Chemical Engineering, 77(3), 489-496 (1999)

5. Simulated Moving Bed Adsorptive Reactor

The synthesis of 1,1- dibutoxyethane was carried out in a Simulated Moving Bed pilot unit LICOSEP 12-26 (Novasep, France) with 12 columns packed with the commercial ion-exchange resin Amberlyst-15 (Rohm & Haas, France). Experimentally the best raffinate purity obtained was 85% with a productivity of 5.04 $kg.L^{-1}.d^{-1}$ and a desorbent consumption of 13.5 $L.kg^{-1}$. The TMBR model was used to construct reaction/separation regions and to study the influence of feed composition, switching time, flow rates and mass-transfer resistances on the SMBR performance. The SMBR process shows a potential to be a competitive, efficient and environmentally friendly way to produce 1,1- dibutoxyethane and other acetals.

5.1. Introduction

The oxygenated compound 1,1-dibutoxyethane (DBE) is produced through the liquid phase acetalization reaction of 1-butanol and acetaldehyde in acidic medium; water is also produced as by-product:

$$2 \times \text{Butanol(A)} + \text{Acetaldehyde(B)} \overset{H^+}{\Leftrightarrow} \text{DBE(C)} + \text{Water(D)}$$

The use of a solid acid catalyst, such as Amberlyst-15, seems to be a good alternative to produce oxygenated compounds, like acetals, avoiding the drawbacks of homogeneous catalysis (Yadav and Pujari, 1999), such as their corrosive nature, the existence of side reactions, and the fact that the catalyst cannot be easily separated from the reaction mixture (Lilja et al., 2002).

Both 1-butanol and acetaldehyde can be produced by means of natural resources (Agirre et al., Ezeji et al., 2007); moreover, 1-butanol has been considered as alternative to ethanol as biofuel (Dürre, 2007). In the last years, the use of biofuels as alternative to conventional petroleum-derived fuels became an important trend towards a sustainable development. Biodiesel, obtained from vegetable oils and animals fats by a transesterification reaction, shows potential to significantly reduce the exhaust emission of particulate matter in a diesel engine; moreover, biodiesel presents other advantages such as: biodegradability, high flash-point, and inherent lubricity in neat form (Knothe et al., 2006). However, biodiesel presents worst performance than conventional diesel in terms of oxidation stability, nitrogen oxides emissions, energy content and cold weather operability (Moser and Erhan, 2008). To overcome these limitations, the use of oxygenated bio-derived additives such as acetals, avoiding the environmental harmful effects of metal based additives, seems to be a good solution (Capeletti et al., 2000).

Acetalization reactions carried out in a conventional batch reactor present low equilibrium conversions (Gandi et al., 2005, Graça et al., 2010, Silva and Rodrigues, 2006). The use of integrated reaction/separation processes appears to be a good alternative in order to enhance the reaction conversion, since they allow the separation of the products from the reaction medium as they are formed, displacing the chemical equilibrium towards product formation (Agar, 1999, Bergeot et al., 2009). Among the integrated reaction/separation processes reactive, chromatography is a very attractive

way to increase the reactants conversion (Sainio et al., 2007) and in terms of energy consumption savings, since it is based on the selective adsorption rather selective evaporation; therefore, the use of high temperatures is not necessary. Moreover, it can be used with temperature-sensitive products such as pharmaceutical or natural products (Lode et al., 2003). When operated discontinuously as in classical batch mode, reactive chromatography presents low efficiency, high desorbent consumption and excessive dilution of the final products. One way to transform the reactive chromatography in a continuous process is by promoting the countercurrent flow between the liquid and the solid phase; this concept is called True Moving Bed (TMB). However, some technical problems arise from the movement of the solid phase, namely, erosion of solid phase caused by particle attrition. These drawbacks were overcome by the invention of Simulated Moving Bed (SMB) concept (Broughton and Gerhold, 1961), where the solid phase is divided for a set of fixed-bed columns and the position of the inlet and the outlet streams move periodically; this change of the position made in the same direction of the liquid phase, simulates the movement of the solid phase in opposite direction. Alternatively, the columns can be mounted on a carousel that rotates continuously or intermittently through different feed and discharge ports; this process was patented by Advanced Separation Technologies (Berry et al., 1988). From the application of the SMB concept to reactive systems results the Simulated Moving Bed Reactor (SMBR) (Kawase et al., 1996, Mazzotti et al., 1996).

The principle of SMBR operation for a reaction of type $2A+B \leftrightarrow C+D$ is schematically represented in *Figure 5.1*. The inlets (feed and desorbent) and outlets (raffinate and extract) define the four sections of the SMBR. Section 1 is located between desorbent and extract stream; Section 2 is located between extract and feed streams; Section 3 is located between feed and raffinate streams; Section 4 is located between raffinate and desorbent stream. The reactant B enters into the reactor by the feed stream and reacts with the excess reactant A, the components C and D are formed as reaction products. The more strongly adsorbed component D is adsorbed by the solid phase and transported towards the extract node. The flow rate in section 1 should be high enough to desorb the component D in order to regenerate the solid phase. The less strongly adsorbed component is transported by liquid phase towards raffinate node. In section 4 the flow rate should be low enough to allow the adsorption of component C by the solid phase in order to regenerate the liquid phase.
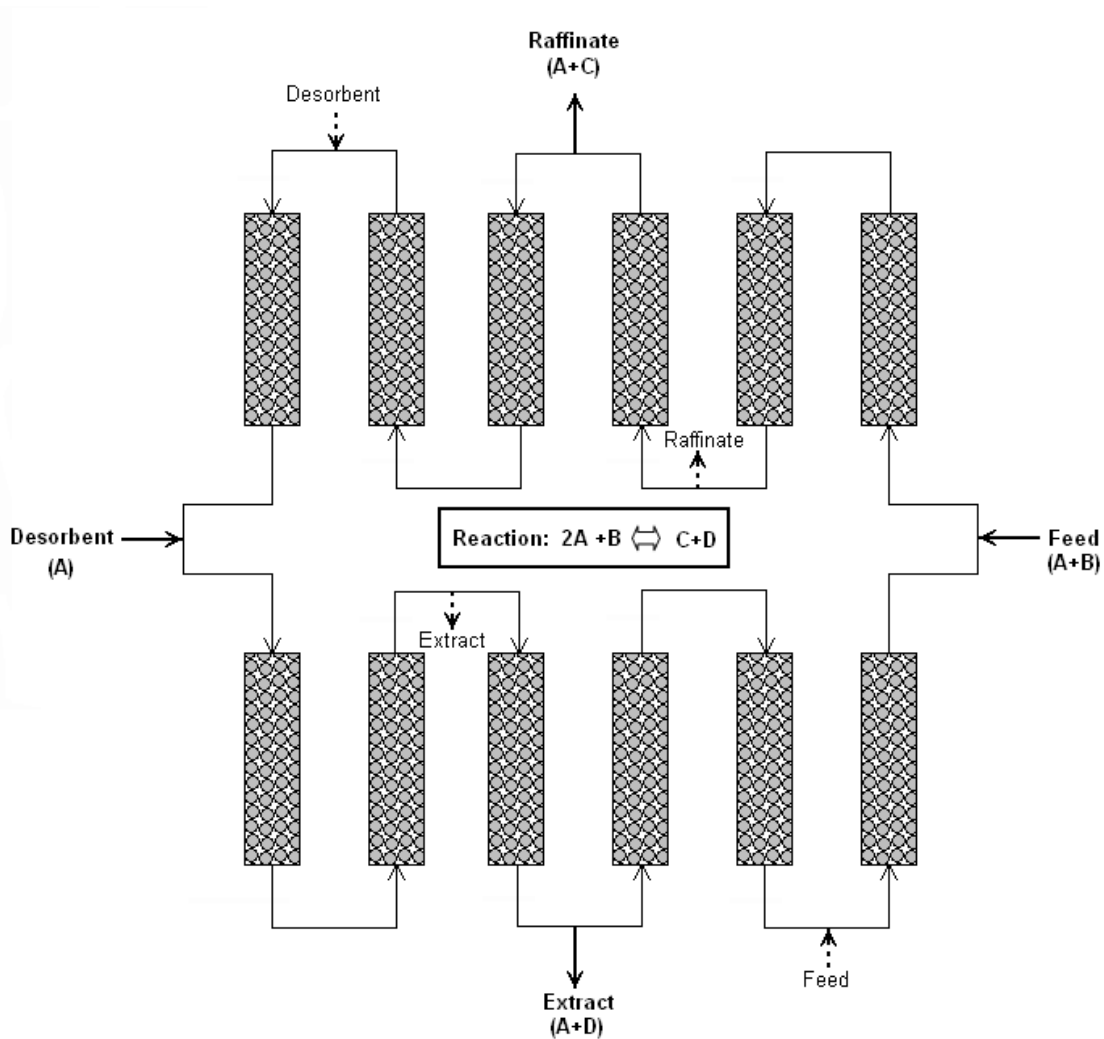
Figure 5.1. Schematic representation of a simulated moving bed reactor. Dashed lines represent the position of the streams in the last period before the present one (continuous lines).

The aim of the present work is the study of the performance and feasibility of the synthesis of 1,1 –dibutoxyethane in a simulated moving bed reactor. The synthesis reaction was carried out experimentally using the SMB pilot unit Licosep 12-26 (Novasep, France) with 12 columns packed with the ion-exchange resin Amberlyst-15 (Rohm & Haas, France). The SMBR model is validated by comparison with experimental data. The applicability of TMBR model in the simulation of SMBR operation is verified. The effect of SMBR parameters (Switching time, feed composition, flow rates, and mass-transfer resistances) in the process performance is studied by simulation.

5.2. Synthesis of 1,1-Dibutoxyethane in a Simulated Moving-Bed Adsorptive Reactor

5.2.1. Experimental Apparatus

The SMBR experiments were carried out in a pilot unit Licosep$^®$ 12-26 by Novasep. It is a continuous chromatographic system constituted by 12 columns connected in series. The columns are Superformance SP 230 $\times$ 26 (length $\times$ ID, mm), by Götec Labortechnik (Mühltal, Germany), packed with Amberlyst-15 (Rohm and Haas). These columns can withstand temperatures up to 60ºC and 60 bar of pressure. The operating temperature was 25ºC. The columns jackets are connected to one other by silicone hoses and to a thermostat bath (Lauda GmbH, Lauda-Königshofen, Germany), in order to ensure the temperature control. A four-port valve (Top-Industrie, France) actuated by the control system is located between every two columns. When required, the valves allow either pumping of feed/desorbent into the system or withdrawal of extract/raffinate streams. The valves work at a minimum air pressure of 6 bar provided by an air compressor. The recycling of the liquid phase is ensured by a positive-displacement three-head membrane pump (Milton Roy, Pont St. Pierre, France), which may deliver flow rates as low as 20 mL/min and up to 120 mL/min and that can hold up to 100 bar of pressure. The inlet and outlet streams are controlled by four pumps (models L-6000 and L-6200, Merck Hitachi, Darmstadt, Germany), connected to a computer by an RS-232 interface. The maximum flowrate in the desorbent and extract pumps is 30 mL/min, whereas in the feed and raffinate pumps the maximum flowrate is 10 mL/min. The internal concentration profiles are determined by collecting samples by a six-port valve located between the twelfth and the first columns. A detailed description of the methodology followed to determine the internal concentration profiles is given in *Appendix D*.

Pulse experiments of tracer (blue dextran solution) were performed in each of the twelve columns in order to verify the homogeneity of packing and to determine the bed porosity. An average Peclet number of 300 was obtained and the mean value for bed porosity was 0.4. The characteristics of the SMBR columns used are presented in *Table 5.1*.

Table 5.1. Characteristics of the SMBR columns

Solid weight	48 g
Length of the bed	23 cm
Internal diameter	2.6 cm
Radius of the particle	375 μm
Bed porosity	0.4
Particle porosity	0.36[1]
Bulk density	390 kg/m^3
Peclet number	300

[1] (Lode et al., 2001)

5.2.2. Chemicals and Catalyst/Adsorbent

The reactants used were 1-butanol (>99.9% pure) and acetaldehyde (99.5% pure) (Sigma-Aldrich, UK).

The SMBR columns were packed with the ion-exchange resin Amberlyst-15 Wet (Rohm & Haas, France).

5.2.3. Experimental Results

The operating conditions used in the SMBR synthesis of DBE are presented in *Table 5.2*. All the experiments were carried out with a SMBR configuration of 3 columns per section (3-3-3-3), flowrate of 45 mL/min in section 1, and at 25ºC. The feed composition was a mixture of 1-butanol and acetaldehyde, with 50% acetaldehyde molar fraction. It was noticed that when 1-butanol and acetaldehyde were mixed the temperature of the solution increased considerably; this exothermic behavior was already reported for the synthesis of 1,1-diethoxyethane from ethanol and acetaldehyde (Prior and Loureiro, 2001). Therefore, before the beginning of each SMBR experiment, the feed solution was placed in a thermostatic bath until the operation temperature was reached.

The SMBR experiments were carried out under conditions of incomplete resin regeneration in section 1 due to equipment limitations (maximum allowable desorbent flow rate of 30 mL/min).

Table 5.2. Operating conditions of the SMBR unit.

Run 1	Run 2	Run 3
$t^* = 3.7$ min	$t^* = 3.5$ min	$t^* = 3.3$ min
$Q_D = 25$ mL/min	$Q_D = 24$ mL/min	$Q_D = 23$ mL/min
$Q_F = 3$ mL/min	$Q_F = 3$ mL/min	$Q_F = 3$ mL/min
$Q_R = 8$ mL/min	$Q_R = 8$ mL/min	$Q_R = 8$ mL/min
$Q_X = 20$ mL/min	$Q_X = 19$ mL/min	$Q_X = 18$ mL/min
$Q_{Recycle} = 20$ mL/min	$Q_{Recycle} = 21$ mL/min	$Q_{Recycle} = 22$ mL/min

Figure 5.2, *Figure 5.3* and *Figure 5.4* compare the experimental and simulated internal concentration profiles. The experimental concentration profiles at the cyclic steady-state were obtained at the middle of the switching time after 10 cycles. There is a good agreement between model and experimental results.

The effect of operating under conditions of incomplete resin regeneration can be perceived looking at the internal concentration profiles; the presence of a considerable amount of water in section 1 and section 4 results from that fact. It can be observed that the minimum concentration of 1-butanol in section 3 decreases from Run 1 to Run3; this is caused by the decrease of the desorbent flow rate and consequently the decrease of the amount of 1-butanol that enters in the reactor.
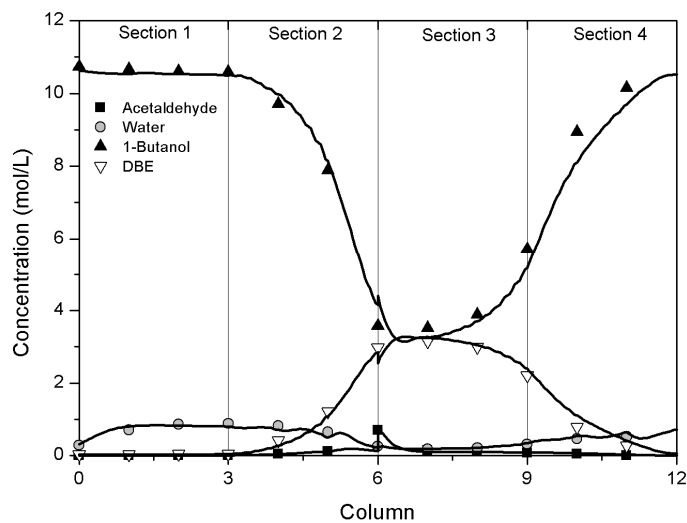
Figure 5.2. Experimental and simulated (by SMBR model) cyclic steady-state concentration profiles at 50% of switching time for Run1.
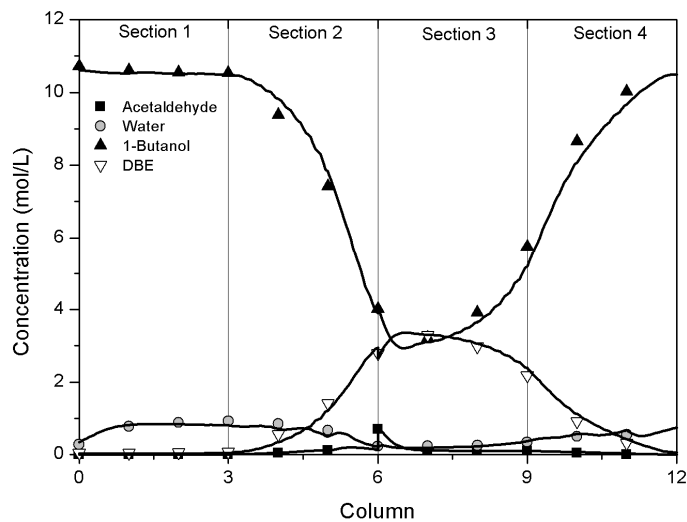
Figure 5.3. Experimental and simulated (by SMBR model) cyclic steady-state concentration profiles at 50% of switching time for Run2.
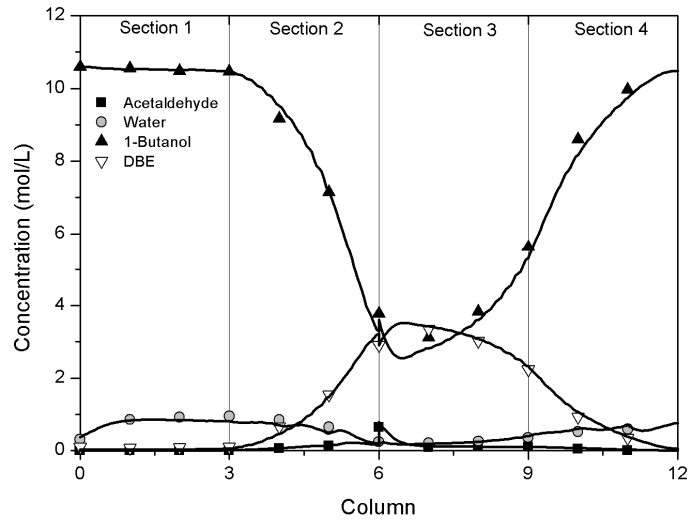
Figure 5.4. Experimental and simulated (by SMBR model) cyclic steady-state concentration profiles at 50% of switching time for Run3.

In order to evaluate the SMBR performance the following criteria are used:

Raffinate Purity (%)

$$PUR = \frac{C_{C,R}}{C_{B,R} + C_{C,R} + C_{D,R}} \times 100 \qquad (5.1)$$

Extract Purity (%)

$$PUX = \frac{C_{C,X}}{C_{B,X} + C_{C,X} + C_{D,X}} \times 100 \qquad (5.2)$$

Acetaldehyde Conversion (%)

$$X = \left(1 - \frac{Q_X C_{B,X} + Q_R C_{B,R}}{Q_F C_{B,F}}\right) \times 100 \qquad (5.3)$$

DBE recovery (%)

$$Rec = \frac{Q_R C_{C,R}}{Q_F C_{B,F}} \times 100 \qquad (5.4)$$

Raffinate Productivity ($kg_{DBE} L_{adsorbent}^{-1} day^{-1}$)

$$PR = \frac{Q_R C_{C,R}}{(1 - \varepsilon) V_{unit}} \qquad (5.5)$$

Desorbent Consumption ($L_{adsorbent} kg_{DBE}^{-1}$)

$$DC = \frac{\left[\left(Q_D C_{A,D} + Q_F (C_{A,F} - 2X C_{B,F}) \right) V_{mol,A} \right]}{Q_R C_{C,R}}$$

$$= \frac{\left[\left(Q_D C_{A,D} + Q_F (C_{A,F} - 2X C_{B,F}) \right) V_{mol,A} \right]}{PR(1 - \varepsilon) V_{unit}} \qquad (5.6)$$

Table 5.3 presents the performance parameters for each SMBR experiment calculated experimentally and by simulation with the SMBR model. It can be observed that the performance parameters are reasonably predicted by the SMBR model. The acetaldehyde conversion is up to 95% for all experiments. In order to obtain greater values of acetaldehyde conversion, higher desorbent flow rates are needed for complete regeneration of the resin in section 1; however, due to equipment limitations the SMBR experiments were performed under conditions of incomplete resin regeneration. Therefore, the water adsorbed in the resin is not completely removed in section 1 and is carried by the resin to section 4, decreasing the capacity of regenerating the liquid phase in this section and contaminating the raffinate stream; the water is also transported to section 3, where the adsorbed water has an inhibitory effect in the reaction rate (see *Equation 5.9*) and consequently the acetaldehyde conversion decreases.

Table 5.3. Performance parameters obtained experimentally and with the SMBR model (inside brackets).

	Run 1	Run 2	Run 3
PUR(%)	85.10 (84.55)	83.22 (83.74)	82.88 (82.23)
PUX(%)	94.80 (94.24)	93.25 (93.38)	90.69 (91.73)
X(%)	97.29 (95.66)	96.19 (95.45)	95.91 (95.04)
Rec(%)	87.63 (96.19)	86.46 (94.76)	88.57 (92.42)
PR($kg_{DBE}L_{adsorbent}^{-1}day^{-1}$)	5.04 (5.53)	4.97 (5.45)	5.09 (5.31)
DC($L_{adsorbent}kg_{DBE}^{-1}$)	13.51 (12.32)	13.38 (12.21)	12.73(12.23)

5.3. Mathematical Model

The mathematical model used in this work considers the intermittent behavior of the SMBR process, axial dispersion flow for bulk fluid phase; plug flow for solid phase, linear driving force (LDF) for the particle mass transfer rate, variation of the interstitial liquid phase velocity with the composition, and multicomponent adsorption equilibrium. Constant column length and packing porosity are also considered.

Bulk fluid mass balance to component i in column k:

$$\frac{\partial C_{ik}}{\partial t} + \frac{\partial (u_k C_{ik})}{\partial z} + \frac{(1-\varepsilon)}{\varepsilon}\frac{3}{r_p}K_{L,ik}\left(C_{ik} - \bar{C}_{p,ik}\right) = D_{ax,k}\frac{\partial^2 C_{ik}}{\partial z^2} \qquad (5.7)$$

where C_{ik} and $\bar{C}_{p,ik}$ are the bulk and the average particle concentrations in the fluid phase of component i in column k, respectively, $K_{L,ik}$ is the global mass transfer coefficient of component i, ε is the bulk porosity, t is the time variable, z is the axial

coordinate, $D_{ax,k}$ is the axial dispersion coefficient in column k, u_k is the interstitial velocity in column k, and r_p is the particle radius.

Pellet mass balance to component i in column k:

$$\varepsilon_p \frac{\partial \bar{C}_{p,ik}}{\partial t} + (1 - \varepsilon_p) \frac{\partial q_{ik}}{\partial t} = \frac{3}{r_p} K_{L.ik}(C_{ik} - \bar{C}_{p,ik}) + v_i \rho_p r(\bar{C}_{p,ik}) \tag{5.8}$$

where q_{ik} is the average adsorbed phase concentration of component i in column k in equilibrium with $\bar{C}_{p,ik}$, ε_p is the particle porosity, v_i is the stoichiometric coefficient of component i, ρ_p is the particle density and r is the chemical reaction rate given by:

$$r = k_c \frac{a_A a_B - \dfrac{a_C a_D}{K_{eq} a_A}}{\left(1 + K_{S,D} a_D\right)^2} \tag{5.9}$$

where a_i are the activities of the components calculated based on the average concentration into particle pores and using the UNIFAC method (Fredenslund et al., 1977), the equilibrium constant based on activities (Sanz et al., 2004), K_{eq}, the kinetic constant, k_c and the adsorption constant of water, $K_{S,D}$, were determined in a previous work (Graça et al., 2010) and are given by:

$$K_{eq} = 9.59 \times 10^{-3} exp\left(\frac{1755.3}{T(K)}\right) \tag{5.10}$$

$$k_c = 2.39 \times 10^9 exp\left(-\frac{6200.9}{T(K)}\right) \tag{5.11}$$

$$K_{S,D} = 2.25 \times 10^{-4} exp\left(\frac{3303.1}{T(K)}\right) \tag{5.12}$$

In order to describe the adsorption equilibrium, the multicomponent Langmuir isotherm was considered:

$$q_i = \frac{Q_i K_i \bar{C}_{p,i}}{1 + \sum_{j=1}^{NC} K_j \bar{C}_{p,j}} \tag{5.13}$$

where Q_i and K_i represent the total molar capacity per volume of resin and the adsorption constant for component i, respectively. The adsorption parameters were measured experimentally (Graça et al., 2010) and are presented in *Table 5.4*.

Table 5.4. Multicomponent Langmuir isotherm parameters at 25ºC

Component	Q(mol/L$_{wet\ solid}$)	K(L/mol)
1-Butanol	8.5	7.5
Acetaldehyde	15.1	0.5
Water	44.9	12.1
DBE	5.8	0.4

The global mass transfer coefficient (K_L) is given by:

$$\frac{1}{K_L} = \frac{1}{k_e} + \frac{1}{\varepsilon_p k_i} \tag{5.14}$$

where k_e and k_i are, respectively, the external and internal mass transfer coefficients to the liquid phase. The methods used to determine k_e and k_i are detailed presented in a previous work (Graça et al., 2010).

The variation of interstitial velocity with the concentration was considered and calculated using the total mass balance:

$$\frac{du_k}{dz} = -\frac{(1-\varepsilon)}{\varepsilon}\frac{3}{r_p}\sum_{i=1}^{NC} K_{L,ik} V_{mol,i}\left(C_{ik} - \bar{C}_{p,ik}\right) \tag{5.15}$$

where $V_{mol,i}$ is the molar volume of component i.

Initial and Danckwerts boundary conditions:

$$t = 0 \qquad\qquad C_{ik} = \bar{C}_{p,ik} = C_{ik,0} \tag{5.16}$$

$$z = 0 \qquad u_j C_{ik} - D_{ax,j}\left.\frac{\partial C_{ik}}{\partial z}\right|_{z=0} = u_j C_{ik,in} \tag{5.17}$$

$$z = L_C \qquad\qquad \left.\frac{\partial C_{ik}}{\partial z}\right|_{z=Lc} = 0 \tag{5.18}$$

From the mass balances at the nodes of the inlet and outlet lines of SMBR results:

For a column inside a section and for extract and raffinate nodes

$$C_{i2}(z = 0) = C_{i1}(z = L_C), C_{i4}(z = 0) = C_{i3}(z = L_C) \tag{5.19}$$

For the desorbent node

$$C_{i1}(z = 0) = \frac{u_4(z = L_C)}{u_1(z = 0)} C_{i4}(z = L_C) + \frac{u_D}{u_1(z = 0)} C_i^D \tag{5.20}$$

For the feed node

$$C_{i3}(z = 0) = \frac{u_2(z = L_C)}{u_3(z = 0)} C_{i2}(z = L_C) + \frac{u_F}{u_3(z = 0)} C_i^F \tag{5.21}$$

where,

$$u_1(z = 0) = u_4(z = L_C) + u_D \tag{5.22}$$

$$u_2(z = 0) = u_1(z = L_C) - u_X \tag{5.23}$$

$$u_3(z = 0) = u_2(z = L_C) + u_F \tag{5.24}$$

$$u_4(z = 0) = u_3(z = L_C) - u_R \tag{5.25}$$

The concept of TMBR can be used as an alternative in order to predict the SMBR process operation. In the TMBR model, the solid phase is assumed to move in opposite direction of the fluid phase, while the inlet and the outlet lines remain fixed. The equivalence between TMBR and SMBR models is made by keeping constant the liquid velocity relative to solid velocity, therefore, the liquid interstitial velocity in TMBR is given by:

$$u_j^{TMBR} = u_j^{SMBR} - u_s \tag{5.26}$$

where u_s is the solid interstitial velocity, that must be evaluated from the value of the switching time interval (t^*) of the SMBR model:

$$u_s = {L_C}/{t^*}$$

(5.27)

The ratio between the fluid interstitial velocity, u_j, and the solid interstitial velocity, u_s, could be defined for each section giving a new parameter:

$$\gamma_j = \frac{u_j}{u_s}$$

(5.28)

From *Equation 5.26*:

$$\gamma_j^* = \gamma_j + 1$$

(5.29)

where γ_j^* and γ_j are the ratio between fluid interstitial velocity and solid interstitial velocity in SMBR and TMBR, respectively,

Figure 5.5, *Figure 5.6*, and *Figure 5.7* present a comparison between the steady-state internal concentration profiles given by the TMBR model and the SMBR model. The simulation of both models was performed using the operation conditions given by *Table 5.2*.
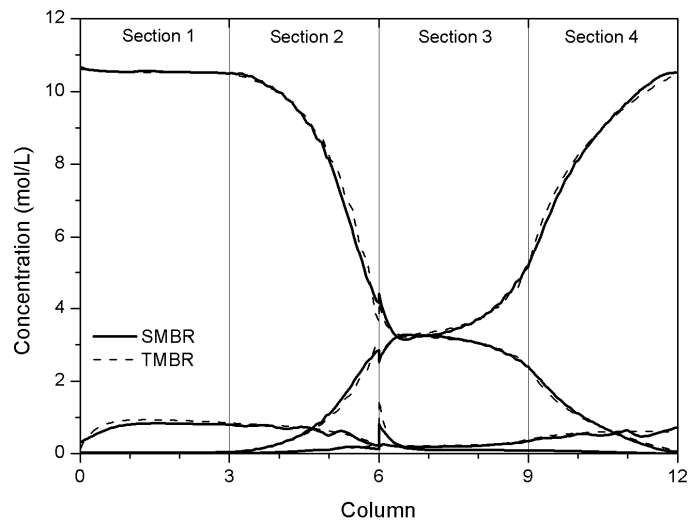
Figure 5.5. Comparison of the SMBR cyclic steady-state concentration profiles calculated by TMBR and SMBR (at 50% of switching time) models, for conditions of Run 1.
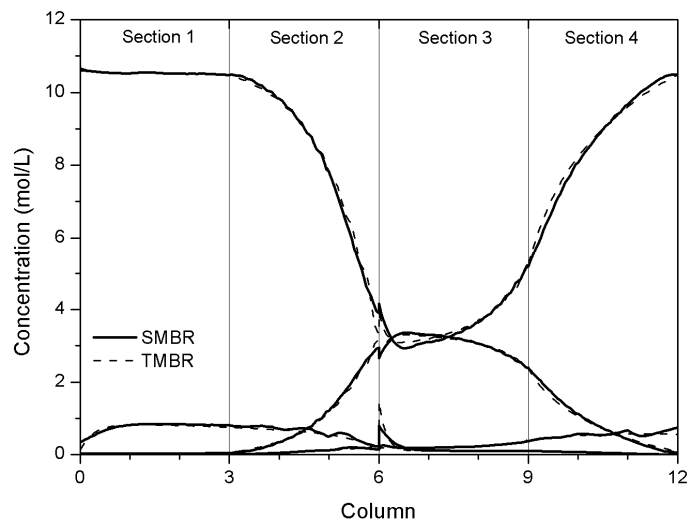
Figure 5.6. Comparison of the SMBR cyclic steady-state concentration profiles calculated by TMBR and SMBR (at 50% of switching time) models, for conditions of Run 2.
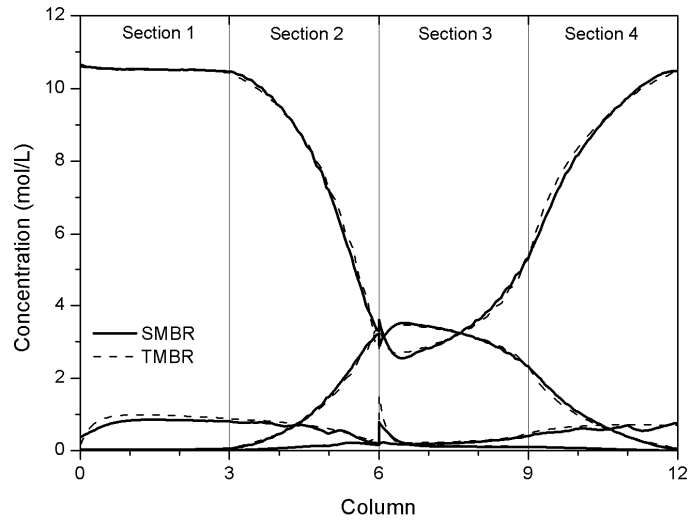
Figure 5.7. Comparison of the SMBR cyclic steady-state concentration profiles calculated by TMBR and SMBR (at 50% of switching time) models, for conditions of Run 3.

5.4. Reaction/Separation Regions

The correct choice of operating conditions is crucial for the successful operation of the SMBR chromatographic reactor. The equilibrium theory applied to non-reactive SMB can be used to determine the adequate operating conditions for SMBR case (Fricke et al., 1999, Sá Gomes et al., 2007) Neglecting axial dispersion and mass-transfer resistance, the constraints of SMBR operation in terms of interstitial velocity ratios (γ_j) are given by the following equations:

$$\gamma_1 > \frac{(1-\varepsilon)}{\varepsilon}\left(\varepsilon_p + \left(1-\varepsilon_p\right)\frac{q_{D1}}{\bar{C}_{p,D1}}\right) \tag{5.30}$$

$$\frac{(1-\varepsilon)}{\varepsilon}\left(\varepsilon_p + \left(1-\varepsilon_p\right)\frac{q_{C2}}{\bar{C}_{p,C2}}\right) < \gamma_2 < \gamma_3 < \frac{(1-\varepsilon)}{\varepsilon}\left(\varepsilon_p + \left(1-\varepsilon_p\right)\frac{q_{D3}}{\bar{C}_{p,D3}}\right) \tag{5.31}$$

$$\gamma_4 < \frac{(1-\varepsilon)}{\varepsilon}\left(\varepsilon_p + (1-\varepsilon_p)\frac{q_{C4}}{\overline{C}_{p,C4}}\right) \tag{5.32}$$

If the above constraints are met it is guaranteed that water (D) is preferentially carried by the liquid phase in section 1 and by the solid phase in the other sections; and DBE (C) is preferentially carried by the solid phase in section 4 and by the liquid phase in the other sections. Both sections 1 and 4 play a very important role in the SMBR operation. In section 1 the solid phase is regenerated by removing the adsorbed water. In section 4 the desorbent is cleaned by adsorbing the DBE. Considering diluted water or DBE in sections 1 and 4, respectively, the critical values of interstitial velocity ratios for these sections can be calculated:

$$\gamma_{1,min} = 6.860 \tag{5.33}$$

$$\gamma_{4,max} = 0.570 \tag{5.34}$$

The reaction/separation region defines the operation region in the γ_2-γ_3 plane where a minimum value of extract and raffinate purity is guaranteed. The reaction/separation region is located above the diagonal γ_2=γ_3, that corresponds to a zero feed flow rate, and above the horizontal branch γ_3=γ_4, that corresponds to a zero raffinate flowrate.

The algorithm for the construction of the reaction/separation region starts by setting a low value of the feed flow rate (0.01 mL/min) and γ_2=$\gamma_{4,max}$; the value of γ_2 is consecutively incremented by steps of 0.05. For each γ_2, the value of γ_3 is given by:

$$\gamma_3 = \frac{(1-\varepsilon)}{\varepsilon}\frac{Q_F}{Q_S} + \gamma_2 \tag{5.35}$$

Where the solid flowrate (Q_S) is given by:

$$Q_S = \frac{(1-\varepsilon)V_c}{t^*} \tag{5.36}$$

For each pair of (γ_2, γ_3) both extract and raffinate purities are calculated. When the last pair of (γ_2, γ_3) that guarantees the purity specifications is reached, the value of γ_2 is reinitiated and the feed flow rate is incremented by a step of 1 mL/min. This procedure is repeated until the maximum feed flow rate that guarantees the purity specification is reached. The reaction/separation region is constructed with the points where minimum purity requirement is achieved.

The minimum acetaldehyde conversion and extract and raffinate purities considered in this work were 95%. All the simulations of the SMBR unit used in the reaction/separation region construction were performed using the equivalent TMBR model.

5.5. Simulated Results

The simulations of the SMBR operation were performed by numerically solving the SMBR and TMBR mathematical models using the general Process Modeling System (gPROMS, version 3.1.5, www.psenterprise.com). The axial coordinate was discretized using the third-order orthogonal collocation in finite elements (OCFEM). The system of ordinary differential equations (ODE's), resulting from the axial discretization, was integrated over the time using DASOLV integrator implementation in gPROMS. For axial discretization were used twenty finite elements. All simulations used a fixed tolerance equal to 10^{-7}.

5.5.1. Effect of γ_1 and γ_4

In order to study the influence of the ratio between liquid and solid interstitial velocities in section 1 and section 4, reaction/separation regions were constructed for different values of γ_1 and γ_4, since the value of the switching time is fixed (t*=3.5 min) and the value of solid interstitial velocity is also fixed; therefore, the variations on γ_1 and γ_4 are due to variations on the liquid interstitial velocity in section 1 and section 4, respectively.

Figure 5.8 shows the influence of γ_1 on the reaction/separation region for a fixed value of $\gamma_4 = 0.385$. The size of the region increases with the increase of γ_1; however, the

position of the vertex point is poorly affected. The increase of the reaction/separation region size is due to for higher values of γ_1 it is possible to operate with higher values of γ_2 with extract flow rate high enough to remove water from the system, preventing the accumulation of water and consequently the contamination of the raffinate stream.
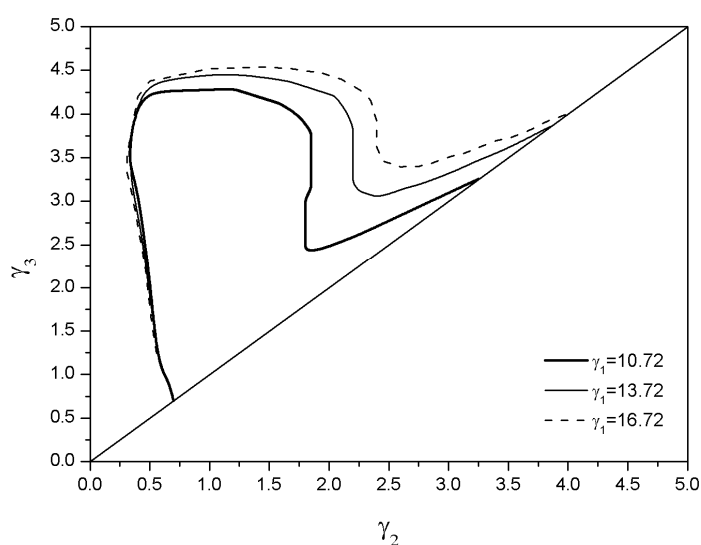
Figure 5.8. Reaction/separation regions for different values of γ_1 ($\gamma_4=0.385$, $t^*=3.5$ min and $x_{B,F}=0.3$).

For fixed values of γ_2, γ_3 and γ_4 the increase of γ_1 corresponds to the increase of both desorbent and extract flow rates. This increase allows a better adsorbent regeneration in section 1 and more water removed from the system; consequently, a best performance is achieved in terms of acetaldehyde conversion and purity for higher values of γ_1 (*Figure 5.9*).

The performance in terms of productivity is little affected by variations in γ_1; however, the desorbent consumption increases for higher values of γ_1 (*Figure 5.10*), since the desorbent flow rate should compensate the increase of the liquid flow rate in section 1.

The size and shape of the reaction/separation region are slightly affected by variations in γ_4 for a fixed value of $\gamma_1= 13.72$ (*Figure 5.11*). Nevertheless, the reduction of the liquid flow rate in section 4 implies a reduction in the liquid flow rate that enters in

section 1; therefore, since the value of γ_1 is fixed, the desorbent flow rate should increase with the decrease of γ_4.
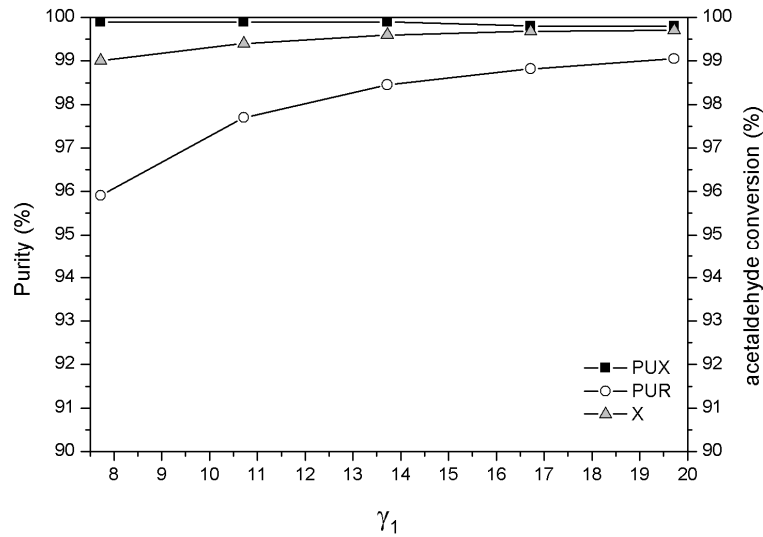
Figure 5.9. Acetaldehyde conversion, extract and raffinate purities for different values of γ_1 ($\gamma_2=1.0$, $\gamma_3=3.0$, $\gamma_4=0.385$, $t^*=3.5$ min and $x_{B,F}=0.3$).
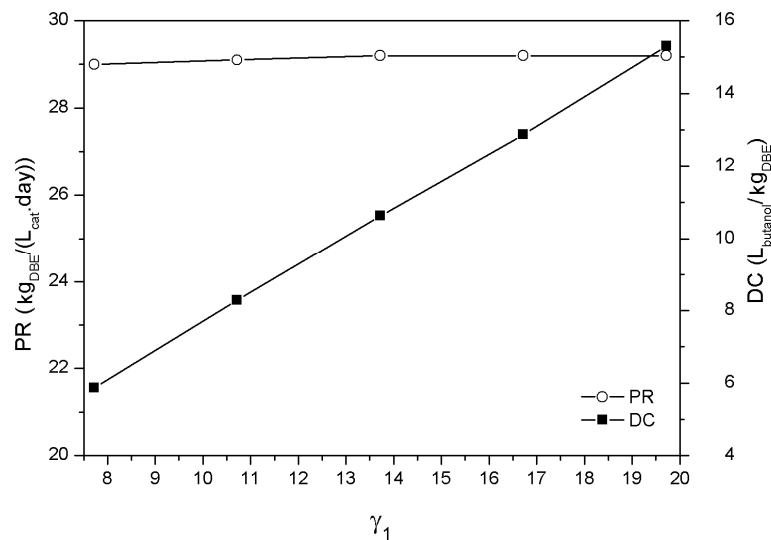
Figure 5.10. Effect of γ_1 in productivity and desorbent consumption ($\gamma_2=1.0$, $\gamma_3=3.0$, $\gamma_4=0.385$, $t^*=3.5$ min and $x_{B,F}=0.3$).
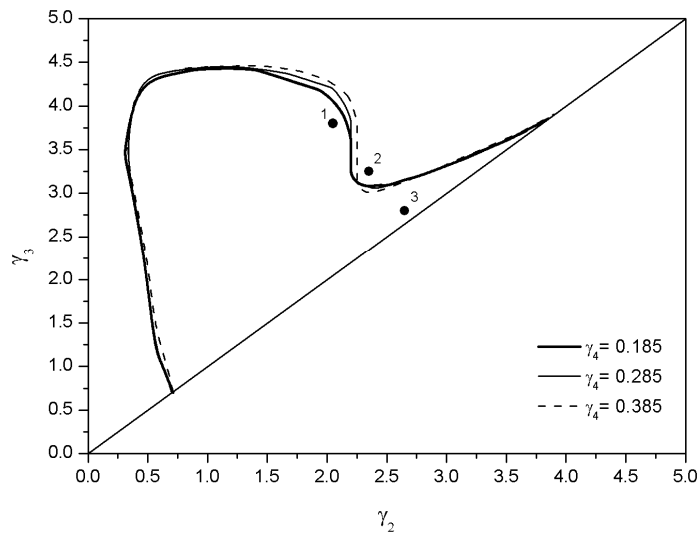
Figure 5.11. Reaction/separation regions for different values of γ_4 ($\gamma_1=13.72$, $t^*=3.5$ min and $x_{B,F}=0.3$).

Since the amount of DBE removed from the system by the raffinate stream increases for lower values of γ_4, the better performance in terms of extract purity is achieved for lower values of γ_4; the acetaldehyde conversion and raffinate purity are slightly affected by γ_4 (*Figure 5.12*).
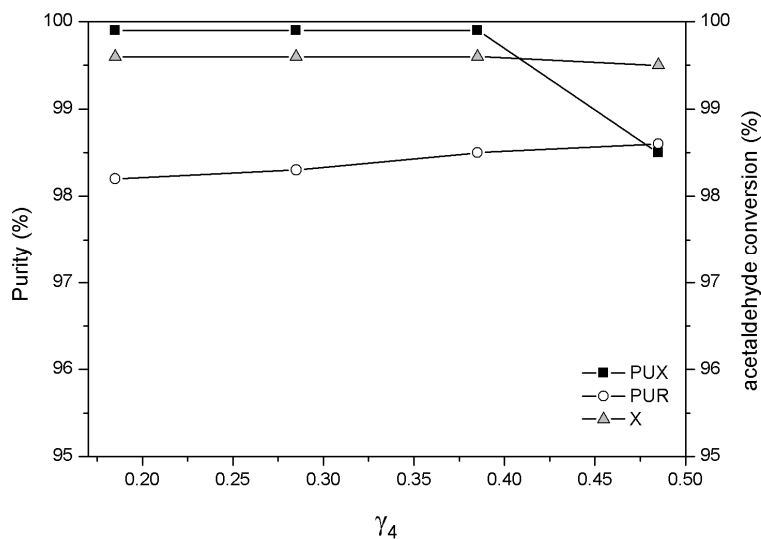
Figure 5.12. Acetaldehyde acetaldehyde conversion, extract and raffinate purities for different values of γ_4 ($\gamma_2=1.0$, $\gamma_3=3.0$, $\gamma_1=13.72$, $t^*=3.5$ min and $x_{B,F}=0.3$).

Figure 5.13 show that both productivity and desorbent consumption are almost not affected by variations on γ_4.
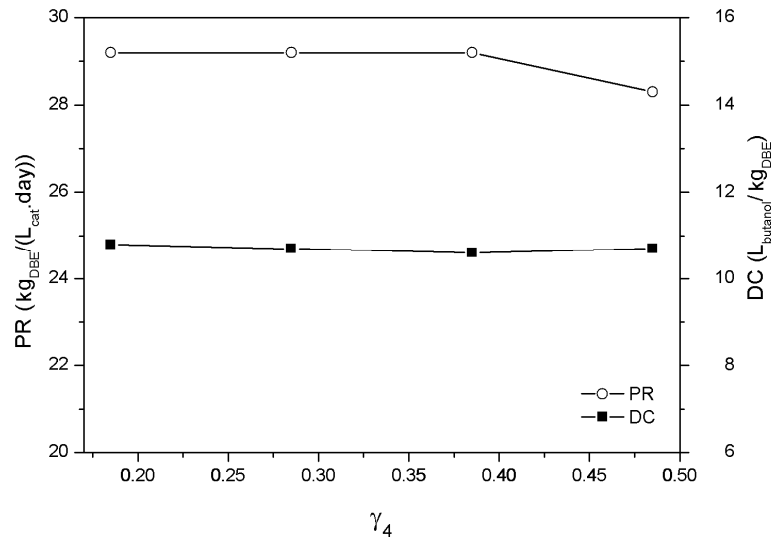
Figure 5.13. Effect of γ_1 in productivity and desorbent consumption ($\gamma_2=1.0$, $\gamma_3=3.0$, $\gamma_1=13.72$, t*=3.5 min and $x_{B,F}=0.3$).

The shape of the reaction/separation regions presented in *Figure 5.11* can be better understood looking at the internal concentration profiles of acetaldehyde (*Figure 5.14*a), DBE *(Figure 5.14*b) and water (*Figure 5.14*c) for three different points in the γ_2-γ_3 plane. The feed flowrate increases from point 3 to point 1 (*Figure 5.11*); however, only the point 2 is out of the reaction/separation region and this is due to contamination of the raffinate stream by water and acetaldehyde on point 2; on the other hand, on point 3 the contamination is compensated by a greater concentration of DBE on the raffinate stream.
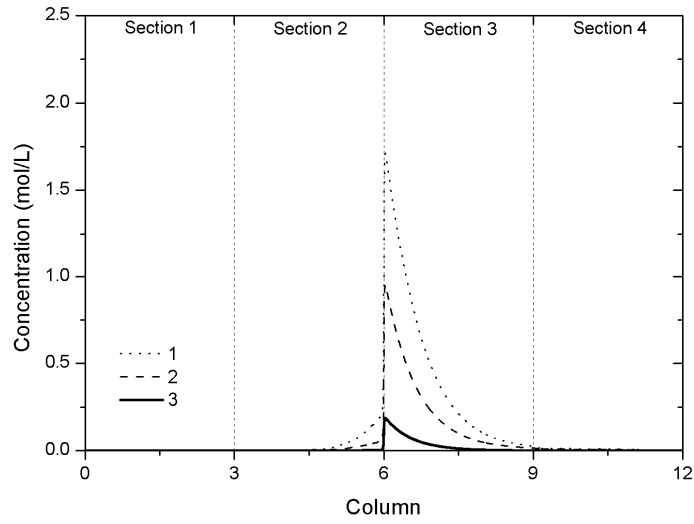
(a)
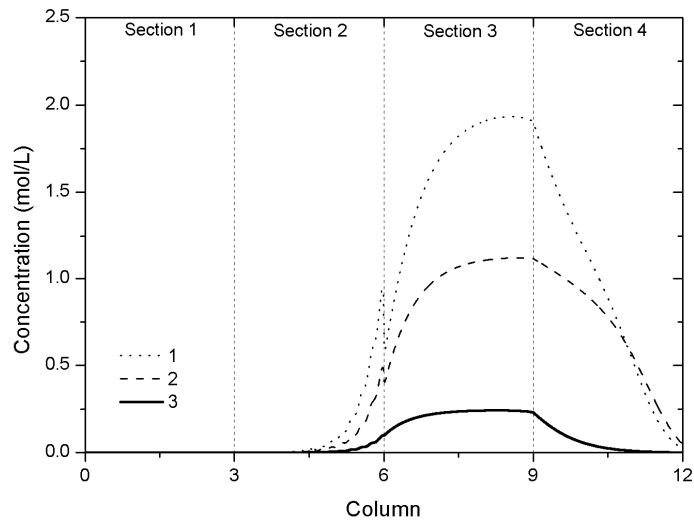
(b)
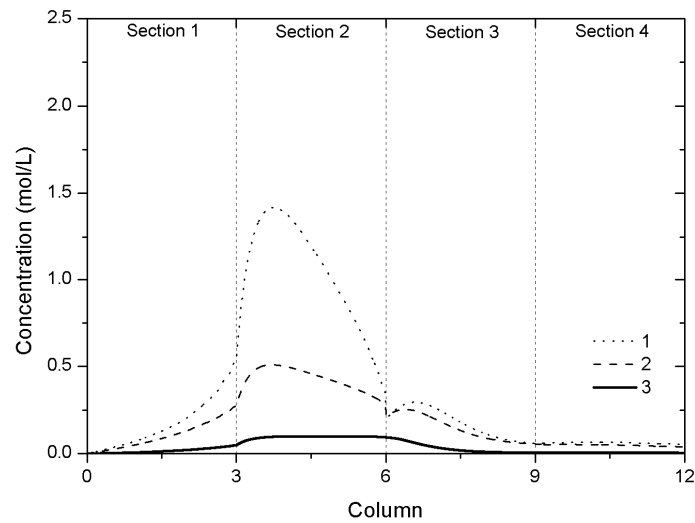
(c)

Figure 5.14. Internal concentration profiles calculated at the points 1, 2 and 3 of Figure 5.11. ($\gamma_1=13.72$, $\gamma_4=0.385$, $t^*=3.5$ min and $x_{B,F}=0.3$). (a) acetaldehyde, (b) DBE, (c) water

5.5.2. Effect of Feed Composition

Reaction/separation regions were constructed for different values of molar fraction in the feed stream. The values of γ_1 and γ_4 used were 13.72 and 0.385, respectively, the switch time was also fixed ($t^*=3.5$ min).

Figure 5.15 shows that the size and the shape of the reaction/separation regions were affected by variations in feed composition. However, it is worth noting that the interception of the reaction/separation region with the line $\gamma_2=\gamma_3$ is always the same for all feed concentrations considered; this fact is due to the decrease of feed flow rate as the operation point approaches to diagonal; therefore, when the distance of operating point from diagonal vanishes the feed flow rate tends to zero. Under this circumstance, the acetaldehyde that enters in the feed stream is immediately diluted and consumed by the large amount of desorbent. Consequently, for any feed composition the unit behavior approaches to a linear diluted system.
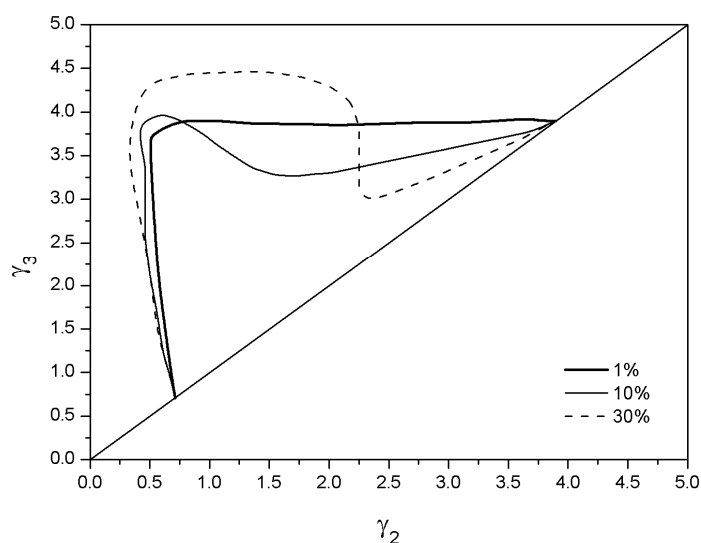
Figure 5.15. Reaction/separation regions for different values of acetaldehyde molar fraction in feed (γ_1=13.72, γ_4=0.385 and t*=3.5 min)

For acetaldehyde molar fraction between 1% and 30 % the position of the vertex point is displaced towards higher values of γ_3 with the increase of the acetaldehyde molar fraction; this can be explained by the more favorable sorption of acetaldehyde at higher concentrations (Lode et al., 2003); consequently, the increase of acetaldehyde in adsorbed phase leads to faster reaction kinetics and a slow propagation velocity of acetaldehyde; therefore, higher liquid flow rates in section 3 are allowable since acetaldehyde has a longer residence time for the reaction.

The separation/reaction regions were constructed for values of acetaldehyde molar fraction in feed below 30%, in order to ensure that 1-butanol is always the excess reactant. *Figure 5.16* shows that the increase of acetaldehyde molar fraction in feed could lead to a lack of 1-butanol in section 3; consequently, the conversion of acetaldehyde in section 3 is drastically reduced and the unconverted acetaldehyde is carried by the liquid phase contaminating the raffinate stream.
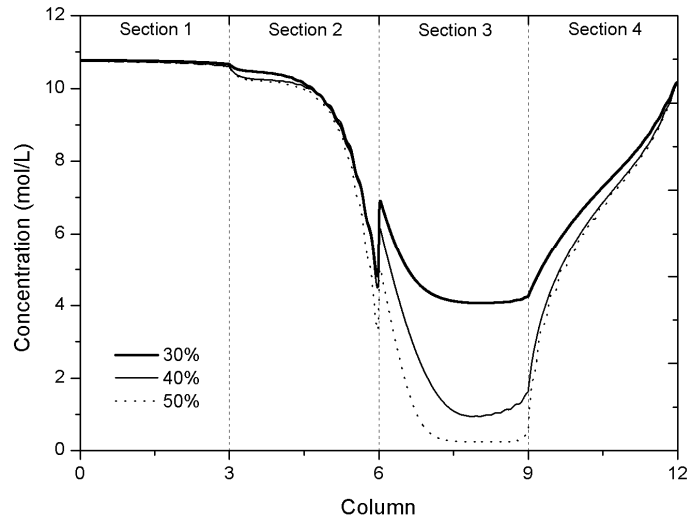
Figure 5.16. Concentration profiles for 1-butanol at steady state for different acetaldehyde molar fraction in feed (γ_2=1.0, γ_3=3.0, γ_1=13.72, γ_4=0.385 and t*=3.5 min).

Figure 5.17 shows the effect of the feed composition in the purity and desorbent consumption. The performance of the SMBR improves with the increase of acetaldehyde molar fraction.
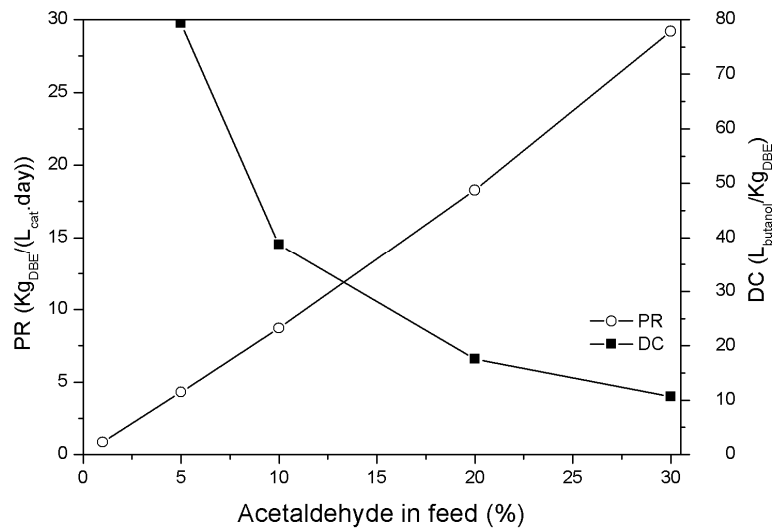
Figure 5.17. Purity and desorbent consumption for different acetaldehyde molar fraction in feed (γ_2=1.0, γ_3=3.0, γ_1=13.72, γ_4=0.385 and t*=3.5 min).

This improvement is due to the fact that for low acetaldehyde molar fraction the desorbent that enters in the feed is higher; consequently, higher values of desorbent consumption are obtained; also, the concentration of DBE in the raffinate increases with the increase of acetaldehyde molar fraction in feed (*Figure 5.18*); therefore, both productivity and desorbent consumptions are optimized when the acetaldehyde molar fraction in the feed is 30%.
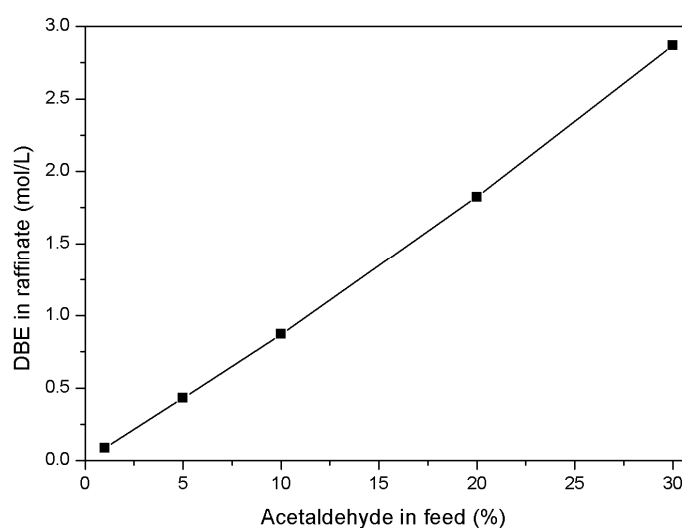
Figure 5.18. DBE concentration in raffinate for different acetaldehyde molar fraction ($\gamma_2=1.0$, $\gamma_3=3.0$, $\gamma_1=13.72$, $\gamma_4=0.385$ and $t^*=3.5$ min).

5.5.3. Effect of Switching Time

The effect of switching time in the reaction/separation region can be observed in *Figure 5.19*. The solid interstitial velocity decreases with the increase of switching time; therefore, for the same value of γ_j, the value of the liquid interstitial velocity in section j has to be smaller for high values of the switching time, in order to compensate the decrease of the solid interstitial velocity. Therefore, higher values of γ_2 and γ_3 are allowed for a long switching time, since the residence time in sections 2 and 3 increases with the decrease of liquid interstitial velocity.
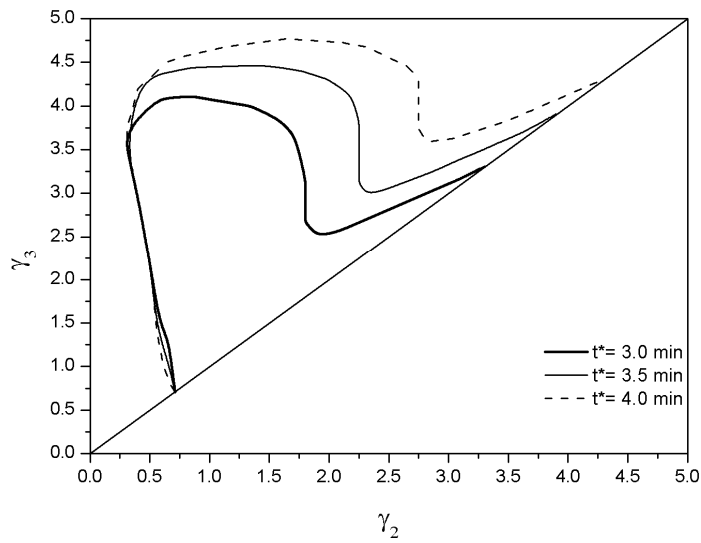
Figure 5.19. Reaction/separation regions for different values of switching time (γ_1=13.72, γ_4=0.385 and $x_{B,F}$=0.3).

In order to study the influence of the switching time in the performance parameters of the SMBR, it was simulated the SMBR operation for different switching times, considering an acetaldehyde molar fraction in feed of 30%, γ_2=1.0 and γ_3=3.0. The results are presented in *Figure 5.20*.
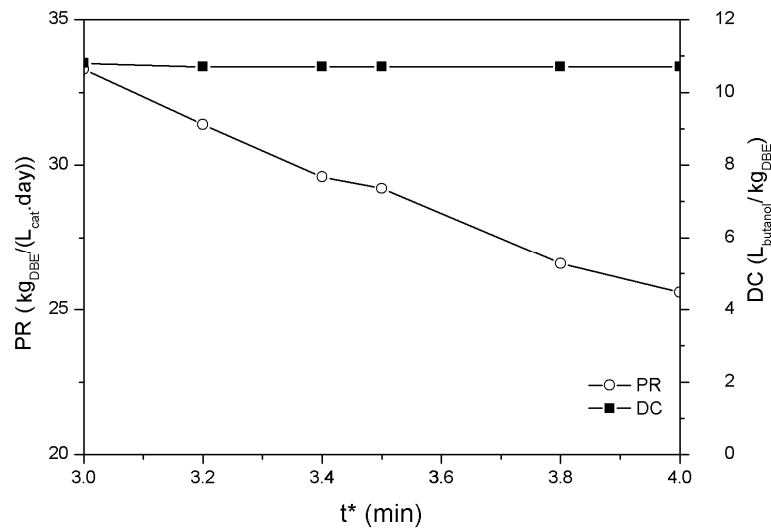
Figure 5.20. Purity and desorbent consumption for different values of switching time (γ_2=1.0, γ_3=3.0, γ_1=13.72, γ_4=0.385 and $x_{B,F}$=0.3).

It can be observed that the productivity decreases by increasing the switching time; this can be explained by the diminution of raffinate flow rate as consequence of the decrease of the liquid interstitial velocity for high values of the switching time. The desorbent consumption is just slightly affected by the switching time, in spite of the reduction of the liquid interstitial velocity for high values of the switching time and consequently a reduction in the desorbent flowrate is observed; this reduction is compensated by the decrease of the productivity.

5.5.4. Effect of Mass-Transfer Resistance

The effect of mass-transfer resistance in the performance parameters of the SMBR operation is presented in *Figure 5.21* and *Figure 5.22*. The value of the performance parameters were obtained by simulation for values of mass-transfer coefficient from ¼ until a value four times bigger than the value calculated by *Equation 5.14*. It can be observed that for mass transfer coefficients below the calculated by *Equation 5.14* all the performance parameters are worse. For mass-transfer coefficients above the calculated ones there is a slight improvement on the performance parameters, therefore, the increase of the mass-transfer coefficient, namely by decreasing the particle size, could lead to an improvement in the SMBR performance.
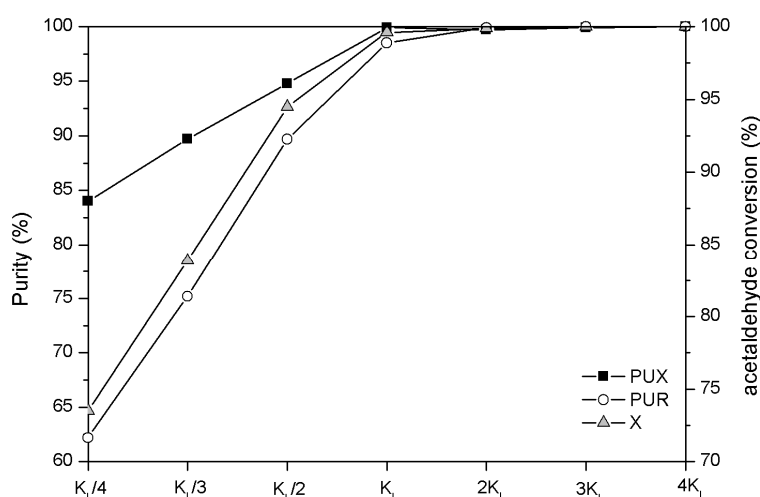
Figure 5.21. Effect of mass-transfer resistance in the purity and acetaldehyde conversion (γ_2=1.0, γ_3=3.0, γ_1=13.72, γ_4=0.385, t*=3.5 min and $x_{B,F}$=0.3).
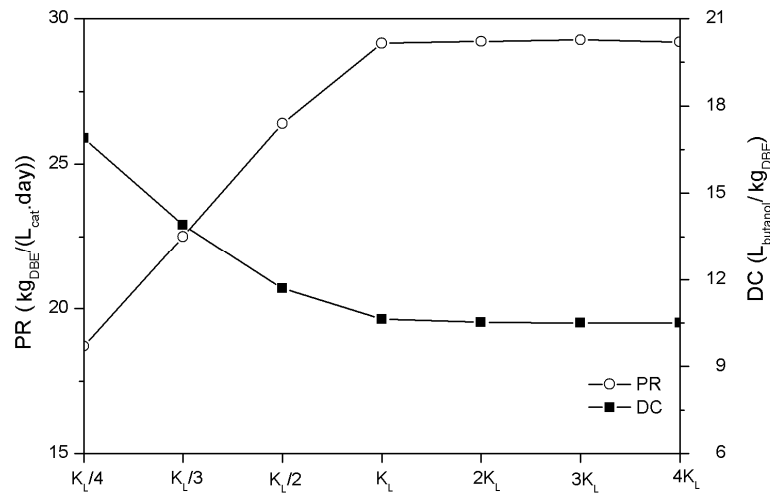
Figure 5.22. Effect of mass-transfer coefficient in the productivity and desorbent consumption ($\gamma_2=1.0$, $\gamma_3=3.0$, $\gamma_1=13.72$, $\gamma_4=0.385$, $t^*=3.5$ min and $x_{B,F}=0.3$).

Figure 5.23 shows that for the value of mass-transfer coefficient calculated by *Equation 5.14* and for a value two times bigger the acetaldehyde is totally consumed inside section 2 and section 3; however, for the higher value of mass-transfer coefficient higher values of feed flow rate could be used, keeping the acetaldehyde inside section 2 and section 3.
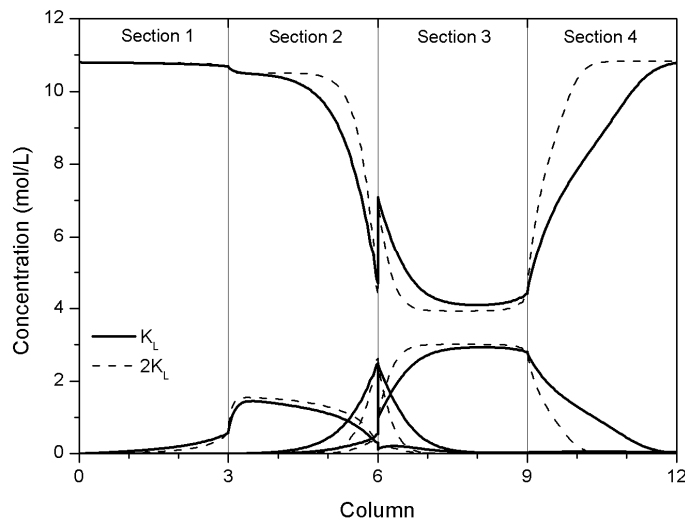
Figure 5.23. Internal SMBR concentration profiles for two different values of mass-transfer coefficients ($\gamma_2=1.0$, $\gamma_3=3.0$, $\gamma_1=13.72$, $\gamma_4=0.385$, $t^*=3.5$ min and $x_{B,F}=0.3$).

5.6. Conclusions

The synthesis of 1,1-dibutoxyethane was carried out by reacting 1-butanol and acetaldehyde, using Amberlyst-15 as catalyst/adsorbent, in a simulated moving bed reactor. The effect of working at conditions of incomplete adsorbent regeneration was verified on the experimental results; however, it was obtained a minimum conversion of 96% and the best raffinate purity of 85.1 %. The comparison between experimental and simulated data shows that both SMBR and TMBR provide a good representation of SMBR operation. The effect of different SMBR parameters on the SMBR performance and on the reaction/separation regions was studied. It was verified that feed composition is the parameter that most influences the best process performance (vertex point). The size of reaction/separation regions increases by increasing both γ_1 and switching time; however, this increase leads to a worse performance in terms of productivity and desorbent consumption. The study of the influence of mass-transfer resistance showed that no significant improvement in the SMBR performance is obtained by decreasing the mass transfer resistance.

5.7. Notation

a liquid phase activity

$\bar{C}_{p,i}$ average particle pore concentration, $\mathrm{mol\,dm^{-3}}$

C_i concentration, $\mathrm{mol\,dm^{-3}}$

D_{ax} axial dispersion, $\mathrm{dm^{-2}\,min}$

DC desorbent consumption, $\mathrm{L_{adsorbent}\,kg_{DBE}^{-1}}$

K adsorption constant, $\mathrm{dm^3\,mol^{-1}}$

k_c kinetic constant, $\mathrm{mol\,g_{cat}^{-1}\,min}$

k_e external mass-transfer coefficient, $\mathrm{dm\,min^{-1}}$

K_{eq} equilibrium constant

k_i internal mass-transfer coefficient, $\mathrm{dm\,min^{-1}}$

K_L global mass-transfer coefficient, dm min^{-1}

$K_{s,D}$ equilibrium adsorption constant

L_C SMBR column length, dm

PR   raffinate productivity, kg_{DBE} $L_{adsorbent}^{-1}$ day^{-1}

PUR   raffinate purity, %

PUX   extract purity, %

Q   adsorption capacity, mol dm^{-3}

q   solid phase concentration, mol dm^{-3}

r   reaction rate, mol g_{cat}^{-1} min

Rec   DBE recovery on raffinate, %

r_p particle radius, mm

t   time coordinate, min

t*   switching time, min

T   temperature, ºC

u   interstitial velocity, dm min^{-1}

u_s interstitial solid velocity, dm min^{-1}

V_m molar volume, dm^3 mol^{-1}

X   conversion of the limiting reactant

z   axial position, dm

Greek letters

γ ration between TMBR liquid and solid interstitial velocities, dimensionless

γ^* ration between SMBR liquid and solid interstitial velocities, dimensionless

ε bed porosity

ε_p particle porosity

ρ_p particle density, g dm^{-3}

υ   stoichiometric coefficient

Subscripts

D   relative to desorbent

F   relative to feed

i   relative to component (i= A, B, C, D)

k   relative to section (k= 1, 2, 3, 4)

R   relative to raffinate

X   relative to extract

0   relative to initial conditions

5.7. References

Agar D. W., "Multifunctional reactors: Old preconceptions and new dimensions", Chem. Eng. Sci. , 54(10), 1299-1305 (1999)

Agirre I., Barrio V. L., Güemez B., Cambra J. F. and Arias P. L., "Catalytic reactive distillation process development for 1,1 diethoxy butane production from renewable sources", Bioresour. Technol., In Press, Corrected Proof,

Bergeot G., Leinekugel-Le-Cocq D., Leflaive P., Laroche C., Muhr L. and Bailly M., "Simulated moving bed reactor for paraxylene production", Chem. Eng. Trans., 17, 87-92 (2009)

Berry W. W., Schemeda R. A. and Kibler H. S., "Device for Continuos Contacting of Fluids and Solids.", (1988)

Broughton D. B. and Gerhold C. G., "Continuous Sorption Process Employng FIxed Bed of Sorbent and Moving Inlets and Outlets.", (1961)

Capeletti M. R., Balzano L., De La Puente G., Laborde M. and Sedran U., "Synthesis of acetal (1,1-diethoxyethane) from ethanol and acetaldehyde over acidic catalysts", Appl. Catal., A, 198(1-2), L1-L4 (2000)

Dürre P., "Biobutanol: An attractive biofuel", Biotechnology Journal, 2(12), 1525-1534 (2007)

Ezeji T. C., Qureshi N. and Blaschek H. P., "Bioproduction of butanol from biomass: from genes to bioreactors", Curr. Opin. Biotechnol., 18(3), 220-227 (2007)

Fredenslund A., Gmehling J. and Rasmussen P., "Vapor-Liquid Equilibria Using UNIFAC", Elsevier, Amsterdam (1977)

Fricke J., Meurer M., Dreisörner J. and Schmidt-Traub H., "Effect of process parameters on the performance of a Simulated Moving Bed chromatographic reactor", Chem. Eng. Sci., 54(10), 1487-1492 (1999)

Gandi G. K., Silva V. M. T. M. and Rodrigues A. E., "Process development for dimethylacetal synthesis: Thermodynamics and reaction kinetics", Industrial and Engineering Chemistry Research, 44(19), 7287-7297 (2005)

Graça N. S., Pais L. S., Silva V. M. T. M. and Rodrigues A. E., "Oxygenated biofuels from butanol for diesel blends: Synthesis of the acetal 1,1-dibutoxyethane catalyzed by amberlyst-15 ion-exchange resin", Ind. Eng. Chem. Res, 49(15), 6763-6771 (2010)

Graça N. S., Pais L. S., Silva V. M. T. M. and Rodrigues A. E., "Dynamic Study of the Synthesis of 1,1- Dibutoxyethane in a Fixed-Bed Adsorptive Reactor.", Submited to Sep. Sci. Technol.), (2010)

Kawase M., Suzuki T. B., Inoue K., Yoshimoto K. and Hashimoto K., "Increased esterification conversion by application of the simulated moving-bed reactor", Chem. Eng. Sci., 51(11), 2971-2976 (1996)

Knothe G., Sharp C. A. and Ryan Iii T. W., "Exhaust emissions of biodiesel, petrodiesel, neat methyl esters, and alkanes in a new technology engine", Energy Fuels, 20(1), 403-408 (2006)

Lilja J., Murzin D. Y., Salmi T., Aumo J., Mäki-Arvela P. and Sundell M., "Esterification of different acids over heterogeneous and homogeneous catalysts and correlation with the taft equation", J. Mol. Catal. A: Chem., 182-183, 555-563 (2002)

Lode F., Houmard M., Migliorini C., Mazzotti M. and Morbidelli M., "Continuous reactive chromatography", Chem. Eng. Sci., 56(2), 269-291 (2001)

Lode F., Francesconi G., Mazzotti M. and Morbidelli M., "Synthesis of methylacetate in a simulated moving-bed reactor: Experiments and modeling", AIChE J. , 49(6), 1516-1524 (2003)

Mazzotti M., Kruglov A., Neri B., Gelosa D. and Morbidelli M., "A continuous chromatographic reactor: SMBR", Chem. Eng. Sci., 51(10), 1827-1836 (1996)

Moser B. R. and Erhan S. Z., "Branched chain derivatives of alkyl oleates: Tribological, rheological, oxidation, and low temperature properties", Fuel, 87(10-11), 2253-2257 (2008)

Prior J. M. V. and Loureiro J. M., "Residual thermodynamic properties in reactor modeling", Chem. Eng. Sci., 56(3), 873-879 (2001)

Sá Gomes P., Leão C. P. and Rodrigues A. E., "Simulation of true moving bed adsorptive reactor: Detailed particle model and linear driving force approximations", Chem. Eng. Sci., 62(4), 1026-1041 (2007)

Sainio T., Kaspereit M., Kienle A. and Seidel-Morgenstern A., "Thermal effects in reactive liquid chromatography", Chem. Eng. Sci., 62(18-20), 5674-5681 (2007)

Sanz M. T., Murga R., Beltrán S., Cabezas J. L. and Coca J., "Kinetic Study for the Reactive System of Lactic Acid Esterification with Methanol: Methyl Lactate Hydrolysis Reaction", Ind. Eng. Chem. Res. , 43(9), 2049-2053 (2004)

Silva V. M. T. M. and Rodrigues A. E., "Kinetic studies in a batch reactor using ion exchange resin catalysts for oxygenates production: Role of mass transfer mechanisms", Chemical Engineering Science, 61(2), 316-331 (2006)

Yadav G. D. and Pujari A. A., "Kinetics of acetalization of perfumery aldehydes with alkanols over solid acid catalysts", Can. J. Chem. Eng., 77(3), 489-496 (1999)

6. Thermal Effects in Non-Isothermal Operation of Adsorptive Reactors

The effect of temperature on the synthesis of 1,1-dibutoxyethane in a fixed-bed adsorptive reactor was studied by performing both adsorption/desorption and reaction/regeneration experiments at 15ºC and 35ºC. The Langmuir type isotherm parameters at 15ºC and 35ºC were obtained from the adsorption/desorption experiments. The reaction/regeneration experiments showed an increase in both conversion and productivity by increasing the temperature. Isothermal and non-isothermal mathematical models were used to simulate the reactor operation with different Damkhöler numbers. Simulated results suggest that the reactor productivity can be improved by using the adiabatic operation mode on fixed-bed adsorptive reactor. The effect of temperature on simulated moving bed adsorptive reactor performance was studied by simulation with both isothermal and non-isothermal mathematical models. Simulated results showed an improvement of SMBR performance with temperature. The SMBR performance can be also improved by using the adiabatic operation mode.

6.1. Introduction

Reactive separation techniques such as chromatographic reactors (Mazzotti et al., 1997) and reactive distillation (Taylor and Krishna, 2000) are commonly used for the conversion enhancement of reversible reactions. These integrated reaction/separation processes are a basic component of process intensification, which the main objective is to develop cheaper, safer and sustainable technologies by reducing the equipment volume, energy consumption and waste formation (Stankiewicz, 2003). The use of the autothermal reactor concept, where a hot reactor effluent is used to heat up a cold reactor feed until reaction temperature, is a common way to use the heat generated by an exothermic reaction to improve the reactor performance in terms of energy consumption (Kolios et al., 2000).

The acetal 1,1-dibutoxyethane (DBE) is produced by the liquid phase reaction of 1-butanol with acetaldehyde in acidic medium:

$$2 \times Butanol\ (A) + Acetaldehyde\ (B) \overset{H^+}{\Leftrightarrow} DBE\ (C) + Water\ (D)$$

This acetalization reaction is slightly exothermic (Graça et al., 2010) with $\Delta H_R = -14.59\ kJ\ mol^{-1}$.

When an exothermic reaction such as the DBE synthesis is carried out in a fixed bed adsorptive reactor or simulated moving bed adsorptive reactor there is continuous generation of heat due to the reaction enthalpy. The heat is also generated or consumed due to the enthalpies of adsorption and mixing. These effects should be considered in the process scale-up because the increase of the column diameter can render the system nearly adiabatic (Sainio et al., 2011). Moreover, Sanio et al.(Sainio et al., 2007) have shown that the conversions on the esterifications of acetic acid with methanol and ethanol, which are also slightly exothermic reactions, are significantly higher for the adiabatic operation mode. Therefore, the adiabatic operation of a fixed-bed adsorptive reactor could be used to improve the reactor performance.

The aim of this work is to study the influence of temperature on the isothermal operation of the fixed-bed adsorptive reactor for the synthesis of 1,1-dibutoxyethane

(DBE). The results obtained with non-reactive pairs allow the calculation of the adsorption parameters at different temperatures, adsorption enthalpies and the development of the non-isothermal model for the synthesis of DBE in a fixed-bed adsorptive reactor. Simulated results allow the comparison between isothermal and non-isothermal operation modes. The adsorption data obtained are used in the simulations of simulated moving bed adsorptive reactor with both isothermal and non-isothermal mathematical models.

6.2. Fixed-Bed Adsorptive Reactor

6.2.1. Experimental Section

The experimental work was performed in a laboratory-scale jacked glass column, packed with the sulfonic acid ion-exchange resin Amberlyst-15 (Silva and Rodrigues, 2002). A thermostatic bath was used to maintain the column at constant temperature during the experiments.

Table 6.1 presents the characteristics of the fixed-bed reactor.

Table 6.1. Characteristics of the Fixed-Bed Column

Solid weight	25 g
Length of the bed	12 cm
Internal diameter	2.6 cm
Radius of the particle	375 μm
Bed porosity[1]	0.36
Peclet number[1]	173
Bulk density	390 kg m^{-3}

[1](Graça et al., 2011)

The experimental concentration histories were obtained by gas chromatography analysis of small samples (1 mL), withdrawn at different times at the column outlet.

6.2.1.1.Adsorption/Desorption Experiments

The adsorption/desorption experiments were performed in a fixed-bed column at 15ºC and 35ºC. Each experiment begins after the column was saturated with pure 1-butanol. Then, the column is fed with non-reactive binary mixtures 1-butanol/water or 1-butanol/DBE until the saturation of the column with the feed mixture. After saturation, the column is regenerated by feeding pure 1-butanol.

At temperatures below 40ºC the binary mixture 1-butanol/water forms two liquid phases for water molar fractions above 0.5 (Graça et al., 2011). The formation of two liquid phases with different densities can lead to backmixing problems during the fixed-bed operation. Therefore, the adsorption/desorption experiments with the pair 1-butanol/water were performed using a water molar fraction below 0.5. *Table 6.2* and *Table 6.3* present the experimental conditions at 15ºC and 35ºC, respectively.

Table 6.2. Experimental conditions for adsorption/desorption with 1-butanol/water and 1-butanol/DBE at 15ºC.

	1-Butanol/water				1-Butanol/DBE			
Run	S1	R1	S2	R2	S3	R3	S4	R4
Q (mL min^{-1})	9.0	9.0	8.0	8.0	9.0	9.0	8.0	8.0
$C_{0,A}$ (mol L^{-1})	10.97	9.38	10.97	9.70	10.97	6.53	10.97	7.38
$C_{0,B}$ (mol L^{-1})	0	8.03	0	6.41	0	1.96	0	1.59
$C_{F,A}$ (mol L^{-1})	9.38	10.97	9.70	10.97	6.53	10.97	7.38	10.97
$C_{F,B}$ (mol L^{-1})	8.03	0	6.41	0	1.96	0	1.59	0

(A) 1-Butanol , (B) Water or DBE

Table 6.3. Experimental conditions for adsorption/desorption with 1-butanol/water and 1-butanol/DBE at 35ºC.

	1-Butanol/water				1-Butanol/DBE			
Run	S1	R1	S2	R2	S3	R3	S4	R4
Q (mL min^{-1})	9.0	9.0	8.0	8.0	9.0	9.0	8.0	8.0
$C_{0,A}$ (mol L^{-1})	10.77	7.6	10.77	9.55	10.77	6.36	10.77	7.22
$C_{0,B}$ (mol L^{-1})	0	9.29	0	6.24	0	1.9	0	1.53
$C_{F,A}$ (mol L^{-1})	9.29	10.77	9.55	10.77	6.36	10.77	7.22	10.77
$C_{F,B}$ (mol L^{-1})	7.6	0	6.24	0	1.9	0	1.53	0

(A) 1-Butanol , (B) Water or DBE

Hydrodynamic problems can also occur due to the difference of densities between adsorbed and desorbed components inside the column. These problems are avoided by using different flow direction in each experiment: when the desorbed component has density higher than the adsorbed component, the top-bottom flow direction is used; when the desorbed component has density lower than the adsorbed component, the bottom-top flow direction is used.

Figure 6.1 and *Figure 6.2* show the time evolution of reactor outlet concentration during adsorption/desorption experiments with 1-butanol/DBE and 1-butanol/water systems, respectively.
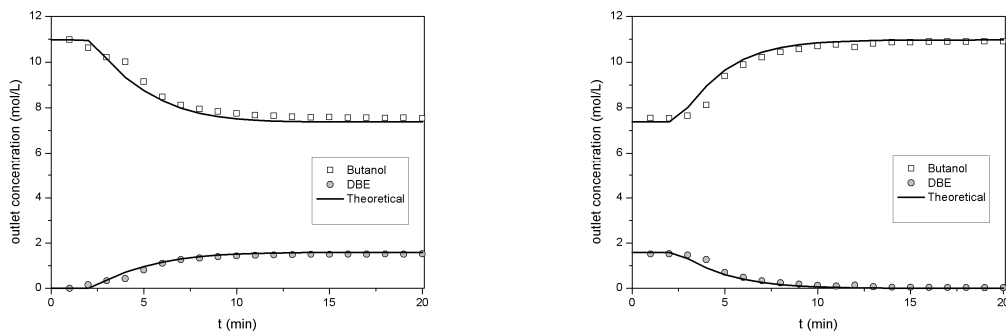
Figure 6.1. Reactor outlet concentration history during an adsorption/desorption experiment with 1-butanol/DBE at T=15ºC and Q= 8 mL min^{-1}.
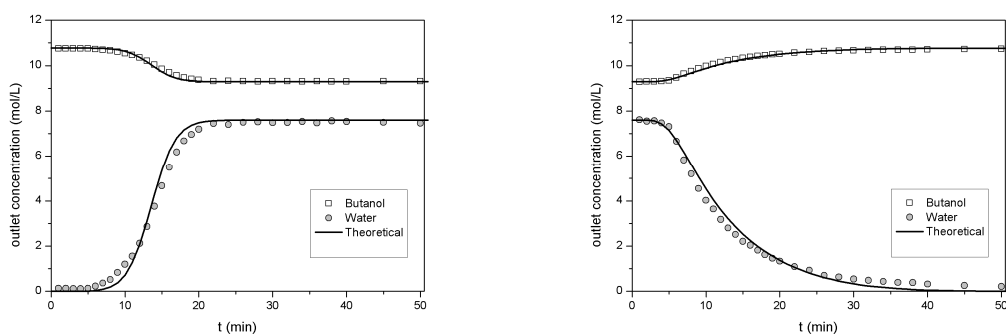
Figure 6.2. Reactor outlet concentration history during an adsorption/desorption experiment with 1-butanol/water at T=35ºC and Q= 9 mL min^{-1}.

The total amount of species retained/leaving the column (amount in interparticle space + amount in particle pores + amount adsorbed in solid phase) are experimentally calculated (See *Section 4.5*)

The multicomponent Langmuir isotherm (*Equation 6.1*) was used in this work in order to describe the adsorption equilibrium.

$$q_i = \frac{Q_i K_i C_{p,i}}{1 + \sum_{j=1}^{NC} K_j C_{p,j}} \tag{6.1}$$

The Langmuir isotherm parameters are optimized by minimizing the difference between experimental and theoretical values of moles adsorbed/desorbed. The experimental and theoretical values of moles adsorbed/desorbed in each experiment are presented in *Table 6.4* and *Table 6.5* (negative values represent the amount of desorbed component).

For all adsorption/regeneration pairs (S and R) of experiments the mass balance closes (number of moles adsorbed = number of moles desorbed) with an error lower than 2%.

Breakthrough experiments with acetaldehyde were not performed, because acetaldehyde reacts with itself to give an acetaldehyde trimer. Therefore, the adsorption parameters of acetaldehyde were determined by a best-fit procedure of the mathematical model with the experimental reaction data.

Table 6.4. Experimental and theoretical values for the number of moles adsorbed/desorbed at 15ºC.

Run	1-Butanol/water				1-Butanol/DBE			
	S1	R1	S2	R2	S3	R3	S4	R4
$n_{exp,A}$ (mol)	-0.192	0.188	-0.166	0.164	-0.173	0.171	-0.139	0.138
$n_{exp,B}$ (mol)	0.968	-0.955	0.839	-0.831	0.076	-0.076	0.061	-0.061
$n_{theo,A}$ (mol)	-0.192	0.192	-0.166	0.166	-0.175	0.175	-0.141	0.141
$n_{theo,B}$ (mol)	0.986	-0.986	0.850	-0.850	0.078	-0.078	0.063	-0.063
Δn_A (%)	-0.14	-2.28	0.16	-1.05	-1.38	-2.56	-1.51	-2.25
Δn_B (%)	-1.90	-3.29	-1.37	-2.35	-3.05	-3.05	-3.50	-3.50

(A) 1-Butanol , (B) Water or DBE

Table 6.5. Experimental and theoretical values for the number of moles adsorbed/desorbed at 35ºC.

Run	1-Butanol/water				1-Butanol/DBE			
	S1	R1	S2	R2	S3	R3	S4	R4
$n_{exp,A}$ (mol)	-0.176	0.177	-0.156	0.157	-0.165	0.165	-0.132	0.132
$n_{exp,B}$ (mol)	0.901	-0.902	0.799	-0.799	0.071	-0.071	0.057	-0.057
$n_{theo,A}$ (mol)	-0.177	0.177	-0.155	0.155	-0.169	0.169	-0.136	0.136
$n_{theo,B}$ (mol)	0.930	-0.930	0.814	-0.814	0.072	-0.072	0.058	-0.058
Δn_A (%)	-0.68	-0.11	0.43	1.06	-2.38	-2.38	-2.80	-2.80
Δn_B (%)	-3.18	-3.07	-1.93	-1.93	-1.64	-1.64	-1.84	-1.84

(A) 1-Butanol , (B) Water or DBE

The Langmuir isotherm parameters at 15ºC and 35ºC are presented in *Table 6.6.*

Table 6.6. Langmuir isotherm parameters at 15ºC and 35ºC.

	15ºC		35ºC	
	Q ($mol\ L_{solid}^{-1}$)	K ($L\ mol^{-1}$)	Q ($mol\ L_{solid}^{-1}$)	K ($L\ mol^{-1}$)
1-Butanol	8.8	7.8	8.4	7.2
Acetaldehyde	15.2	0.6	15	0.4
Water	45.0	12.9	44.0	11.4
DBE	6.0	0.8	5.0	0.1

Figure 6.3 presents the graphical representation of the monocomponent Langmuir isotherm for each component at different temperatures.

The different values of molar capacity, Q_i, for different components or for different temperatures are not in agreement with the theoretical foundations of the Langmuir isotherm; therefore, in this work, the Langmuir isotherm should be looked as an empirical description of the adsorption phenomena that satisfactorily represents the experimental data. Previous works showed that the Langmuir model can satisfactorily represent the experimental adsorption data on ion-exchange resins (Gandi et al., 2006, Graça et al., 2011, Silva and Rodrigues, 2002).
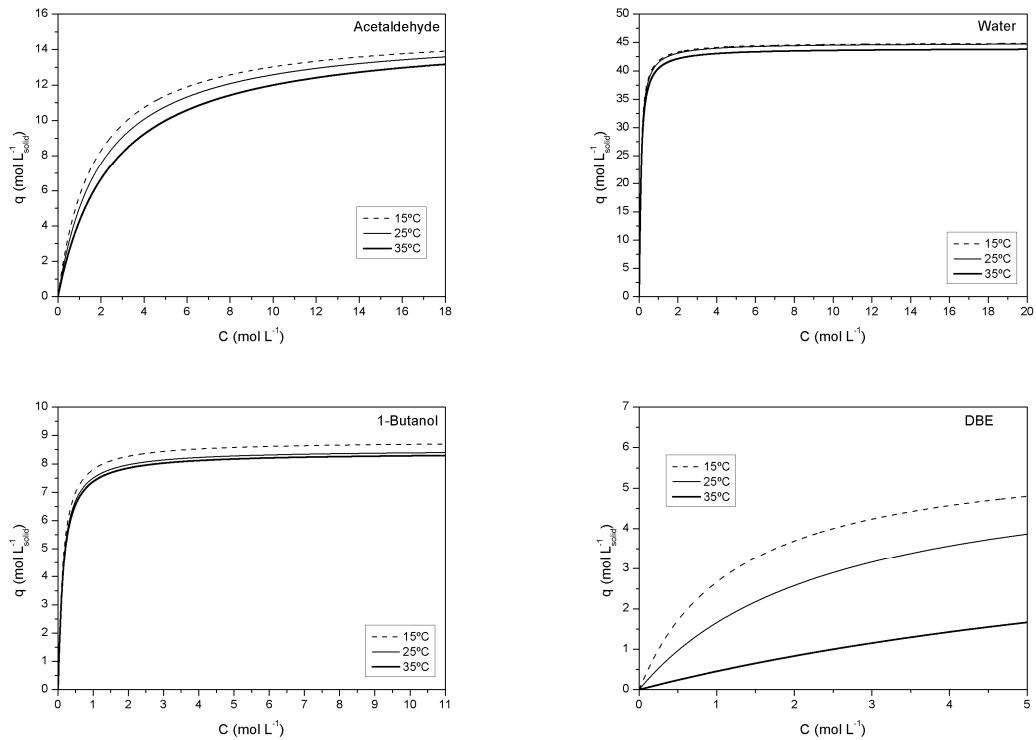
Figure 6.3. Monocomponent Langmuir isotherms at different temperatures.

6.2.1.2. Reaction Experiments

Reaction experiments were performed at 15ºC and 35ºC in a fixed-bed column; a binary mixture of 1-butanol/acetaldehyde was fed to the column previous saturated with 1-butanol, the column outlet concentration was determined by collect and analyse small samples (1 mL) at different times. After each reaction the column was regenerated with pure 1-butanol.

Figure 6.4 and *Figure 6.5* show the time evolution of concentration of the column outlet during reaction and regeneration at 15ºC and 35ºC, respectively.
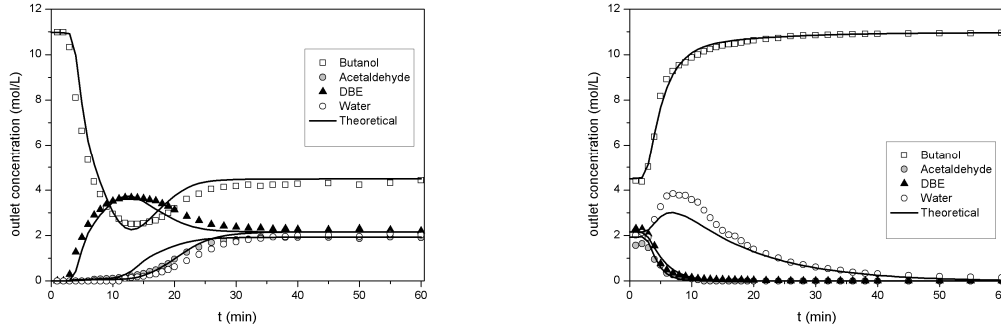
Figure 6.4. Concentration histories in a fixed-bed adsorptive reactor, reaction (left) and regeneration (right) experiments. Q= 8 mL min^{-1} and T=15ºC
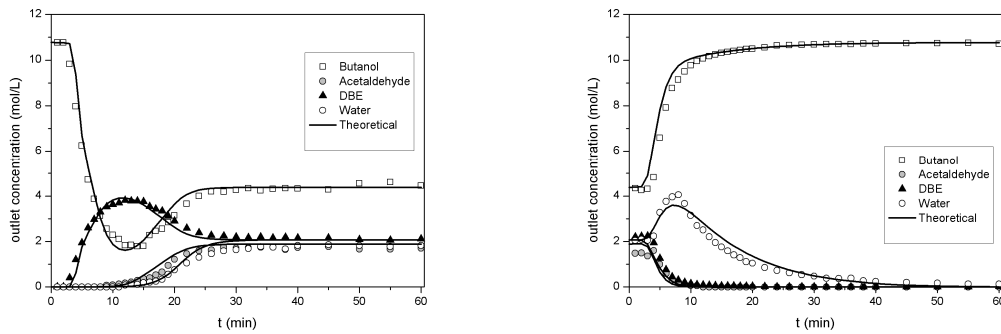
Figure 6.5. Concentration histories in a fixed-bed adsorptive reactor, reaction (left) and regeneration (right) experiments. Q= 8 mL min^{-1} and T=35ºC

Conversion (*Equation 6.2*) and productivity (*Equation 6.3*) were calculated in order to evaluate and compare the fixed-bed reactor performance. The conversion was calculated based on unreacted amount of acetaldehyde eluted in both reaction and regeneration steps. The productivity was calculated based on the amount of DBE (n_C) that can be collected with a purity (*Equation 6.4*) above 95%.

$$X = \frac{C_{B,F}t_{feed} - \int_0^{t_{end}} C_{B,out}(t)dt}{C_{B,F}t_{feed}} \qquad (6.2)$$

$$PR = \frac{n_C}{tw_{cat}}\bigg|_{PUR>0.95} \qquad (6.3)$$

$$PUR = \frac{C_{C,out}}{C_{B,out} + C_{C,out} + C_{D,out}}$$

(6.4)

Table 6.7 shows the experimental performance results at two different temperatures and two different flowrates. It can be seen that conversion increases by increasing the temperature and decreases by increasing the flowrate. This can be explained based on the combination of two factors, the increase of reaction rate with the increase of temperature and the decrease of reactants residence time with the increase of flowrate, i.e., at low temperature (low reaction rate) a longer reactant residence time (low flowrate) is required in order to ensure a high reactant conversion.

Table 6.7. Experimental conversion and productivity for the fixed-bed adsorptive reactor.

	15°C		35°C	
Q (mL min^{-1})	8	9	8	9
X(%)	64.28	62.77	65.36	62.90
PR(mol hr^{-1} kg^{-1})	49.57	57.39	52.17	57.39

The Damkhöler number expressed by *Equation 6.5* represents the ratio between reactant mean residence time and reaction characteristic time.

$$Da = \frac{(1 - \varepsilon)\rho_b L_c \Re_0}{u_0 C_{B,F}}$$

(6.5)

where $\Re_0$ and $C_{B,F}$ are the reaction rate and acetaldehyde concentration at reactor inlet conditions, respectively.

The simulated results were obtained considering the same reaction and regeneration times used in reaction/regeneration experiments (60 min for each step)

The effect of Da on conversion at three different temperatures is shown in *Figure 6.6*. It can be observed that at sufficiently high values of Da the conversion is always higher for lower temperatures. This fact is due to for high values of Da the residence time of the reactant is higher as compared with reaction characteristic time, and therefore, the conversion depends mainly on the chemical equilibrium position. Since K_{eq} decreases with the increase of temperature (exothermic reaction) the conversion will be lower at high temperatures. However, at low temperatures the low reaction rate has to be compensated by using a low feed flowrate or a bigger column length in order to obtain high values of Da. Consequently, the productivity of the fixed-bed adsorptive reactor could decrease in such conditions.
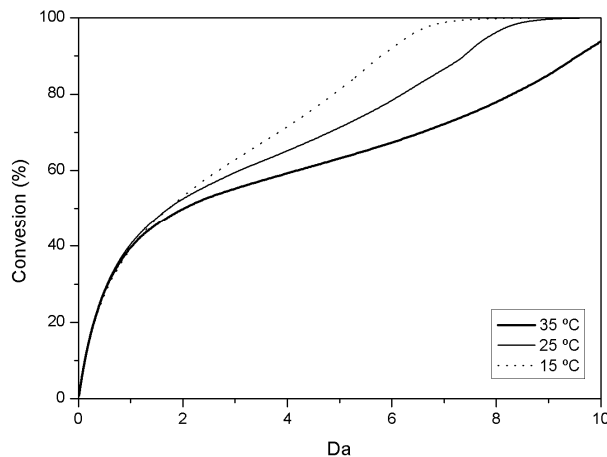
Figure 6.6. Simulated values of conversion as function of Damköhler number.

Figure 6.7 shows the influence of Da on fixed-bed adsorptive reactor productivity at three different temperatures. If the value of Da is too small, that corresponds to use a high value of feed flowrate or a small column length, the small amount of DBE produced due to low reactant residence time is rapidly contaminated with the great amount of unreacted acetaldehyde or desorbed water, consequently, the purity restriction is not achieved. For sufficiently high values of Da it is possible to obtain DBE in the column outlet within the minimum purity restriction. The maximum productivity is obtained for the three temperatures at the same Da≈2.7. However, the best productivity is obtained at 35ºC, since the greater reaction rate allows processing a

higher feed flowrate. It can be noticed at 35ºC a rapid decrease of productivity for values of Da bellow 2.7. This can be explained by the favourable effect of the high temperatures in water desorption, therefore, at sufficiently high flowrate or small column length (low Damkhöler), the desorbed water contaminates the column outlet in a short period of time.
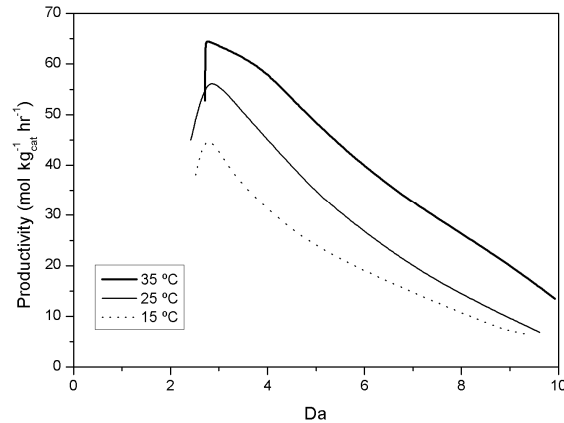
Figure 6.7. Simulated values of productivity as function of Damkhöler number.

6.2.2. Mathematical Model

In order to simulate the adiabatic operation of the fixed-bed adsorptive reactor, it was used a non-isothermal model that results from coupling the mass balances (See *Section 4.3*) with the following energy balances:

Fluid phase energy balance:

$$\rho_L C_p^L \left(\frac{\partial T}{\partial t} + u \frac{\partial T}{\partial z} \right) + h_L \frac{3}{r_p} \frac{(1 - \varepsilon)}{\varepsilon} (T - T_S) + \frac{U_W}{\varepsilon} \frac{4}{d_C} (T - T_W) = \lambda_e \frac{\partial^2 T}{\partial z^2} \qquad (6.6)$$

Solid phase energy balance:

$$\frac{3}{r_p} h_L (1 - \varepsilon)(T - T_s)$$

$$= \alpha \rho_L C_p^L \frac{\partial T_s}{\partial t} - (1 - \varepsilon)(1 - \varepsilon_p) \sum_{i=1}^{n} \left(-\Delta H_i^{ads}\right) \frac{\partial \bar{q}_i}{\partial t} \qquad (6.7)$$

$$- \rho_b \Re\left(\bar{C}_{p,i}\right)\left(-\Delta H^R\right)$$

Initial and Danckwerts boundary conditions:

$$t = 0 \qquad T = T_s = T_F \qquad (6.8)$$

$$z = 0 \qquad uT - D_{ax,h} \left.\frac{\partial T}{\partial z}\right|_{z=0} = uT_F \qquad (6.9)$$

$$z = L_c \qquad \left.\frac{\partial T}{\partial z}\right|_{z=L_c} = 0 \qquad (6.10)$$

The parameter α represents the heat capacity ratio between particle and liquid phases:

$$\alpha = \frac{\rho_b C_p^p}{\rho_L C_p^L} \qquad (6.11)$$

In the case of ion-exchange resins and common liquids, the heat capacity ratio is close to unity (Sainio et al., 2007).

In this model was considered that the heat is generated by the reaction and by the adsorption of species, and the consumption of heat is due to desorption of species. Previous work (Graça et al., 2010) showed that the reaction of DBE synthesis is

exothermic with $\Delta H^R = -14593.6$ J mol^{-1}. The isosteric heat of adsorption, ΔH_i^{ads}, is determined by the Clausius-Clapeyron equation (*Equation 6.12*).

$$\Delta H_i^{ads} = R \left(\frac{\partial \ln C_i}{\partial \left(1/T \right)} \right)_q \tag{6.12}$$

The variation of ΔH_i^{ads} with catalyst loading for each component is presented in *Figure 6.8.*
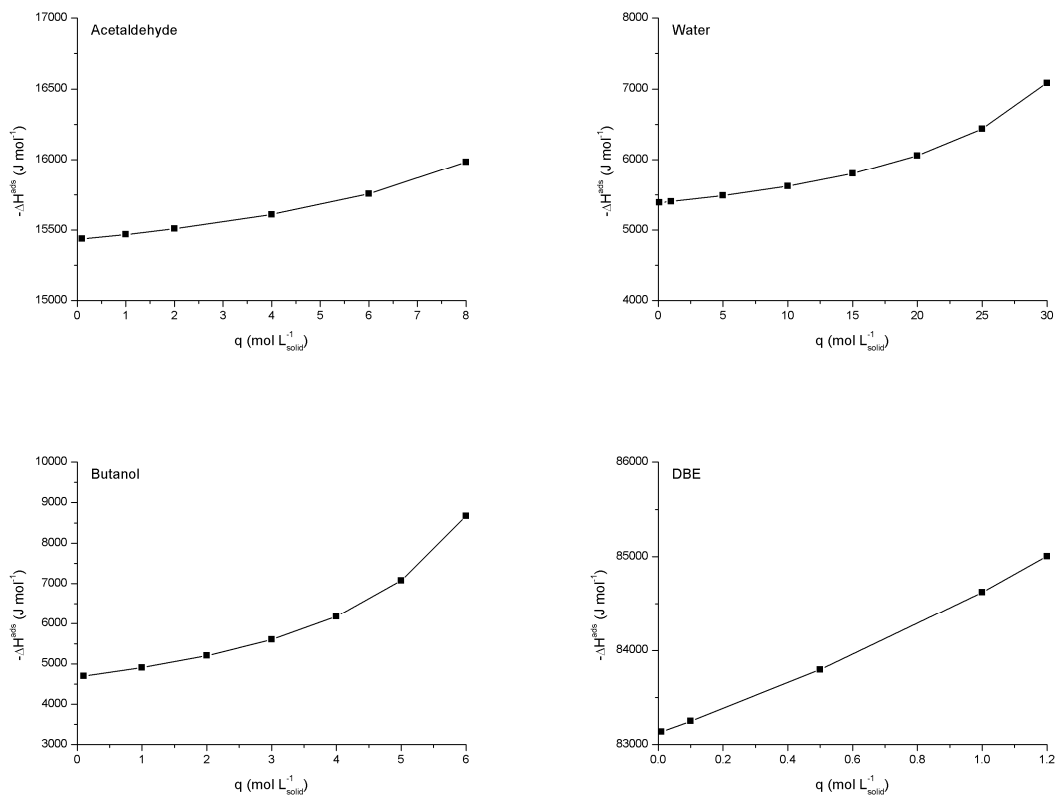
Figure 6.8. Isosteric heat adsorption for different values of catalyst loading.

The temperature dependency of K_i is described with a Van't Hoff type of relation (*Equation 6.13*) using enthalpy of adsorption (*Table 6.8*)

$$K_i = K_i^{ref} exp\left[\frac{-\Delta H_i^{ads}}{R}\left(\frac{1}{T} - \frac{1}{T^{ref}}\right)\right] \tag{6.13}$$

Table 6.8. Enthalpy of adsorption.

Component	ΔH_i^{ads} (J mol^{-1})
1-Butanol	-6961.5
Acetaldehyde	-15802.4
Water	-6379.3
DBE	-84533.3

The liquid-particle heat-transfer coefficient, h_L, was estimated using the Chilton-Colburn analogy and the Wilson and Geankopolis correlation(Ruthven, 1984).

$$Nu_p = \frac{1.09}{\varepsilon}\left(Re_p Pr\right)^{0.33} \tag{6.14}$$

where $Nu_p = h_L d_p/\lambda_L$ and $Re_p = \rho d_p u_0/\eta$ are, respectively, the Nusselt and Reynolds numbers, relative to particle and $Pr = \eta C_p^L/\lambda_L$ is the Prandtl number.

The liquid phase thermal conductivity, λ_L, was estimated by the equation proposed by Sato-Riedel (Reid et al., 1987) extended to liquid mixtures (Pandey et al., 2007).

$$\lambda_L = \frac{\left(\frac{1.11}{\sum x_i M_i}\right)\left[3 + 20\left(1 - \frac{T}{\sum x_i T_{ci}}\right)^{2/3}\right]}{\left[3 + 20\left(1 - \frac{\sum x_i T_{bi}}{\sum x_i T_{ci}}\right)^{2/3}\right]} \tag{6.15}$$

where T_{bi} and T_{ci} are the normal boiling point and the critical temperature of component i.

The effective axial thermal conductivity, λ_e, was estimated from the analogy between mass and heat transfer ($Pe_m = Pe_h$) (Julcour et al., 1999, Julcour et al., 2002), where $Pe_m = uL_c/D_{ax}$ and $Pe_h = uL_c\rho_L C_p^L/\lambda_e$.

6.2.3. Simulated Results

The effect of the heat exchange between the reactor bed and the reactor jacket was studied by simulation of the fixed-bed reactor operation for different values of overall heat transfer coefficient on the reactor wall (U_W). *Figure 6.9* shows the outlet temperature during a reaction/regeneration experiment (regeneration step begins at t=60 min). It can be noticed high variations on the outlet temperature of U_W=0 (adiabatic operation).
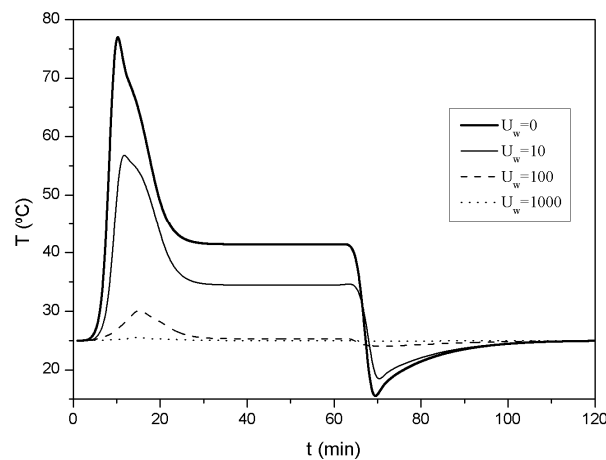
Figure 6.9. Simulated time evolution of reactor outlet temperature during a reaction/regeneration experiment for different values of overall heat exchange coefficient. (T_0=25ºC, Q=8 mL min^{-1} and $C_{F,B}$= 3.92 mol L^{-1})

These variations become smaller with the increase of U_W due to the increase of the heat transfer between the reactor bed and the jacket, for a sufficiently high value of overall heat transfer coefficient (U_W=1000) isothermal operation can be considered. During the reaction step (between t=0 and t=60 min) a positive variation on temperature, relatively

to reactor initial temperature (25ºC), occurs mainly due to the heat generated inside the reactor by the exothermic reaction; during the regeneration step (between t=60 and t=120 min) a negative variation on temperature, relatively to reactor initial temperature, occurs mainly due to the endothermic desorption of water.

In order to better understand the temperature evolution inside the reactor, the temperature history at three different positions inside the reactor column was simulated considering adiabatic operation (see *Figure 6.10*). These results show the development of a thermal wave that grows stronger as it travels along the reactor. This self-amplifying nature indicates that the temperature front travels with approximately the same velocity of the reaction front. The increase of temperature at reaction front leads to a higher reaction rate, which further increases the temperature, due to the exothermic nature of reaction.
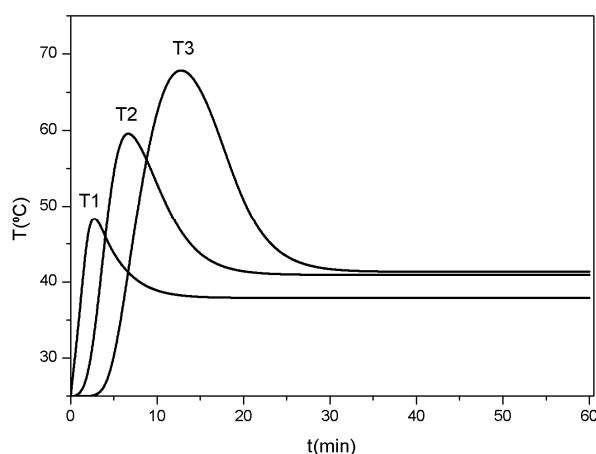
Figure 6.10. Temperature histories at three different column positions ($T_1=0.2$ cm, $T_2=0.8$ cm and $T_3=1.2$ cm) during a reaction feed step. (T=25ºC, Q=8 mL min^{-1} and and $C_{F,B}$= 3.92 mol L^{-1})

Figure 6.11 shows the simulated results of productivity for different values of overall heat transfer coefficient (U_W). The results obtained show that the best performance in terms of productivity is obtained using the adiabatic operation mode (U_W=0). The best performance for the adiabatic operation is due to the increase of reaction rate; therefore, higher values of feed flowrate (low Damkhöler number) could be used leading to higher values of productivity.
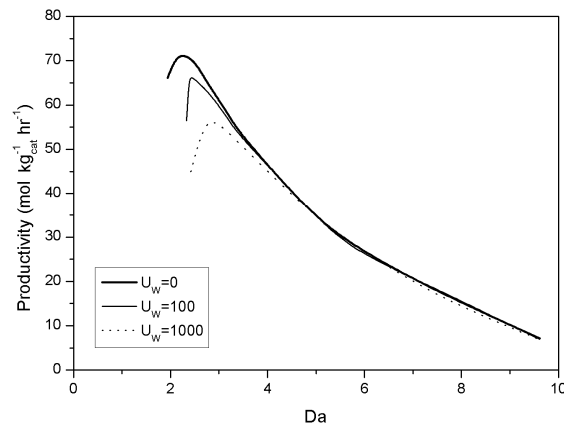
Figure 6.11. Effect of overall heat exchange coefficient on reactor productivity. $T=25^oC$, $Q=8$ mL min^{-1} and $C_{F,B}= 3.92$ mol L^{-1})

6.3. Simulated Moving Bed Adsorptive Reactor

The effect of temperature on the isothermal operation of the simulated moving bed (SMB) adsorptive reactor is studied by simulation with the isothermal True Moving Bed (TMB) adsorptive reactor model (*see Section 5.3*). The effect of temperature in the reaction/separation regions is shown in *Figure 6.12*. The size of the reaction/separation regions increases with the increase of temperature.
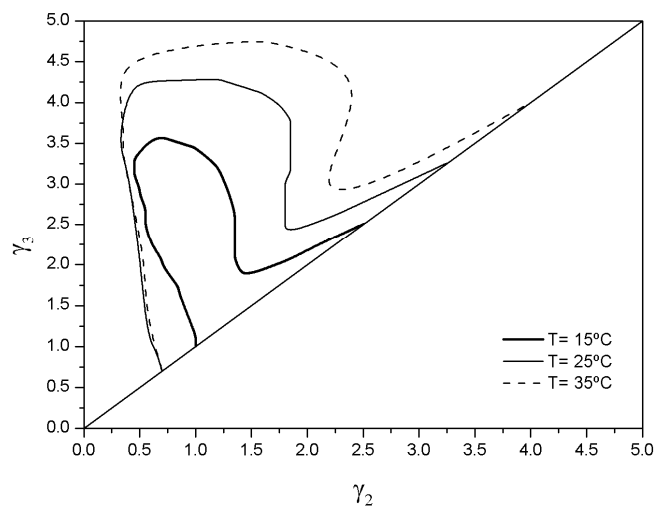
Figure 6.12. Reaction/separation Regions at different temperatures ($\gamma_1=10.72$, $\gamma_4=0.385$, t*=3.5 min and $x_{B,F}=0.3$) .

The increase of temperature allow the use of higher flowrates in sections 2 and 3 since the increase of reaction rate with temperature avoids the contamination of the raffinate stream with unconverted acetaldehyde (*Figure 6.13a*). Due to the increase of acetaldehyde conversion the production of DBE and water also increases. However, the increase of temperature improve the regeneration of solid phase in section 4 due to the exothermic nature of the adsorption, therefore, the amount of water removed from the system by the extract stream increases (*Figure 6.14*) reducing the total amount of water inside the reactor (*Figure 6.13c*).
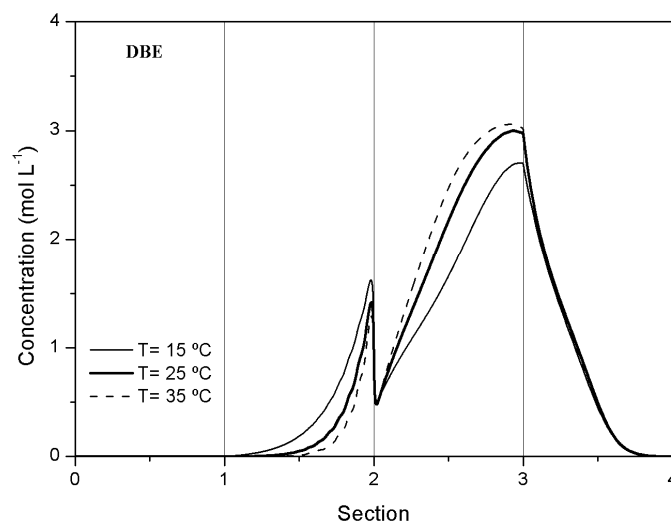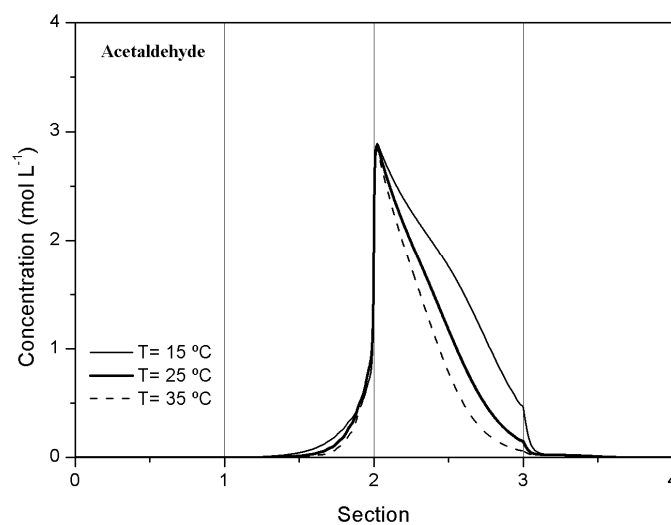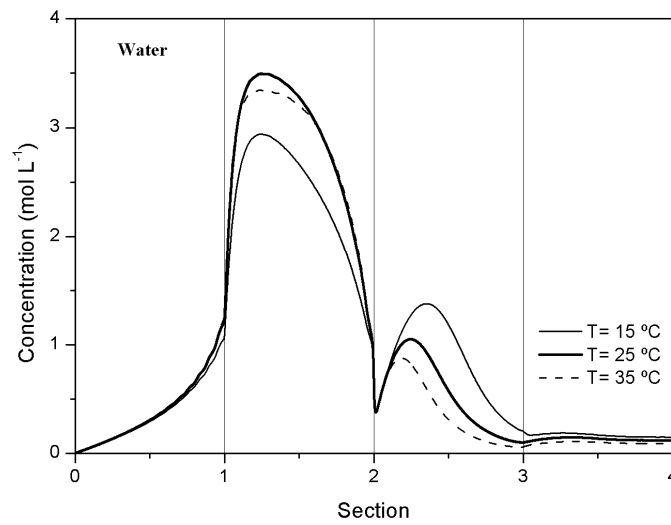
Figure 6.13. Effect of temperature on the TMBR steady-state concentration profiles ($\gamma_1 = 10.72$, $\gamma_4 = 0.385$, $\gamma_2 = 1$, $\gamma_3 = 4.58$, $t^* = 3.5$ min and $x_{B,F} = 0.3$) .
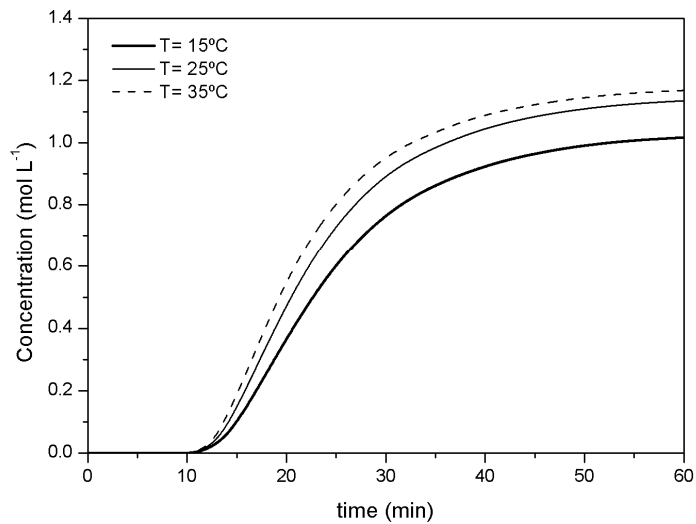
Figure 6.14. Water concentration on extract at different temperatures ($\gamma_1 = 10.72$, $\gamma_4 = 0.385$, $\gamma_2 = 1$, $\gamma_3 = 4.58$, $t^* = 3.5$ min and $x_{B,F} = 0.3$) .

The increase of acetaldehyde conversion and the improvement of solid phase regeneration in section 4 lead to the improvement of all performance parameters (*see Section 5.2.5*) with the increase of temperature *Table 6.9.*

Table 6.9. Performance parameters obtained by simulation with TMBR model at different temperatures (γ_1=10.72, γ_4=0.385, γ_2=1, γ_3=4.58, t*=3.5 min and $x_{B,F}$=0.3)

	Temperature		
	15ºC	25ºC	35ºC
PUX (%)	99.9	100.0	100.0
PUR (%)	80.0	92.2	96.1
X (%)	85.2	95.2	98.0
Rec (%)	85.2	94.9	97.4
PR($kg_{DBE}L_{adsorbent}^{-1}day^{-1}$)	45.2	49.8	50.6
DC($L_{adsorbent}kg_{DBE}^{-1}$)	9.5	8.5	8.2

6.3.1. Non-Isothermal Mathematical Model

The non-isothermal operation of simulated moving bed adsorptive reactor is studied by simulation with the non-isothermal true moving bed adsorptive reactor model. The mathematical model results from coupling mass balance equations (*see Section 5.3*) with de following energy balance equations:

Energy Balances:

Bulk fluid energy balance to section j:

$$\frac{\partial T_j}{\partial t} + u_j \frac{\partial T_j}{\partial z} + \frac{h_{L,j}}{\rho_L C_p^L} \frac{3}{r_p} \left(T_j - T_{s,j}\right) + \frac{4}{d_C} \frac{U_W}{\varepsilon \rho_L C_p^L} \left(T_j - T_W\right) = \frac{\lambda_{e,j}}{\rho_L C_p^L} \frac{\partial^2 T_j}{\partial z^2} \qquad (6.16)$$

Solid phase energy balance:

$$\alpha \rho_L C_p^L \left(\frac{\partial T_{s,j}}{\partial t} + u_s \frac{\partial T_{s,j}}{\partial x} \right)$$

$$= \frac{3}{r_p} h_{L,j} (1 - \varepsilon)(T_j - T_{s,j}) \tag{6.17}$$

$$+ (1 - \varepsilon)(1 - \varepsilon_p) \sum_{i=1}^{NC} (-\Delta H_i^{ads}) \frac{\partial q_{ij}}{\partial t} + \rho_b \Re(-\Delta H^R)$$

Initial and Danckwerts boundary conditions:

$$t = 0 \qquad T_j = T_{s,j} = T_{j,in} \tag{6.18}$$

$$z = 0 \qquad u T_j - D_{ax,h} \left. \frac{\partial T_j}{\partial z} \right|_{z=0} = u_j T_{j,in} \tag{6.19}$$

$$z = L_j \qquad \left. \frac{\partial T_j}{\partial z} \right|_{z=L_j} = 0 \tag{6.20}$$

For a column inside a section and for extract and raffinate nodes

$$\left. T_j \right|_{z=L_c} = \left. T_{j+1} \right|_{z=0} \tag{6.21}$$

For the desorbent node

$$u_1 \rho_L C_p^L \left(T_1|_{z=0} - T_4|_{z=L_c}\right) = u_D \rho_D C_p^D \left(T_D - T_4|_{z=L_c}\right) \tag{6.22}$$

For the feed node

$$u_3 \rho_L C_p^L \left(T_3|_{z=0} - T_2|_{z=L_c}\right) = u_F \rho_F C_p^F \left(T_F - T_2|_{z=L_c}\right) \tag{6.23}$$

where,

$$u_1 = u_4 + u_D \tag{6.24}$$

$$u_2 = u_1 - u_X \tag{6.25}$$

$$u_3 = u_2 + u_F \tag{6.26}$$

$$u_4 = u_3 - u_R \tag{6.27}$$

6.3.2. Simulated Results

If the heat generated by the reaction and by desorption of components is not removed from the SMBR through the reactor wall, a thermal wave develops inside the reactor and a steady-state temperature profile is formed (*Figure 6.15*).

The effect of the overall heat-transfer coefficient on the reaction/separation regions is presented on *Figure 6.16*. The size of region increases by reducing the values of overall heat-transfer coefficient on the wall, allowing higher values of γ_3, however, for low

values of γ_3 (low feed flowrate) the size and the shape of region are poorly influenced by the overall heat-transfer coefficient. This is related with the amount of reactant fed and consequently the amount of heat generated by the reaction, which influences the amplitude of steady-state temperature profiles (*Figure 6.17*).
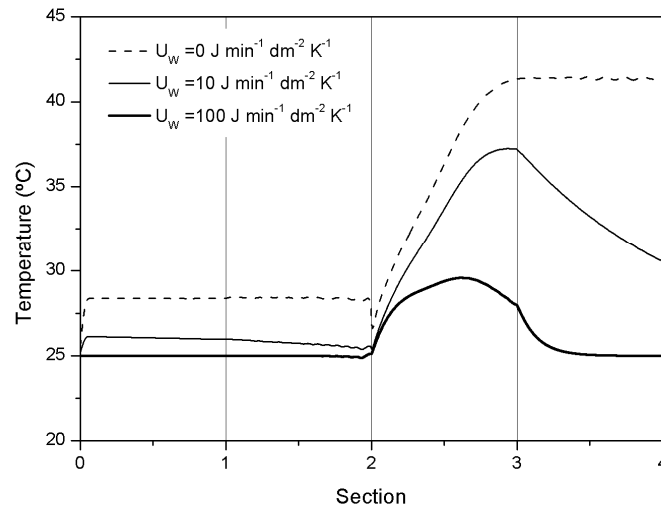
Figure 6.15. Steady-state temperature profiles inside the TMBR for different values of overall heat-transfer coefficient on the wall ($T_F=25°C$, $T_D=25°C$, $\gamma1=10.72$, $\gamma_4=0.385$, $\gamma_2=1$, $\gamma_3=4.58$, $t^*=3.5$ min and $x_{B,F}=0.3$)
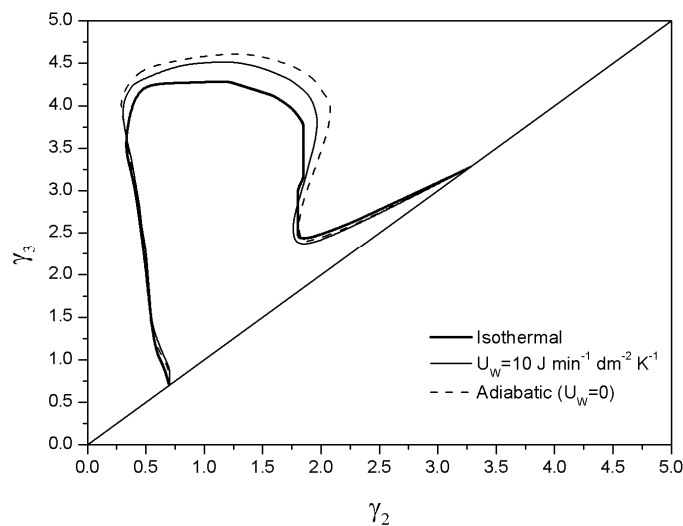
Figure 6.16. Effect of overall heat-transfer coefficient on the wall on reaction/separation regions ($T_F=25°C$, $T_D=25°C$, $\gamma_1=10.72$, $\gamma_4=0.385$, $t^*=3.5$ min and $x_{B,F}=0.3$)
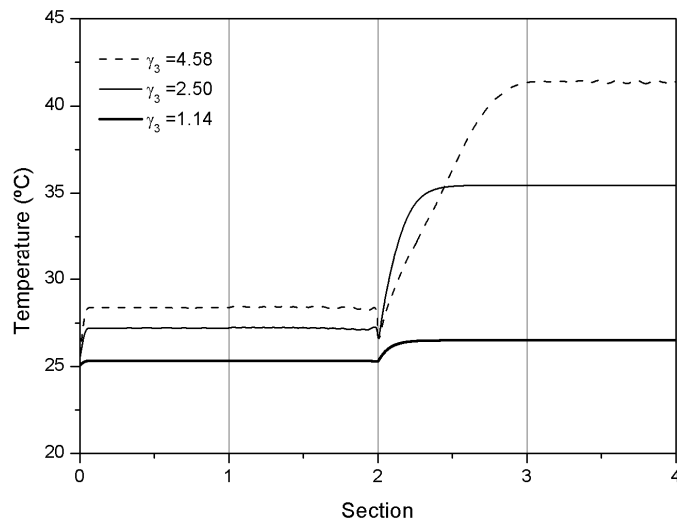
Figure 6.17. Effect of section 3 flowrate on TMBR steady-state temperature profiles (T_F=25ºC, T_D=25ºC, $γ_1$=10.72, $γ_4$=0.385, $γ_2$=1, t=3.5 min and $x_{B,F}$=0.3).*

When operated adiabatically the performance of the TMBR with an initial temperature of 25ºC is close to the performance of an isothermal TMBR at 35ºC (*Table 6.10*). However, for high values of $γ_2$ the performance of isothermal TMBR at 35ºC is better (*Figure 6.18*).

Table 6.10. Performance parameters obtained by simulation with TMBR model on adiabatic and isothermal operation ($γ_1$=10.72, $γ_4$=0.385, $γ_2$=2.3, $γ_3$=4.1, t=3.5 min and $x_{B,F}$=0.3).*

	Temperature		
	25ºC	35ºC	25ºC (Adiabatic)
PUX (%)	99.9	100.0	100.0
PUR (%)	92.4	95.5	94.1
X (%)	97.7	98.7	98.3
Rec (%)	96.1	96.9	96.7
PR($kg_{DBE}L_{adsorbent}^{-1}day^{-1}$)	25.2	25.1	25.4
DC($L_{adsorbent}kg_{DBE}^{-1}$)	13.0	12.1	12.9
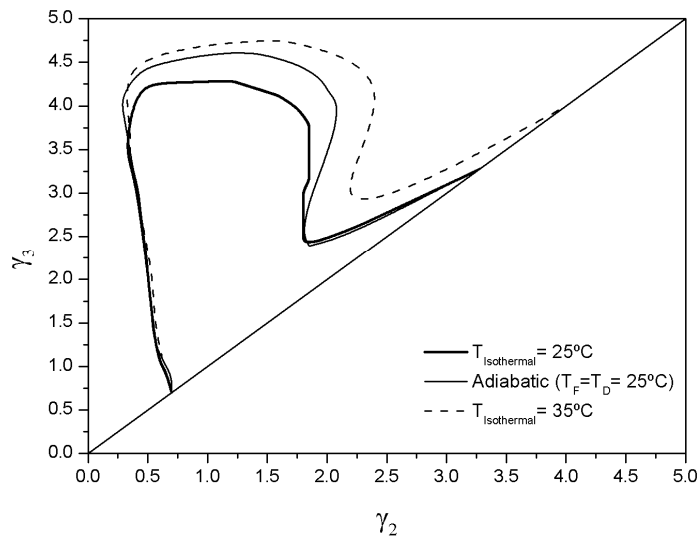
Figure 6.18. Reaction/separation regions for TMBR (γ_1=10.72, γ_4=0.385, t=3.5 min and $x_{B,F}$=0.3)*

This difference on performance can be perceived looking at *Figure 6.19*.
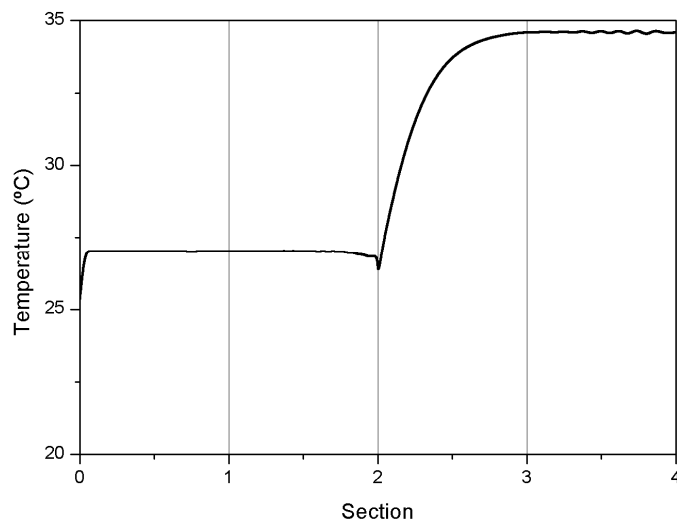
Figure 6.19. Steady-state temperature profile for the adiabatic operation of SMBR (T_F=25ºC, T_D=25ºC, γ_1=10.72, γ_4=0.385, γ_2=2.3, γ_3=4.1, t=3.5 min and $x_{B,F}$=0.3)..*

The steady-state temperature profile of adiabatically operated TMBR is close to 35ºC on section 3 and 4; however, the temperature on sections 1 and 2 decreases due to the colder desorbent that enters in the begin of section 1. Since the performance of solid

phase regeneration in section 1 increases with the temperature and consequently, more water is removed from the system by the extract stream. Therefore, for higher temperatures on sections 1 and 2, is possible to operate with higher values of γ_2 without contaminating the section 3 with water (*Figure 6.20c*).
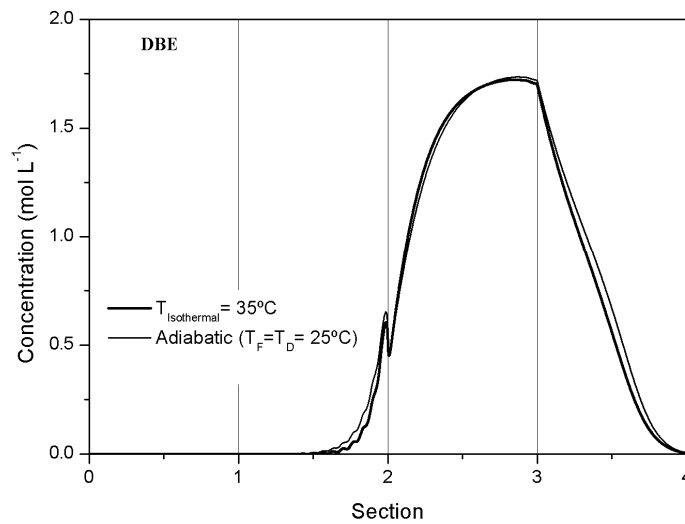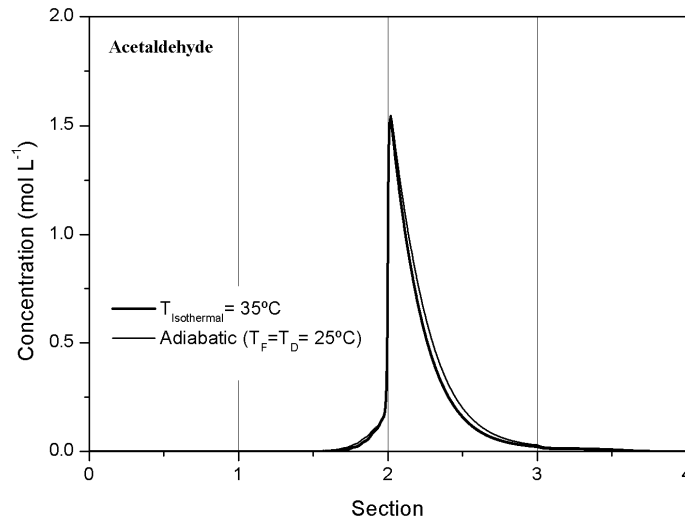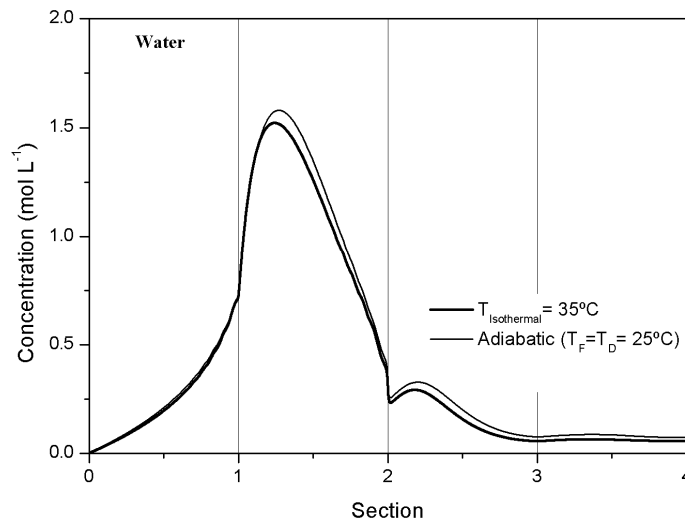
Figure 6.20. Steady-state concentration profiles for isothermal and adiabatic operation ($T_F=25^oC$, $T_D=25^oC$, $\gamma_1=10.72$, $\gamma_4=0.385$, $\gamma_2=2.3$, $\gamma_3=4.1$, $t^*=3.5$ min and $x_{B,F}=0.3$)

The temperature on sections 1 and 2 can be increased by decreasing the value of γ_1 (or decrease the desorbent flowrate) (*Figure 6.21*).
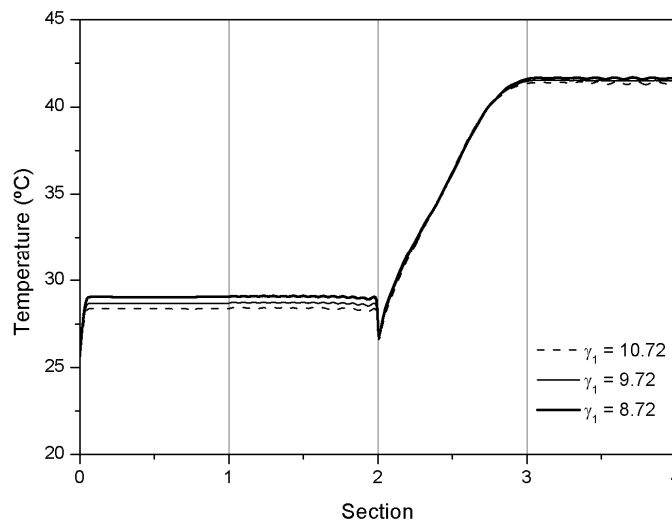
Figure 6.21. Influence of section 4 flowrate on adiabatic steady state temperature profiles ($T_F=25^oC$, $T_D=25^oC$, $\gamma_1=10.72$, $\gamma_4=0.385$, $\gamma_2=1$, $\gamma_3=4.58$, $t^*=3.5$ min and $x_{B,F}=0.3$).

However, as can be seen in *Figure 6.22* and *Figure 6.23* only the desorbent consumption improves with the decrease of γ_1. This suggests that the decrease of γ_1 is note compensated by the increase of the temperature in terms of solid phase regeneration performance.
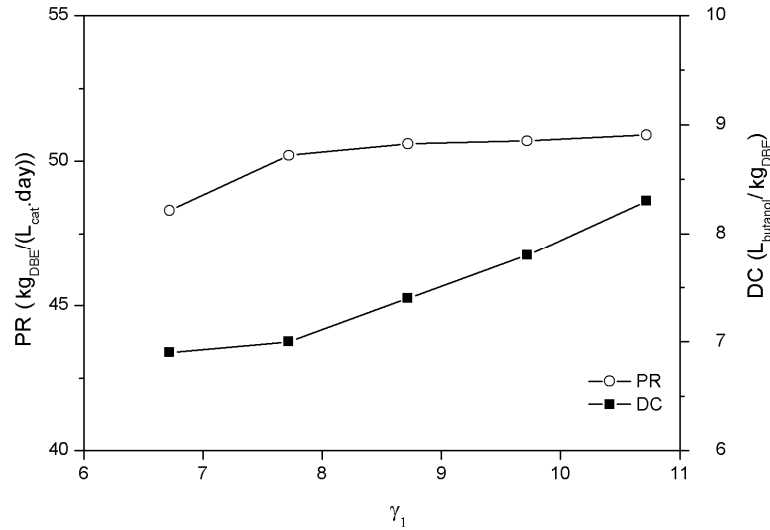
Figure 6.22. Effect of γ_1 on productivity and desorbent consumption ($T_F=25^oC$, $T_D=25^oC$, $\gamma_4=0.385$, $\gamma_2=1$, $\gamma_3=4.58$, $t^*=3.5$ min and $x_{B,F}=0.3$).
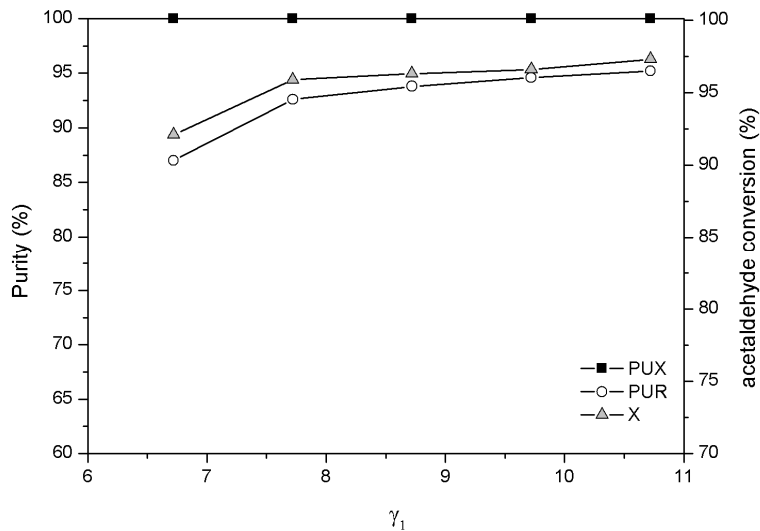
Figure 6.23. Effect of γ_1 on extract and raffinate purities and acetaldehyde conversion ($T_F=25^oC$, $T_D=25^oC$, $\gamma_4=0.385$, $\gamma_2=1$, $\gamma_3=4.58$, $t^*=3.5$ min and $x_{B,F}=0.3$).

The effect of reducing γ_1 on adiabatic reaction/separation is presented in *Figure 6.24*. The decrease of region size with the decrease of γ_1 is due mainly to a worse performance in terms of solid phase regeneration in section 1 caused by the reduction of γ_1 which is not compensated by the increase of temperature.
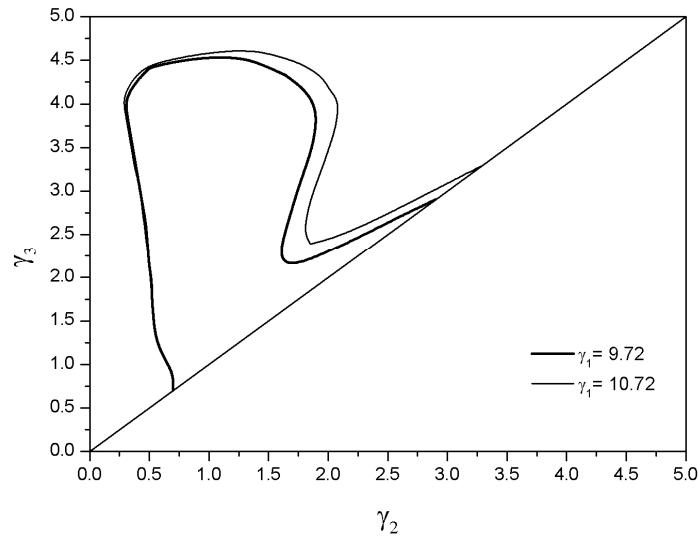
Figure 6.24. Effect of γ_1 on adiabatic reaction/separation region (T_F=25ºC, T_D=25ºC, γ_1=10.72, γ_4=0.385, t*=3.5 min and $x_{B,F}$=0.3).

The temperature on section 1 and 2 can be increased by increasing the temperature of the desorbent stream (T_D). A possible way to heat the desorbent stream is by use the hot raffinate stream (*Figure 6.27*)
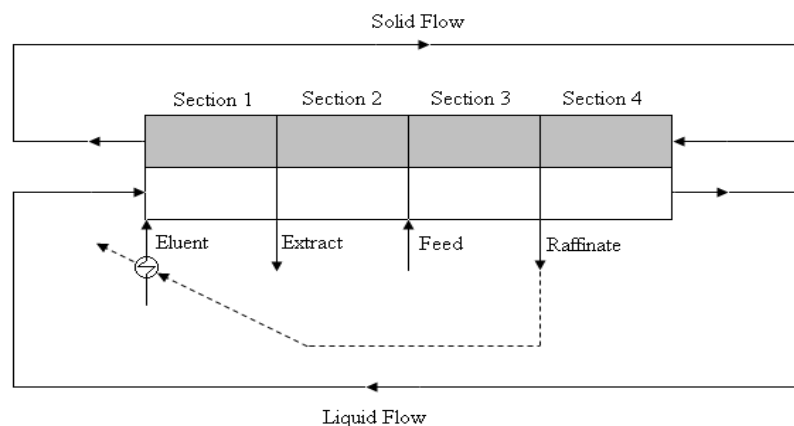
Figure 6.25. Schematic representation of TMBR with heated desorbent stream.

The effect of desorbent temperature on steady-state TMBR temperature profiles is presented on *Figure 6.26.* The increase of desorbent temperature increases the temperature in all TMBR section.
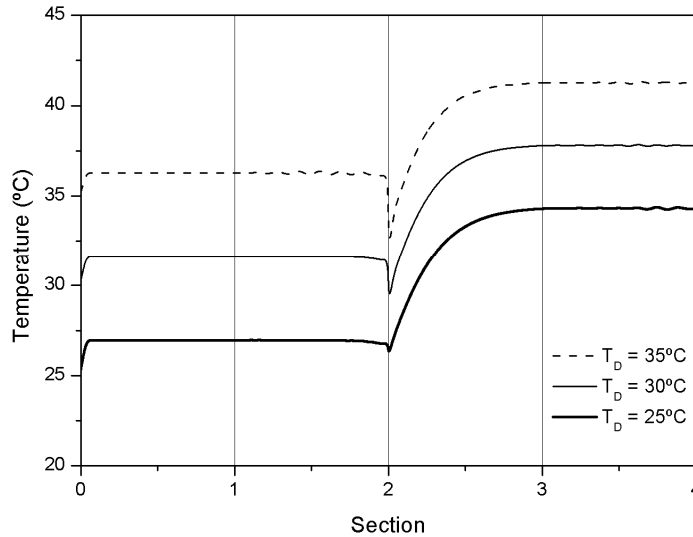
Figure 6.26. Effect of desorbent temperature on the adiabatic steady-state temperature profiles ($T_F=25^oC$, $\gamma_1=10.72$, $\gamma_4=0.385$, $\gamma_2=2.5$, $\gamma_3=4.1$, $t^*=3.5$ min and $x_{B,F}=0.3$).

The adiabatically operated SMBR with a starting temperature of 25ºC and a desorbent temperature of 35ºC presents a slight increase of reaction/separation region for high values of γ_2 (*Figure 6.27*).This is due to the increase of the temperature on sections 1 and 2.

Table 6.11 shows that the performance of an adiabatically operated SMBR with a starting temperature of 25ºC can be improved by increasing the temperature of the desorbent stream.
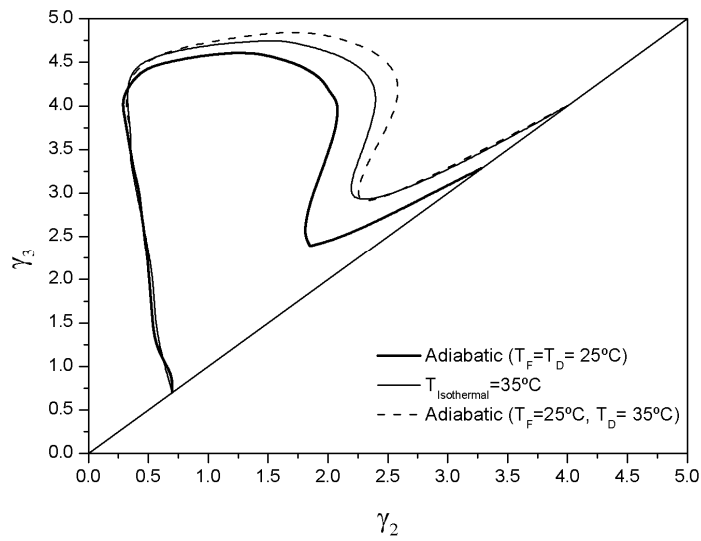
Figure 6.27. Effect of desorbent temperature on reaction/separation regions (γ_1=10.72, γ_4=0.385, t*=3.5 min and $x_{B,F}$=0.3)

Table 6.11. Effect of desorbent temperature on performance parameters (γ_1=10.72, γ_4=0.385, γ_2=2.5, γ_3=4.1, t*=3.5 min and $x_{B,F}$=0.3).

	Adiabatic (25ºC)			Isothermal (35 ºC)
	T_D= 25ºC	T_D= 30ºC	T_D= 35ºC	
PUX (%)	100.0	100.0	100.0	100.0
PUR (%)	93.2	94.5	95.5	94.8
X (%)	97.9	98.3	98.6	98.4
Rec (%)	96.3	96.6	96.7	96.5
PR($kg_{DBE}L_{adsorbent}^{-1}day^{-1}$)	25.3	25.4	24.4	25.1
DC($L_{adsorbent}kg_{DBE}^{-1}$)	13.0	12.9	12.9	13.0

6.4. Conclusions

Adsorption/desorption experiments with the non-reactive binary mixtures of 1-butanol/water and 1-butanol/DBE were performed in a fixed-bed column at 15ºC and 35ºC. The Langmuir isotherm parameters were estimated by minimizing the error

between the experimental and theoretical number of moles adsorbed/desorbed for all adsorption/desorption experiments.

The reaction of DBE synthesis was performed in a fixed-bed adsorptive reactor at 15ºC and 35ºC, experimental results show an increase of conversion and productivity for the higher temperature, that results mainly from the increase of reaction rate with temperature.

In order to better understand the influence of reaction rate and reactant residence time, the conversion and productivity were calculated by simulation of isothermal fixed-bed reactor model. Results show that the best operation in terms of productivity can be obtained at 35ºC and Da≈2.7.

Simulations with the adiabatic non-isothermal fixed-bed adsorptive reactor model show an improvement of reactor productivity relatively to isothermal operation; this can be explained by the development of a thermal wave inside the reactor that travels with the reaction front increasing the reaction rate.

The adsorption data obtained experimentally in the fixed-bed adsorptive reactor at different temperatures is used in the simulation of the simulated moving bed adsorptive reactor operation with both isothermal and non-isothermal models.

Simulated results show that the performance of an isothermally operated SMBR can be improved by increasing the temperature, due mainly to the increase of the reaction rate and the improvement of solid phase regeneration performance in section 1.

Simulations of the non-isothermal operation of SMBR show that a steady-state temperature profile can be formed. The temperature increases in sections 3 and 4 mainly due to the reaction heat; however, the temperature decreases in section 1 and 2 due to the colder desorbent stream. The temperature in section 1 and 2 can be increased by decreasing the desorbent flowrate; however, simulated results showed that the increase of temperature does not compensate the decrease of γ_1. As alternative the temperature of sections 1 and 2 can be increased by increasing the temperature of desorbent stream. Simulated results showed an improvement in the SMBR performance with the increase of desorbent stream temperature.

6.5. Notation

a_i liquid phase activity, dimensionless

C_i liquid phase concentration, mol dm^{-3}

$\bar{C}_{p,i}$ average pore concentration, mol dm^{-3}

C_p^L liquid phase heat capacity, J g^{-1} K^{-1}

C_p^p particle phase heat capacity, J g^{-1} K^{-1}

Da Damkhöler number, dimensionless

D_{ax} liquid phase axial dispersion coefficient, dm^2 min^{-1}

DC   desorbent consumption, L$_{adsorbent}$ kg$_{DBE}^{-1}$

d_c reactor column diameter, dm

h_L liquid-particle heat-transfer coefficient, J min^{-1} dm^{-2} K^{-1}

k_c kinetic constant, mol g^{-1} min^{-1}

K_{eq} equilibrium constant, dimensionless

K_i adsorption constant, dm^3 mol^{-1}

$K_{L,i}$ global mass-transfer coefficient, dm min^{-1}

$K_{s,D}$ water adsorption constant, dimensionless

L_c reactor column length, dm

M_i molar mass, g mol^{-1}

n number of moles, mol

Nu_p particle Nusselt number, dimensionless

Pe_h thermal Peclet number, dimensionless

Pe_m mass Pectlet number, dimensionless

Pr Prandtl number, dimensionless

PR   raffinate productivity, kg$_{DBE}$ L$_{adsorbent}^{-1}$ day^{-1}

PUR   raffinate purity, %

PUX   extract purity, %

Q liquid flowrate, $dm^3 \, min^{-1}$

Q_i adsorbent molar capacity, $mol \, dm^{-3}$

q_i solid phase concentration, $mol \, dm^{-3}$

$\bar{q}_i$ average solid phase concentration, $mol \, dm^{-3}$

R ideal gas constant, $J \, K^{-1} \, mol^{-1}$

Rec   DBE recovery on raffinate, %

$\mathfrak{R}$ reaction rate, $mol \, g^{-1} \, min^{-1}$

$\mathfrak{R}_0$ reaction rate at reactor feed conditions, $mol \, g^{-1} \, min^{-1}$

Re_p particle Reynolds number, dimensionless

r_p particle radius, dm

t time coordinate, min

t*   switching time, min

T temperature, K

T_{bi} normal boiling temperature, K

T_{ci} critical temperature, K

T_s solid phase temperature, K

T_w wall temperature, K

u liquid interstitial velocity, $dm \, min^{-1}$

u_0 liquid superficial velocity, $dm \, min^{-1}$

u_s interstitial solid velocity, $dm \, min^{-1}$

U_w overall heat-transfer coefficient on the wall, $J \, min^{-1} \, dm^{-2} \, K^{-1}$

V reactor volume, dm^{-3}

$V_{mol,i}$ molar volume, $mol \, dm^{-3}$

w_{cat} catalyst mass, kg

X conversion, %

x_i molar fraction, dimensionless

z axial coordinate, dm

ΔH_R reaction enthalpy, J mol^{-1}

ΔH_i^{ads} adsorption enthalpy, J mol^{-1}

Greek letters

γ ration between TMBR liquid and solid interstitial velocities, dimensionless

γ^* ration between SMBR liquid and solid interstitial velocities, dimensionless

α solid-liquid heat capacities ratio, dimensionless

ε bed porosity, dimensionless

ε_p particle porosity, dimensionless

η liquid viscosity, g dm^{-1} min^{-1}

λ_e effective thermal conductivity, J min^{-1} dm^{-1} K^{-1}

λ_L liquid thermal conductivity, J min^{-1} dm^{-1} K^{-1}

ρ_L liquid density, g dm^{-3}

ρ_b bed density, g dm^{-3}

ρ_p particle density, g dm^{-3}

v_i stoichiometric coefficient, dimensionless

Subscripts

D relative to desorbent

F relative to feed

i relative to component (i= A, B, C, D)

k relative to section (k= 1, 2, 3, 4)

R   relative to raffinate

X   relative to extract

0   relative to initial conditions

6.6. References

Gandi G. K., Silva V. M. T. M. and Rodrigues A. E., "Synthesis of 1,1-dimethoxyethane in a fixed bed adsorptive reactor", Ind. Eng. Chem. Res., 45(6), 2032-2039 (2006)

Graça N. S., Pais L. S., Silva V. M. T. M. and Rodrigues A. E., "Oxygenated biofuels from butanol for diesel blends: Synthesis of the acetal 1,1-dibutoxyethane catalyzed by amberlyst-15 ion-exchange resin", Ind. Eng. Chem. Res., 49(15), 6763-6771 (2010)

Graça N. S., Pais L. S., Silva V. M. T. M. and Rodrigues A. E., "Dynamic study of the synthesis of 1,1-dibutoxyethane in a fixed-bed adsorptive reactor", Sep. Sci. Technol., 46(4), 631-640 (2011)

Julcour C., Stüber F., Le Lann J. M., Wilhelm A. M. and Delmas H., "Dynamics of a three-phase upflow fixed-bed catalytic reactor", Chem. Eng. Sci., 54(13-14), 2391-2400 (1999)

Julcour C., Chaudhari R. V., Le Lann J. M., Wilhelm A. M. and Delmas H., "Dynamic modeling of three-phase upflow fixed-bed reactor including pore diffusion", Chem. Eng. Process., 41(4), 311-320 (2002)

Kolios G., Frauhammer J. and Eigenberger G., "Autothermal fixed-bed reactor concepts", Chem. Eng. Sci., 55(24), 5945-5967 (2000)

Mazzotti M., Neri B., Gelosa D. and Morbidelli M., "Dynamics of a Chromatographic Reactor: Esterification Catalyzed by Acidic Resins", Ind. Eng. Chem. Res., 36(8), 3163-3172 (1997)

Pandey J. D., Dey R., Soni N. K., Chandra P. and Yadav M. K., "Estimation of thermal conductivity of binary liquid mixtures employing new approach", Indian J. Chem. Technol., 14(6), 638-641 (2007)

Reid R. C., Prausnitz J. M. and Poling B. E., "Properties of Gases and Liquids", McGraw-Hill, New York (1987)

Ruthven D. M., "Principles of Adsorption and Adsorption Processes", Wiley, New York (1984)

Sainio T., Kaspereit M., Kienle A. and Seidel-Morgenstern A., "Thermal effects in reactive liquid chromatography", Chem. Eng. Sci., 62(18-20), 5674-5681 (2007)

Sainio T., Zhang L. and Seidel-Morgenstern A., "Adiabatic operation of chromatographic fixed-bed reactors", Chem. Eng. J., 168(2), 861-871 (2011)

Silva V. M. T. M. and Rodrigues A. E., "Dynamics of a fixed-bed adsorptive reactor for synthesis of diethylacetal", AIChE J., 48(3), 625-634 (2002)

Stankiewicz A., "Reactive separations for process intensification: An industrial perspective", Chem. Eng. Process., 42(3), 137-144 (2003)

Taylor R. and Krishna R., "Modelling reactive distillation", Chem. Eng. Sci., 55(22), 5183-5229 (2000)

7. Conclusions and Suggestions for Future Work

This work was focused on the implementation and improvement of the synthesis of the acetal 1,1-dibutoxyethane in a simulated moving bed adsorptive reactor. The main results and conclusions are the following:

Thermodynamic and rection kinetic data of the 1,1-dibutoxyethane synthesis were measured in a batch reactor by reacting 1-butnol and acetaldehyde in liquid phase, using Amberlyst 15 as catalyst. The reaction equilibrium constant based on activities was experimentally determined in the temperature range 20 ℃-40 ℃ at 6 atm, K_a=0.00959exp[1755.3/T(K)].

The standard properties of reaction at 298.15 K were estimated: ΔH^0=-14.59 kJ mol^{-1}, ΔG^0= -3.07 kJ mol^{-1}, ΔS^0=-38.64 J mol^{-1} K^{-1}. Kinetic experiments were performed in the temperature range 10 ℃-50 ℃ at 6 atm. A two-parameter kinetic law based on a Langmuir-Hinshelwood rate expression, using activity coefficients from the UNIFAC method, was used:

$$\Re = k_c \frac{a_A a_B - \dfrac{a_C a_D}{K_a a_A}}{(1 + K_{s,D} a_D)^2}$$

and parameters are given by:

$$k_c = 2.39 \times 10^9 exp\left(-\frac{6200.9}{T(K)}\right)$$

$$K_{s,D} = 2.25 \times 10^{-4} exp\left(\frac{3303.1}{T(K)}\right)$$

The activation energy of reaction is 51.55 kJ mol^{-1}.

The synthesis of 1,1-dibutoxyethane in a fixed-bed adsorptive reactor using Amberlyst-15 was studied. The adsorption of non-reactive pairs was investigated experimentally, at 25 ºC, by frontal chromatography in a fixed-bed adsorber. The Langmuir type isotherm parameters were by minimizing the error between experimental and theoretical number of moles adsorbed/desorbed for all adsorption/desorption experiments.

Component	Q (mol/L_{solid})	K (L/mol)
1-Butanol	8.5	7.5
Acetaldehyde	15.1	0.5
Water	44.9	12.1
DBE	5.8	0.4

In order to avoid the immiscibility of liquid phase, the liquid-liquid equilibrium for the mixture 1-butanol/water was studied. It was concluded that, for a fixed-bed operation at 25ºC, the molar fraction of 1-butanol should be higher than 50% in order to prevent the formation of two liquid phases.

The 1,1-dibutoxyethane production and column regeneration were performed in the fixed-bed adsorptive reactor. For the chromatographic reactor, the mathematical model was derived assuming axial dispersion, isothermal operation, external and internal mass transfer resistances, fluid velocity variations with the composition and multicomponent Langmuir isotherm:

$$q_i = \frac{Q_i K_i C_{p,i}}{1 + \sum_{j=1}^{NC} K_j C_{p,j}}$$

Experimental and simulated results of adsorptive reactor show a selective separation between water and DBE over the resin, where DBE is the less retained component and easily displaced by water, the more retained component.

The synthesis of 1,1- dibutoxyethane was carried out in a Simulated Moving Bed pilot unit LICOSEP 12-26 with 12 columns packed with the commercial ion-exchange resin Amberlyst-15. The TMBR model was used to construct reaction/separation regions and to study the influence of feed composition, switching time, flow rates and mass-transfer resistances on the SMBR performance.

The effect of temperature on the synthesis of 1,1-dibutoxyethane in a fixed-bed adsorptive reactor was studied by performing both adsorption/desorption and reaction/regeneration experiments at 15ºC and 35ºC. The Langmuir type isotherm parameters were obtained from the adsorption/desorption experiments:

	15ºC		35ºC	
	Q ($mol\ L_{solid}^{-1}$)	K ($L\ mol^{-1}$)	Q ($mol\ L_{solid}^{-1}$)	K ($L\ mol^{-1}$)
1-Butanol	8.8	7.8	8.4	7.2
Acetaldehyde	15.2	0.6	15	0.4
Water	45.0	12.9	44.0	11.4
DBE	6.0	0.8	5.0	0.1

The reaction/regeneration experiments showed an increase in both conversion and productivity by increasing the temperature. Simulated results suggest that the reactor productivity can be improved by using the adiabatic operation mode on fixed-bed adsorptive reactor.

The effect of temperature on simulated moving bed adsorptive reactor performance was studied by simulation with both isothermal and non-isothermal mathematical models. Simulated results showed that the SMBR performance can be improved by using the adiabatic operation mode.

As future work, alternative SMBR operation modes, such as asynchronous shifting of inlet/outlet ports and feed flow modulation should be considered.

A further implementation of temperature measure devices on the fixed-bed and simulated moving bed experimental apparatus will allow to obtain experimental temperature profiles for the non-isothermal operation mode and determine the non-isothermal mathematical models parameters based on experimental data.

The non-isothermal operation of SMBR should be performed experimentally and optimized.

Appendix A: Thermodynamic Properties

1. Literature available data

1.1. Physical Properties

Table A. 1. Physical Properties

	Acetaldehyde	Butanol	DBE	Water
Molecular Weight(g/mol)	44.053	74.122	174.28	18.015
Melting Temperature – Tf(K)	149.65 [a]	193.25 [a]	233.06 [c]	273.15 [a]
Nomal boiling Temperature – Tb(K)	293.02 [a]	390.15 [a]	490.02 [c]	373.15 [a]
Critical Temperature – Tc(K)	461 [b]	562.93 [b]	669.45 [c]	647.13 [b]
Critical Pressure - Pc(K)	55.5 [b]	44.13 [b]	23.89 [c]	221.20 [b]
Critical Volume – Vc(cm³/mol)	157 [b]	274.5 [b]	625.5 [c]	57.1 [b]
Acentric factor- ω	0.317 [b]	0.595 [b]	0.621 [d]	0.344 [b]

[a] R.H. Perry and D.W.Green, Perry's Chemical Engineers Handbook (7th Edition), McGraw-Hill(1997)
[b] C.L. Yaws, Chemical Properties HandBook, McGraw-Hill(1999)
[c] (Section 2.1) Joback Method – Poling, E.B., Prausnitz, J.M., O'Connell, J.P., The properties of gases and liquids, McGraw-Hill (2001)
[d] (Section 2.2) Lee-Kesler correlation

1.2. Liquid Heat Capacity

$$C_p(J\ mol^{-1}K^{-1}) = A + BT + CT^2 + DT^3 \tag{A.1}$$

Table A. 2. Constants used for liquid heat capacity calculation.

	Acetaldehyde[a]	Butanol[a]	Water[a]	DBE[b]
A	45.056	83.877	92.053	360.66
B	0.44853	0.56628	-3.9953E-2	
C	-1.6602E-3	-1.7208E-3	-2.1103E-4	
D	2.700E-6	2.2780E-6	5.3469E-7	
Tmin(K)	151	185	273	
Tmax(K)	415	507	615	

[a] C.L. Yaws, Chemical Properties HandBook, McGraw-Hill(1999)
[b] Conner, A.Z., Elving, P.J., Steingiser, Specific Heats of Acetaldehyde and Acetaldehyde Dibutyl Acetal, Vol. 69, No. 6, 1947

1.3. Reaction Thermodynamic Data

Table A. 3. Standard Thermochemistry Data

	Acetaldehyde[a]	Butanol[a]	DBE[b]	Water[c]
ΔH^0_f (kJ/mol)	-192.2	-327.3	-577.56	-283.83
ΔG^0_f (kJ/mol)	-127.6	-162.5	-218.55	-237.129
S^0 (J/mol.K)	160.4	225.8	503.45	69.91

[a] Speight, J.G, Lange's HandBook of Chemistry, McGraw-Hill (2005)
[b] Experimental Data
[c] D.Wagman, W.Evans, V.Parker, R. Schumm, I.Halow, S.Bailey, K. Churney, R.Nutall, The NBS Tables of Chemical Thermodynamic Properties, J.Phys.Chem.Ref.Data.11 (1982)

1.4. Vapor Pressure

$$log_{10}P_V(mmHg) = A - \frac{B}{T} \tag{A.2}$$

$$log_{10}P_V(bar) = A - \frac{B}{C + T} \tag{A.3}$$

Table A. 4. Constants used for vapor pressure calculation.

	Acetaldehyde [a]	Butanol [a]	Water [a]	DBE [b]
Equation	A.3	A.3	A.3	A.2
A	3.68639	4.5460	6.20963	8.232
B	822.894	1351.555	2354.731	2470
C	-69.899	-93.34	7.559	-
Tmin(K)	293.3	295.7	293	303.55
Tmax(K)	377.4	390.9	343	464.05

[a] Lange's HandBook(2005)
[b] A.Z.Conner,P.J.Elving, S. Steingiser, Vapor-Liquid Equilibria in Binary System Acetaldehyde Dibutyl Acetal – n-Butanol, Publicker Industries Inc., Philadelphia (1947)

2. Properties Estimation

2.1. Joback Method

$$T_f = 122 + \sum_k N_k T_{fk} \tag{A.4}$$

$$T_b = 198 + \sum_k N_k T_{bk} \tag{A.5}$$

$$T_c = T_b \left[0.584 + 0.965 \sum_k N_k T_{ck} - \left(\sum_k N_k T_{ck} \right)^2 \right]^{-1} \tag{A.6}$$

$$P_c = \left[0.113 + 0.0032 N_{atoms} - \sum_k N_k P_{ck} \right]^{-2} \tag{A.7}$$

$$V_c = 17.5 + \sum_k N_k V_{ck} \tag{A.8}$$

Table A. 5. Parameters used on Joback method.

	T_{fk} (K)	T_{bk} (K)	T_{ck} (K)	P_{ck} (bar)	V_{ck} (cm^3/mol)
CH$_3$	-5.10	23.58	0.0141	-0.0012	65
CH$_2$	11.27	22.88	0.0189	0.000	56
CH	12.64	21.74	0.0164	0.0020	41
-O-	23.05	31.22	0.0098	0.0048	82

2.2. Lee-Kesler Correlation

$$P_r = \frac{P}{P_c} \tag{A.9}$$

$$T_r = \frac{T_b}{T_c} \tag{A.10}$$

$$lnP_r = f^{(0)} + \omega f^{(1)} \tag{A.11}$$

$$f^{(0)} = 5.92714 - 6.09648T_r^{-1} - 1.28862lnT_r + 0.169347T_r^6 \tag{A.12}$$

$$f^{(1)} = 15.2518 - 15.6875T_r^{-1} - 13.4721lnT_r + 0.43577T_r^6 \tag{A.13}$$

$$\omega = \frac{-lnP_r - 5.92714 + 6.09648T_r^{-1} + 1.28862lnT_r - 0.169347T_r^6}{15.2518 - 15.6875T_r^{-1} - 13.4721lnT_r + 0.43577T_r^6} \tag{A.14}$$

Appendix B: GC Calibration

1. Pure Component

Calibration of water:

sample	$V_{inj}(\mu L)$	$n(\mu mol)$	A(u.a.)	R.C.(%)
1			0.335388	
2	0.1	5.539859	0.329351	0.010
3			0.340923	
4			1.007416	
5	0.3	1.000053	0.984401	0.020
6			1.008343	
7			1.643759	
8	0.5	1.664635	1.68704	0.030
9			1.663105	

y = 16.629x
R² = 0.9995
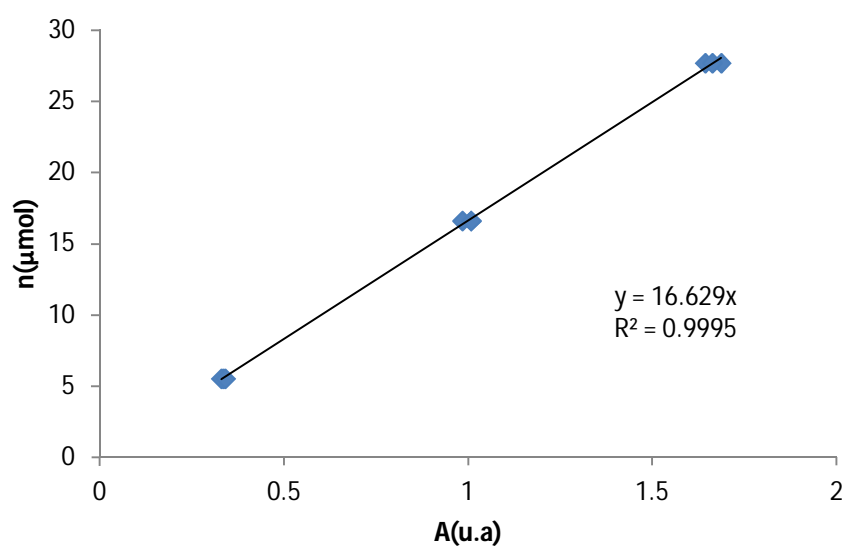
Calibration of Butanol:

sample	$V_{inj}(\mu L)$	$n(\mu mol)$	A(u.a.)	R.C.(%)
1			0.192951	
2	0.1	1.087429	0.196478	0.002
3			0.194021	
4			0.608649	
5	0.3	3.262288	0.613457	0.001
6			0.608518	
7			1.010625	
8	0.5	5.437147	0.99966	0.022
9			0.981145	

y = 5.4276x
R² = 0.9991
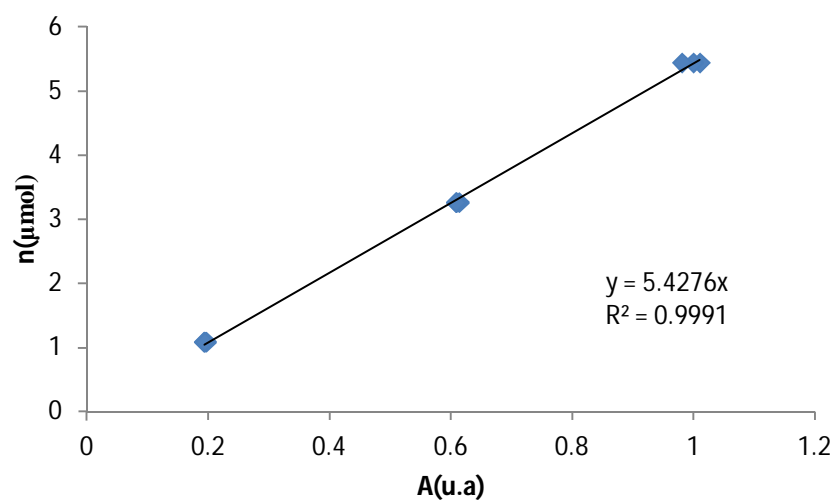
Calibration of Acetaldehyde:

sample	$V_{inj}(\mu L)$	n(µmol)	A(u.a.)	R.C.(%)
1			0.11662	
2	0.05	0.878426	0.12425	0.043
3			0.110149	
4			0.230694	
5	0.1	1.756852	0.220958	0.020
6			0.217889	
7			0.308514	
8	0.15	2.635278	0.321522	0.019
9			0.322487	
10			0.634848	
11	0.3	5.270555	0.616088	0.022
12			0.637969	
13			1.01586	
14	0.5	8.784259	1.023082	0.005
15			1.023082	
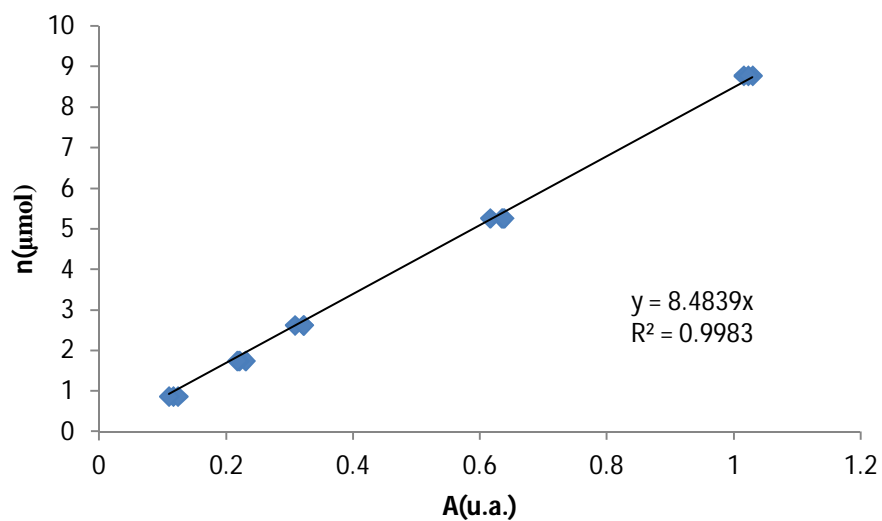
Calibration of DBE:

sample	n(µmol)	A(u.a.)	R.C.(%)
1		0.041925	
2	0.101465	0.040259	0.007
3		0.043626	
4		0.088947	
5	0.198434	0.080393	0.026
6		0.081287	
7		0.136146	
8	0.334598	0.138401	0.006
9		0.132802	
10		0.270047	
11	0.660931	0.271761	0.007
12		0.263623	
13		0.449336	
14	1.12616	0.44456	0.002
15		0.442987	

$y = 2.5029x$
$R^2 = 0.9991$
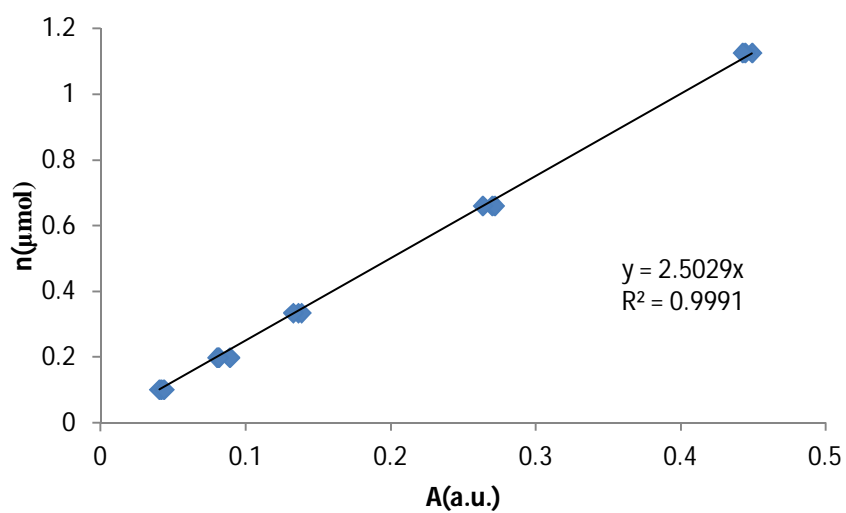
2. Muticomponent mixtures

The molar fraction of each component is calculated accordingly to:

$$x_i = \frac{f_i A_i}{\sum f_n A_n} \tag{B.1}$$

Water/Butanol:

Sample	$x_{Butanol}$(real)	$x_{Butanol}$(calculated)	Error(%)
1		0.857737	1.85
2	0.84212	0.860647	2.20
3		0.860647	2.16
4		0.013729	-0.09
5	0.015692	0.013041	-0.14
6		0.013378	-0.11

Water/Acetaldehyde:

Sample	$x_{Acetaldehyde}$(real)	$x_{Acetaldehyde}$(calculated)	Error(%)
1		0.427247	-2.34
2	0.43748	0.423132	-3.28
3		0.422788	-3.36
4		0.160994	0.44
5	0.160289	0.15972	-0.35
6		0.160713	0.26

Butanol/Acetaldehyde:

Sample	$x_{Acetaldehyde}$(real)	$x_{Acetaldehyde}$(calculated)	Error(%)
1		0.538282	-1.58
2	0.54692	0.55175	0.88
3		0.533304	-2.49
4		0.398931	-3.35
5	0.41274	0.393265	-4.72
6		0.406535	-1.50

Water/Butanol/Acetaldehyde:

Component	Sample	x(real)	x(calculated)	Error(%)
	1		0.37509	0.41
Acetaldehyde	2	0.37356	0.37547	0.51
	3		0.37205	-0.41
	1		0.28680	-3.20
Water	2	0.29629	0.29037	-2.00
	3		0.28053	-5.32
	1		0.33810	2.41
Butanol	2	0.33015	0.33416	1.21
	3		0.34743	5.23

Appendix C: Liquid-Liquid Equilibrium Calculation

In the liquid-liquid equilibrium the following condition has to be verified:

$$\gamma_i^\alpha x_i^\alpha = \gamma_i^\beta x_i^\beta \tag{C.1}$$

where, x_i^α and x_i^β are the molar fractions of component i in the phases α and β, respectively; γ_i^α and γ_i^β are the activity coefficients of component i in the phases α and β, respectively.

From the overall mass balance:

$$z_i = x_i^\alpha L_1 + x_i^\beta L_2 \tag{C.2}$$

where, z_i is the overall molar fraction of component i, L_1 and L_2 are the molar fractions of the phases α and β, respectively.

The distribution ratio of component i is defined from *Equation C.1*:

$$k_i = \frac{x_i^\alpha}{x_i^\beta} = \frac{\gamma_i^\beta}{\gamma_i^\alpha} \tag{C.3}$$

From *Equation C.2* and *Equation C.3* the molar fraction of component i in each liquid phase is given by:

$$x_i^\beta = \frac{z_i}{1 + L_1(k_i - 1)}$$
(C.4)

and

$$x_i^\alpha = \frac{k_i z_i}{1 + L_1(k_i - 1)}$$
(C.5)

Knowing that $\Sigma\, x_i^\alpha = \Sigma\, x_i^\beta = 1$, the following expression is obtained:

$$F(L_1) = \sum_{i=1}^{c} \frac{z_i}{1 + L_1(k_i - 1)} - \sum_{i=1}^{c} \frac{k_i z_i}{1 + L_1(k_i - 1)} = \sum_{i=1}^{c} \frac{z_i(k_i - 1)}{1 + L_1(k_i - 1)} = 0 \quad \text{(C.6)}$$

The value of L_1 is obtained by solving the *Equation C.6* then x_i^β and x_i^α are calculated with *Equation C.4* and *Equation C.5*, and k_i from *Equation C.3*. The composition of the two liquid phases is calculated by this iterative process until the condition in the *Equation C.1* is verified.

In this work the activity coefficients for the binary mixture 1-butanol/water were calculated by the UNIFAC and UNIQUAC methods.

Table C.1 presents the relative molecular volume and surface area parameters used in both methods.

Table C.1. Relative molecular volume and surface area of pure components parameters (Reid et al., 1987)

Molecule(i)	Group Identification			$\upsilon_k^{(i)}$	r_k	q_k
	Name	No. Main	No. Sec			
Butanol (1)	CH$_3$	1	1	1	0.9011	0.848
	CH$_2$	1	2	3	0.6744	0.540
	OH	5	15	1	1.0000	1.200
Water (2)	H$_2$O	7	17	1	0.8200	1.400

The interaction parameters used in the UNIFAC method are presented in *Table C.2*.

Table C.2. Interaction parameters (Fredenslund et al., 1977)

$a_{m,n}$	1	5	7
1	0	986.5	1318
5	156.4	0	353.5
7	300	-229.1	0

In the UNIQUAC method the activity coefficients are calculated by the following equation:

$$\ln \gamma_i = 1 - \frac{\Phi_i}{x_i} + \ln\frac{\Phi_i}{x_i} + 5q_i\left(1 - \frac{\Phi_i}{x_i} + \ln\frac{\Phi_i}{x_i}\right) + q_i\left(1 - \ln S_i - \sum_j \frac{\theta_j \tau_{ij}}{S_j}\right) \quad (C.7)$$

where, Φ_i and θ_j are calculates based on the parameters r and q (*Table C.1*). The parameter τ_{ij} is calculated base on the by binary energy interaction parameter A_{ij} and is given by:

$$\tau_{ij} = \exp\left(-\frac{A_{ij}}{T}\right) \tag{C.8}$$

where, $A_{ii}=A_{jj}=0$ and $A_{ij} \neq A_{ji}$. The parameter A_{ij} is calculated by the *Equation C.9*.

$$A_{ij} = a_{ij} + b_{ij}T + c_{ij}T^2 \tag{C.9}$$

The coefficients of *Equation C.9* are presented in *Table C.4*.

Table C.4. 1-Butanol (1) and water (2) interaction parameters at 273-363 K (Winkelman et al., 2009)

	a_{ij}	b_{ij}	$10^4 c_{ij}$
A_{12}	155.31	1.0822	-43.711
A_{21}	-579.36	2.7517	-6.7700

References

Fredenslund A., Gmehling J. and Rasmussen P., "Vapor-Liquid Equilibria Using UNIFAC", Elsevier, Amsterdam (1977)

Reid R. C., Prausnitz J. M. and Poling B. E., "The Properties of Gases and Liquids", McGraw-Hill, New York (1987)

Winkelman J. G. M., Kraai G. N. and Heeres H. J., "Binary, ternary and quaternary liquid-liquid equilibria in 1-butanol, oleic acid, water and n-heptane mixtures", Fluid Phase Equilibria, 284(2), 71-79 (2009)

Appendix D: Experimental Determination of the Internal Concentration Profiles in a Licosep 12-26

In this appendix is described the methodology followed to determine the internal concentration profiles of Licosep 12-26 SMB pilot unit, as indicated in the Licosep 12-26 *Instruction Manual.*

The Licosep 12-26 internal concentration profiles are determined by collecting samples from the system through a 6-port valve. To build up complete internal profiles, one full cycle is necessary, one sample being collected at each half-time period.

Figure D.1 presents a typical SMB internal concentration profile in the case of an 12-column configuration. This figure shows the concentration measured at different positions, relatively to the inlet and outlet lines of an equivalent TMB, the eluent line being at position 1.
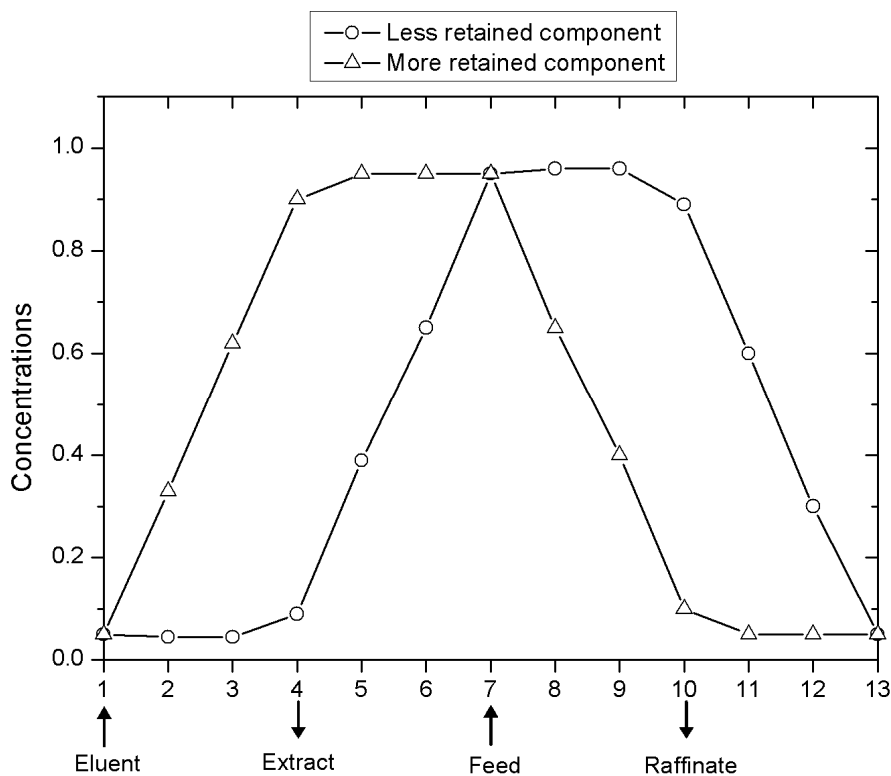

Figure D.1. Typical SMB internal concentration profiles (12-column configuration)

In *Table D.1* the eluent line position and its corresponding abscissa in *Figure D.1* are given.

Table D.1. Relation between the position of the eluent line and the abscissa in Figure D.1

Eluent line position	Abscissa in *Figure D.1*
E1	1
E2	12
E3	11
E4	10
E5	9
E6	8
E7	7
E8	6
E9	5
E10	4
E11	3
E12	2

To understand the meaning of the abscissa in *Figure D.1*, it must be kept in mind that the 6-port valve is fixed whereas the injection and collection points of the SMB move. The valve will appear successively in section 1, 2, 3 and 4, close to or far from the eluent line. The abscissa in *Figure D.1* is related to the number of columns standing between the valve and the eluent line.

The procedure to withdraw a sample from the Licosep 12-26 through the 6 port valve involves the following steps:

- The valve being in its "load" position, wash and fill the injection loop with the eluent using the adapted syringe.

- Switch the valve to its "inject" position.

- Wash the valve. Pump air through it, using (empty) syringe, to dry its internal tubings and thus avoid an undesirable later dilution of the sample withdrawn.

- When at the half-time period (use a chronometer for example), switch the valve to its "load" position. The sample sought is now trapped in the injection loop.

- Put a vial at the purge outlet of the valve and pump air through the valve to make the sample flow out from the vent/waste exit.

The recycling pump used in Licosep 12-26 introduces a dead volume V_d, which delays the concentrations leaving the last and entering the first columns. Fpr the recycling pump used (a three-head membrane pump, Milroyal, Pont St. Pierre, France) this dead volume is equal to 21 mL. The *Separex* group proposed a dead volume correction accomplished by using a period desynchronization. The injection or collection lines which have passed the last column, during a given cycle, are shifted with a delay given by:

$$t_d = \frac{21}{\dfrac{(Q_1^* + Q_2^* + Q_3^* + Q_4^*)}{4}} \qquad (D.1)$$

The 6-port valve used to collect samples from Licosep 12-26 is located after the recycling pump and just before the inlet of the first column. Therefore, excepting at the beginning of a new full cycle (when the eluent inlet is at the inlet of the first column), a new fraction only begins t_d minutes later from the beginning of a new switch time interval. *Table D.2* presents the right moments for the withdrawal of samples at half-time period.

Table D.2. Moments of withdrawal of samples at half-time period (Licosep 12-26 with 12 columns, $t_{1/2}=t^*/2$)

Eluent line position	E1	E2 to E12
Moment of withdrawal	$t_{1/2}$	$t_{1/2} + t_d$